IAHR AIRH

Supported by Spain Water and IWHR, China

IAHR 2017

37th IAHR WORLD CONGRESS

13-18 August, 2017

Kuala Lumpur, Malaysia

KEYNOTE

INFLUENCE OF MORPHOLOGICAL CHANGES ON ECOLOGY: A CASCADE OF SCALES

SILKE WIEPRECHT[(1)], LYDIA SEITZ[(2)] & STEFAN HAUN[(3)]

[(1,2,3)]Institute of Modeling Hydraulic and Environmental Systems, University Stuttgart, Germany
e-mail (wieprecht@iws.uni-stuttgart.de)

ABSTRACT

For the understanding of morphological processes, it is not sufficient to only investigate river sections. On the macro scale, the catchment plays an important role especially for the available quantity of material fluxes and its composition in the river. Intense river works in the last decades and centuries (straightening, reservoirs, dams, dikes etc.) strongly alter the characteristics of our rivers. In particular, the lack of bed load material severely affects the dynamic processes in rivers and ecological important instream structures. In some examples, the attempt is made to enhance the ecological situation in a river by individual river restoration measures. Depending on the availability of material, very different results can be achieved. These effects can also be proven very well with the help of long-term morphological models. Another option is to bring back sediments into the transport cycle, e.g. by flushing reservoirs. On one hand, this can help to increase the morphological dynamics, but on the other hand the grain sorting effect upstream of reservoirs changes the characteristics of the river bed downstream. Due to changes of material composition, the granular structure on the micro and pico-scale of the river bed may be heavily altered. It occurs that, although the meso-scale structure seems to be good, there are still not enough acceptable habitats for aquatic species available. However, alterations on the micro and pico-scale, like colmation and clogging processes, e.g. due to flushing of reservoirs or changes in wash load fluxes from the catchment, can influence the biological communities in rivers. Depending on sediment texture and content of pollutants and/or nutrients, effects like biofilm growth occur, which then additionally alter sediment transport characteristics.

Keywords: Morphology; alluvial form; ecological impact.

1 INTRODUCTION

Morphology of a river is the result of interaction between discharge, sediment transport and the bed material composition. In a natural river section, depending on the hydrograph and the sediment input from upstream, a specific combination of river bed width and its related morphologic form will occur. Many attempts exist to describe the relation between river morphology and its influencing factors (e.g. Schumm, 1985; Rosgen, 1994; Montgomery and Buffington, 1997). Yalin and da Silva (2001); Ahmari and da Silva (2011) specifically investigated the interaction of river bed width, water depth, grain size distribution and the developing alluvial forms. A multitude of nature data and laboratory results show empirically, that the different alluvial forms mainly depend on the parameters discharge, bed width and grain size. However, the influence of altering boundary conditions, as the reduction of sediment input from upstream, fine sediment intrusion as a result e.g. from land erosion or reservoir flushing, as well as grain sorting effects due to changing hydrological conditions is not considered. These are parameters of paramount influence on the habitat conditions of an aquatic ecosystem.

Frissell et al. (1986) assumed that the river morphology and the development of aquatic stream communities are largely determined by the organization, structure, and dynamics of the physical stream habitat, together with the pool of species available for colonization. Also, biological patterns in streams are mainly adjusted to and controlled by physical patterns, e.g. alluvial forms, bed forms, grain size, flow velocity etc. Frissell et al. (1986) considered stream systems as hierarchically organized systems incorporating, from the catchment scale on successively lower levels, river systems, stream segments, pool-riffles, grain structures down to microhabitat subsystems. The authors stated that the hierarchy is spatially nested, which means that a system at one level forms the environment of its subsystems at lower levels. Thus, any disturbance on a higher level will influence the following levels. As a consequence, e.g. variations in land use patterns on the macro scale can be identified down to the pico-scale with a shift of the grain size composition. Habitats at all levels, each segment, reach, pool/riffle system, or grain composition play a particular structural and functional role (physically and biologically) in the stream system and is affiliated to a specific location in the watershed. In the following two examples shall highlight the above statements.

2 FROM MACRO TO PICO: INFLUENCE OF LAND USE ON THE AQUATIC COMMUNITY

In many regions worldwide, a severe change in land use can be observed. Forestor mixed cultivated areas disappear and more and more agricultural monoculture develops. Due to wind and rainfall, the open land is prone to high soil erosion and valuable fertile soil is washed out. Figure 1 shows exemplarily the forest cover change in Fako Division in Cameroon between 2010 and 1986. According to the presented data a severe loss of forest, mainly due to increased cocoa farming activities (85%; red colored areas) and plantation development for rubber and palm oil (11%; brown colored areas) occurred.

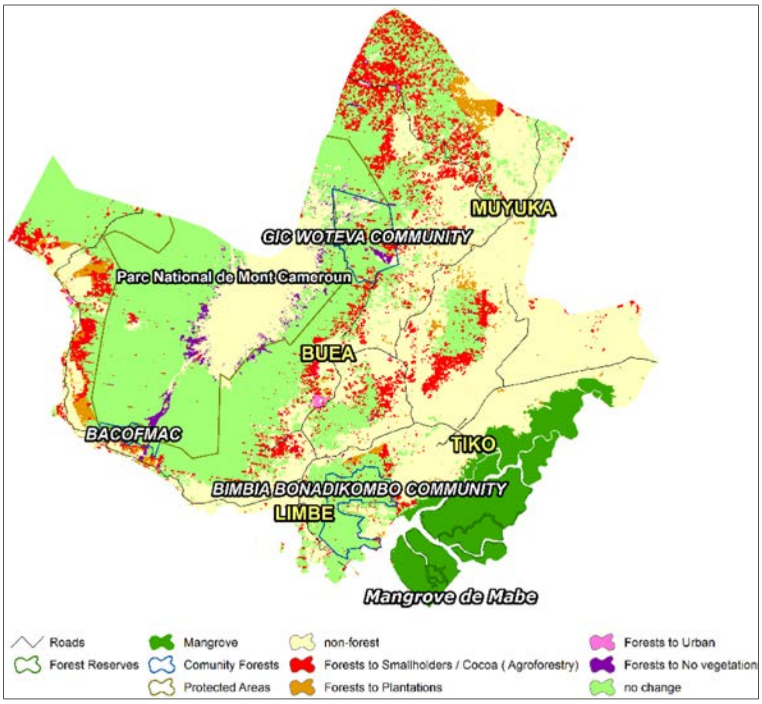

Figure 1. Forest cover change between 1986 and 2010 in Cameroon, Fako Division (Carodenuto et al., 2015).

The eroded fine particles are transported by wind and water and finally introduced into river systems. The fine sediments deposit on top of the river bed or even infiltrate into the river bed and clog the pores. The first one is called outer colmation, whereas the latter one refers to inner colmation (Schälchli, 1995). Essentially, colmation is a naturally occurring process. However, it can be intensified by anthropogenic activities such as agricultural land use (Schälchli, 1995). The deposited fine sediments reduce the pore space which results in a reduction of living space for spawn, juvenile fish and macro invertebrates (Figure 2). The decline of hydraulic conductivity results in a limited exchange of oxygen rich surface water with the hyporheic zone (Sear et al. 2008; Lisle 1989).

Figure 2. Exemplary images of different degrees and forms of outer colmation (picture: IWS, University Stuttgart).

Land erosion models can give an overview of the amount of lost soil and support the evaluation of the ecological status of river systems. The model results for a region in the South of Germany are shown in Figure 3 (Wieprecht et al. 2014).

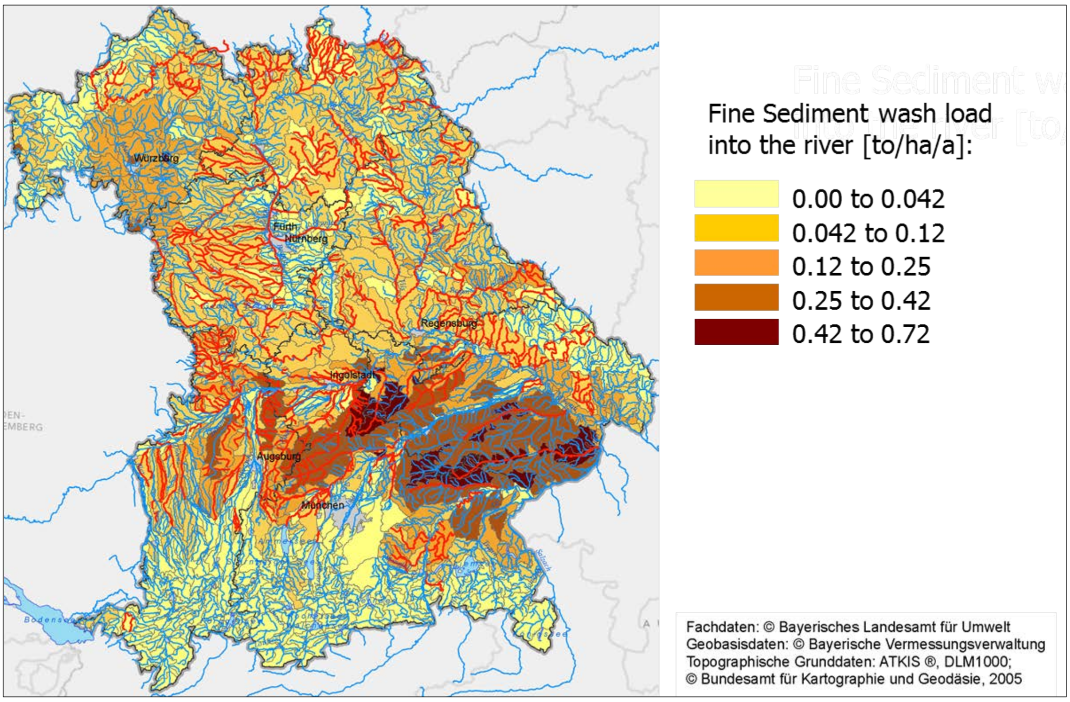

Figure 3. Results from land erosion model of wash load intrusion (MONERIS) into rivers in South Germany (Wieprecht et al., 2014, data and map see:http://www.umweltatlas.bayern.de).

Information about the existing degree of colmation in this region is provided through the characterization of the physiography of the river systems which is carried out during the biological monitoring of macrozoobenthos. The river bed composition is classified at the existing survey stations and they are considered as representative for the river system. The classification follows the parameter “loose”, “little colmation”, “heavy colmation”, “cemented”, and “muddy”. The data of field sampling (Figure 4) shows a clear relation with the results from the land erosion model. Especially the high sediment intrusion, given in the Danube catchment, results in rivers and river sections with heavy colmation, up to cemented or muddy conditions.

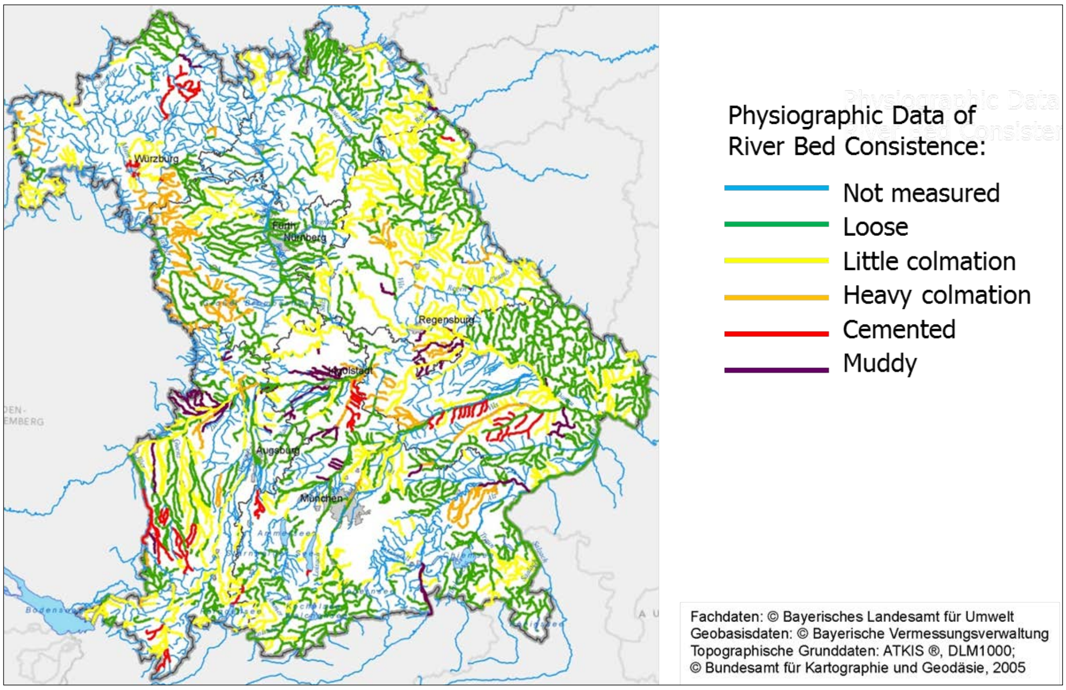

Figure 4. River bed composition of rivers in South Germany based on physiographic field data (Wieprecht et al., 2014, data and map see: http://www.umweltatlas.bayern.de).

Figure 5 refers to the general degradation of macrozoobenthos in the same region and serves as an indicator for its ecological status. It defines the relation of the (natural) reference situation of a river section compared to the actual situation. Of specific interest here, is the number of species individuals and the species assemblage. Obviously, a coincidence of the areas and sections with high wash load (Figure 3), a high colmation degree (Figure 4) and unsatisfactory to poor ecological conditions (Figure 5) can be observed.

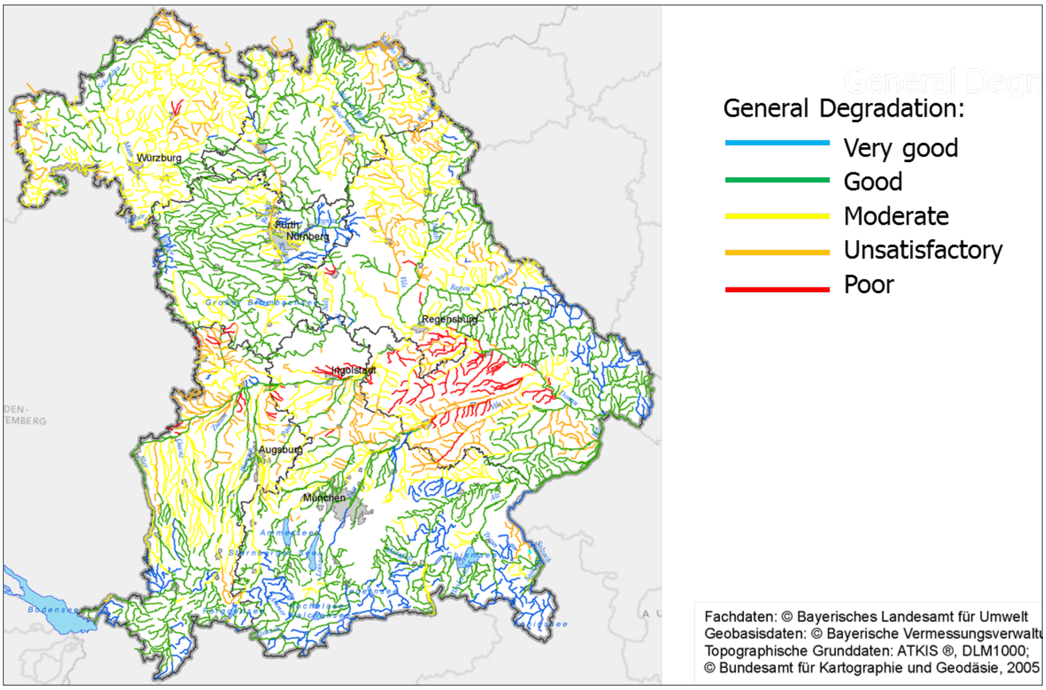

Figure 5. General degradation of rivers in South Germany based on macrozoobenthos data (Wieprecht et al., 2014, data and map see: http://www.umweltatlas.bayern.de).

3 MESO AND MICRO: PREDICTION OF STRUCTURAL AND ECOLOGICAL CHANGES ON A LONGTERM

Anthropogenic interventions on rivers, like river straightening or a fixation of the river bed, disturb their typical morphodynamic behavior and prevent the formation of natural alluvial forms. Ongoing river bed erosion often occurs as a result together with a strong negative ecological influence on the waterbody. The given example of the river Iller has in total 32 hydraulic structures on a total length of 56.6 km with an observed ongoing tendency of river bed degradation. For the benefit of a reduction of the erosion together with an ecological improvement, river training measures shall be realized. Here, the implementation of revetments in combination with a river bed widening was chosen and their applicability on river bed stabilization shall be investigated. For ecological reasons, only a minimum number of revetments shall be applied. However, the aim of a potential equilibrium stage of the river bed shall be reached and has highest priority, while the water level during mean flow conditions has to be kept at the same level. In addition to the implementation of revetments, areas were defined, where the actual river bank fixation shall be removed which allowed the river Iller to supply itself with sediments from the river banks. Figure 6 and Table 1 provide an overview of the location and dimensions of the suggested revetments as well as the widening sections.

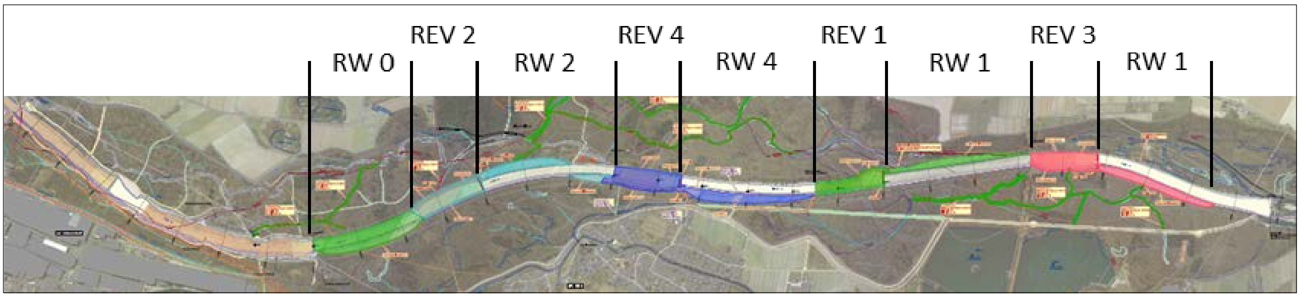

FIGURE 6. Overview of the study site including locations of revetments and river widening sections, Wieprecht et al. (2016).

Table 1. Overview of the location and length of the revetments and corresponding river widening.

Description	abbr.	Location between [km]	
River widening 0	RW 0	13.60	13.10
Revetment 2	REV 2	13.10	12.80
River widening 2	RW 2	12.80	12.20
Revetment 4	REV 4	12.20	11.90
River widening 4	RW 4	11.90	11.30
Revetment 1	REV 1	11.30	11.00
River widening 1	RW 1	11.00	10.35
Revetment 3	REV 3	10.35	10.05
River widening 3	RW 3	10.05	9.50

A coupled 1d-2d numerical model for a simulation period of 50 years was applied to show potential morphological changes. Multiple grain sizes and a multi-layer concept were applied to take into account the natural grain size distribution as well as bed armoring effects.

Finally, a habitat quality simulation was performed with the fuzzy logic model CASiMiR (Schneider, 2001). The model evaluates the quality of physical habitats for all three life stages of the predominant species of grayling (Thymallus thymallus) based on rules and preferences formulated by fish biologists.

Firstly, the status quo was investigated with a 50 year simulation of the morphological development (Figure 7). It reveals that the actual existing stabilization which measures between km 14.6 – 13.6 (upper section) and km 11.4 – 11.0 (middle section) considerably contributes to mitigating the erosion tendencies. Nevertheless, between the two structures and especially locally behind them, severe erosion is predicted with a magnitude of up to 2 m. The revetment at km 11.4 would act as a new pivot point, where the slope upstream can be expected to reduce from 0.16 % to 0.07 % (Figure 7). The chronological sequence of the simulation results indicates that most of the erosion will appear in the first 30 years. As a result of the ongoing river bed degradation, the simulated water level after the prognosis period of 50 years can be expected to be severely lower than the actual water level for a mean annual flow. These results prove once again the necessity of additional river stabilization measures in the remaining section.

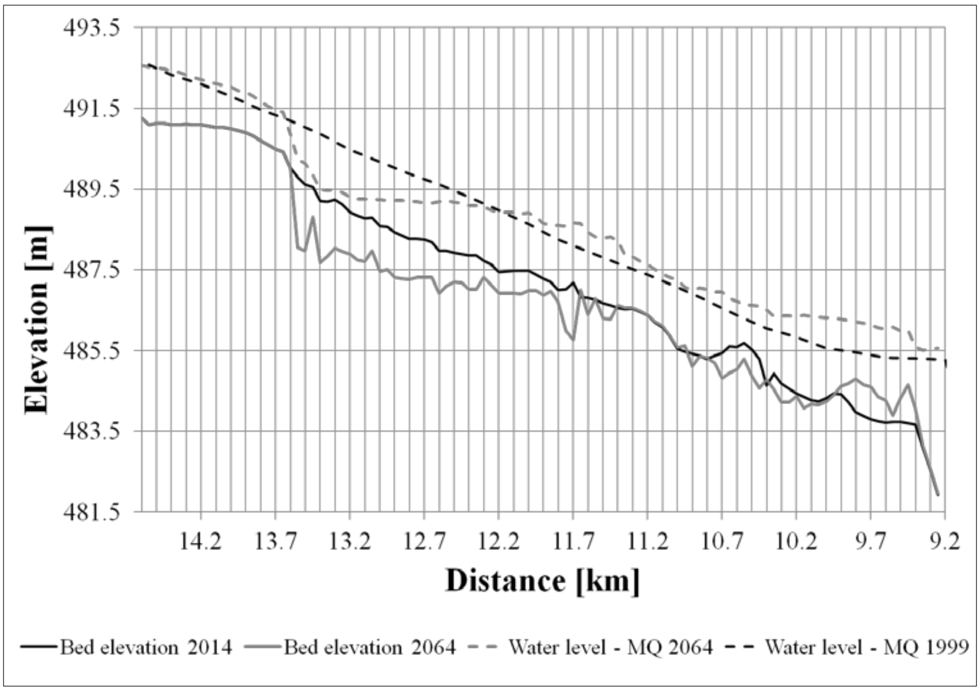

Figure 7. Bed level evolution and corresponding water level for MQ (Status Quo and 50 years prognosis), Wieprecht et al. (2016).

In total, six scenarios were set up and compared to the status-quo simulation in order to evaluate the effects and the necessity of the individual training structures in combination with a river bed widening and to formulate recommendations on their dimensions. The scenario simulations, indicated that all scenarios (2-4 revetments) have positive effects on the river bed stabilization. However, the erosion tendency decreased only in the vicinity of revetments and in the widened sections. Four revetments together with the river bed widening are found out to be one option to completely avoid further erosion processes. Figure 8 represents exemplarily the results of two scenarios.

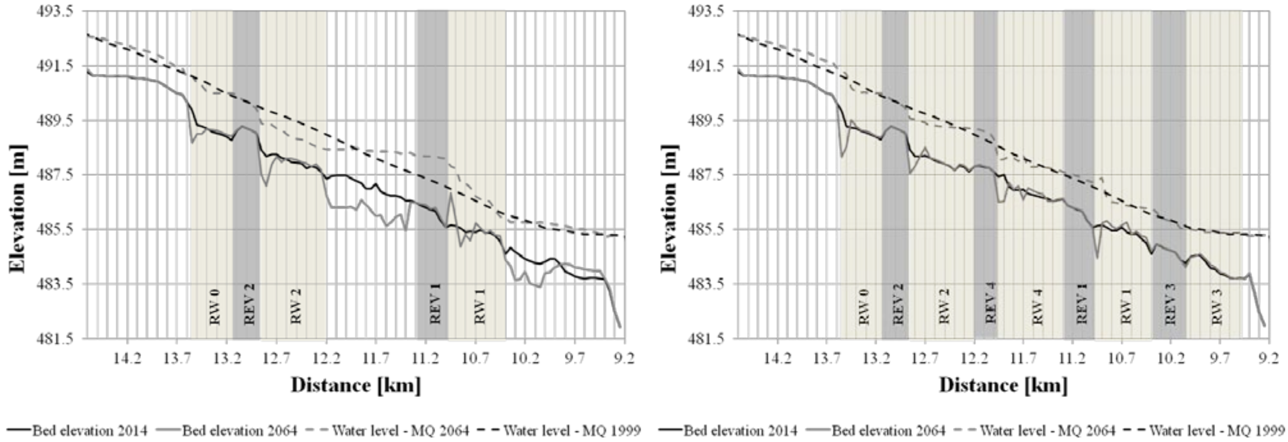

Figure 8. Bed level evolution and corresponding water level for MQ (Status Quo and 50 years prognosis) for two revetments and 20 m river widening (left) and for four revetments and 40 m river widening (right), Wieprecht et al. (2016).

Although the measures contribute to a stabilization effect of the river bed, the amount of bed load material available in the system is not sufficient for the formation of natural or at least nature-like morphologic structures, which are essential for the provision of good physical habitat conditions. The performed habitat quality study reflects the modest morphologic conditions and shows that the implementation of the planned river training structures result only in a slight increase of the habitat quality for the site-specific fish species of the grayling (Thymallus thymallus). Most profitable are the measures for adult species, while for juvenile fish an increase of areas with good and very good habitat quality can be predicted (due to reduced flow velocity, shallow water areas and finer sediment). For the youngsters, the spawning fish, only an increase of areas with mainly a medium quality (Suitability Index SI up to 0.5) can be achieved (Figure 9).

Figure 9. Results of the habitat modeling for adult (left), juvenile (center), and spawning (right) grayling for different scenarios. For each age stage, the physical habitat quality conditions for the status quo and the scenario of four revetments (initial state at the moment of completion and after 50 years of morphological simulation) are given. (SI = Habitat Suitability Index; 1 = best; 0 = worst), Wieprecht et al. (2016).

4 SUMMARY

Morphologic structures are one of the key parameters for a good ecological situation of rivers and streams. Their occurrence and forms are a result of the sensitive interaction between decisive parameters, such as hydrology (intensity of floods), hydraulic conditions (water depth, flow velocity, shear stress), sediment parameters (availability of material, bed load/suspended load transport, grain size distribution, sorting effects, erosion/deposition processes) and anthropogenic interventions (provision of space, fixation of river bed, narrowing activities, straightening, structures as dams, weirs, sills etc.). As the interplay of the mentioned drivers represents a fragile but well balanced meshwork, the alteration of only one factor can have a huge impact on the whole system. Hence, a shift in land use patterns in the catchment, representing the meso-scale, can be seen down to the composition of the grain size distribution in a river section (on the pico-scale) and negative ecological effects become noticeable.

Aiming at an improvement of the ecological situation, often changes in morphological structures are introduced. These measures shall on one hand stabilize our mostly straightened and thus eroding rivers and on the other hand shall ensure the increase of structural variability. In order to achieve the required effect, primarily large scale structures and a minimum dimension of self-dynamic development is essential. The example of the river Iller clearly proves, that measures such as revetments, glides or ramps serve as eco-friendly stabilization measures against erosion. However, the sustainable, ecologically positive impact (here verified via expected habitat quality for the adult, juvenile and spawning grayling) largely fails to appear.

REFERENCES

Ahmari, H. & Da Silva, A.M.F. (2011). Regions of Bars,Meandering and Braiding in Da Silva and Yalin's Plan. *Journal of Hydraulic Research*, 49(6), 718-727.

Carodenuto, S., Merger, E., Essomba, E., Panev, M., Pistorius, T. & Amougou, J. (2015). A Methodological Framework for Assessing Agents, Proximate Drivers and Underlying Causes of Deforestation: Field Test Results from Southern Cameroon. *Forests*, 6(1), 203-224.

Frissell, C.A., Liss, W.J., Warren, C.E. & Hurley, M.D. (1986). A Hierarchical Framework for Stream Habitat Classification: Viewing Streamsin a Watershed Context, *Environmental Management,* 10(2), 199-214.

Lisle, T.E. (1989). Sediment Transport and Resulting Deposition in Spawning Gravels, North Coastal California. *Water Resources Research,* 25(6), 1303–19.

Montgomery, D.R. & Buffington, J.M. (1997). Channel-reachmorphology in Mountain Drainage Basins. *Geological Society of America Bulletin* 109(5), 596-611.

Rosgen, D.L. (1994). A Classification of Natural Rivers. *CATENA* 22(3), 169-199.

Schälchli, U. (1995). Basic Equations for Siltation of Riverbeds. *Journal of Hydraulic Engineering*, 121(3), 274-287.

Schneider, M. (2001). Habitat–und Abflussmodellierung für Fließgewässer mit unscharfen Berechnungsansätzen. Dissertation, *Mitteilungen des Instituts für Wasserbau*, Heft 108, Universität Stuttgart, Eigenverlag. (In German)

Schumm, S.A. (1985). Patterns of Alluvial Rivers. *Annual Review of Earth and Planetary Sciences,* 13(1), 5-27.

Sear, D.S., Frostickl L.B., Rollingson, D. & Lisle, T.E. (2008). The Significance and Mechanics of Fine-Sediment Infiltration and Accumulation in Gravel Spawning Beds. *American Fisheries Society Symposium* 65.

Wieprecht, S., Haun, S., Seitz, L. & Kikillus, A. (2016) *Morphologische Studie Untere Iller (Morphological study of Lower Iller)*, Internal Report of Institute of Modelling Hydraulic and Environmental Systems, Universität Stuttgart (In German)

Wieprecht, S., Heinrich, T., Gruber, M. & Leo, F. (2014). *Rahmenkonzept Sedimentmanagement Bayern (Frame Concept for the sediment management in Bavaria)*, Internal Reportof Institute of Modelling Hydraulic and Environmental Systems, Universität Stuttgart (In German)

Yalin, S. and Da Silva, A.M.F. (2001). *Fluvial Processes*. IAHR Monograph, IAHRInternational Association of Hydraulic Engineering and Research, Delft, TheNetherlands.

Proceedings of the 37th IAHR World Congress
August 13 – 18, 2017, Kuala Lumpur, Malaysia

FLOOD MODELLING AND HAZARD ASSESSMENT FOR EXTREME EVENTS IN RIVERINE BASINS

ROGER FALCONER(1), JUNQIANG XIA(2), DONGFANG LIANG(3), & DAVOR KVOČKA(1)

(1)Hydro-environmental Research Centre, School of Engineering, Cardiff University, Cardiff, U.K.
(2) State Key Laboratory of Water Resources & Hydropower Engineering Science, Wuhan University, Wuhan, China.
(3)School of Engineering, University of Cambridge, Cambridge, U.K.
FalconerRA@cardiff.ac.uk, xiajq@whu.edu.cn, d.liang@eng.cam.ac.uk, Kvockad@cf.ac.uk

ABSTRACT

Extreme flood events, particularly in short steep river basins, are complex to model computationally and can cause: large loss of property, severe risk to people and debris (such as vehicles) to move and float, which in turn can significantly exacerbate the damage and extent of flooding. It is therefore desirable to be able to model as accurately as possible to predict peak elevations, inundation extent and velocities, and assess the degree of safety of people and vehicles during flash floods. In the paper, details are given to show the need for shock capturing algorithms for accurate modelling of flash floods, followed by new mechanics based formulae and experimental data to assess the flood hazard risk to people and vehicles during extreme flood events. For the mechanics based formulae and experimental data, empirical curves relating water depths and corresponding critical velocities for children and adults, developed supported by previous researchers, are used to assess the degree of people safety, and a new incipient velocity formula is used to evaluate the incipient velocity of vehicles. The developed model is applied to several real case studies of floods, including: Glasgow, Boscastle and Borth in the UK. According to the analysis of model predictions, the following conclusions have been obtained: (i) simulated results for the Glasgow flood show that children would be in danger of standing in the flooded streets in a small urban area; and (ii) simulations for the Boscastle flood indicate that vehicles in the car park would be flushed away by the high velocity flood, which indirectly testified to the predictive accuracy of the incipient formula for vehicles. Therefore, the developed integrated TVD model can be used to assess flood hazard risk to people and vehicles in flash floods, and these predictions can be used in flood risk management, particularly for the short steep river basins prevalent in many countries.

Keywords: Flood modeling; flood hazard; shock capturing; flash floods; river hydraulics.

1 INTRODUCTION

In recent years, there has been an increasing awareness of extreme flood events associated with climate change, urbanization, etc., particularly with regard to higher peak flows and their impact along steep river basins. Furthermore, recent flood events in the UK have led to a comprehensive government review of natural flood resilience (Defra, 2016), where the key findings provided by the Met Office have indicated uplifts in extreme rainfall intensity of between 20% and 30% for each of the six standard climatological regions of England and Wales over the next 20-30 years. These findings were based on climate impact modelling, together with an analysis of monthly rainfall records for the six regions. Extreme hydrological events commonly occur across parts of the world, particular for short steep river basins, leading to rivers flowing in the trans-critical hydraulic regime during high flood events, and where river banks are also often protected by levees (e.g. through the city of Cardiff), which can breach. The main difficulty in modeling such extreme flood events (including levee breeches), and trans/supercritical flows, is that conventional numerical models, such as the Alternating Direction Implicit scheme (Stelling et al., 1986), do not accurately model steep water level gradients and artificial damping needs to be introduced, either indirectly through the numerical scheme or through increased friction. To overcome this inaccuracy, the Hydro-environmental Research Centre (HRC) has been involved in developing an efficient shock capturing TVD (Total Variation Diminishing) numerical model, specifically focused on accurately predicting flood elevations and inundation extent for such events (Liang et al., 2006). The model has been refined and tested against a number of idealized cases. The model was then applied to the extreme flood event occurring at Boscastle, UK, in August 2004, where over 200mm of rainfall fell in 5hr (a 1 in 400 year event), causing extensive damage to property and infrastructure. The predicted water elevations along the centerline of the main channel were compared with observed data, with good agreement generally being obtained between both sets of results. More recently, this model study was extended and comparisons were undertaken for a range of schemes for this site, with the predicted peak flood elevations and inundation extent varying significantly for the various schemes considered (Kvocka et al., 2015).

The model was then extended to predict supercritical flow interactions in flood events with buildings. Simulations were first undertaken, both with and without buildings, on an idealized floodplain and downstream of a levee breech. The test simulations were repeated with the building being replaced by: (i) high roughness values, and (ii) treating the building as a porous media, with the porosity and permeability both being varied (Liang et al., 2007). It was found that when the Manning roughness coefficient was high, or when the hydraulic conductivity was low, then the downstream wake characteristics and the upstream and downstream water elevations were similar to those predicted by treating the building as a solid block. This approach was then tested for flood inundation of part of Glasgow, where the three methods of representing buildings were compared. The simulations showed that the porous media method was most flexible as part of the buildings could be occupied by water. This approach offers considerable potential opportunities for modelling a range of water quality parameters associated with flooding in buildings etc.

For the case of the Boscastle flood, as referred to above, one of the main factors exacerbating the increase in flood risk was the fact that over 100 cars were picked up by the flood from an upstream car park and transported downstream to the open sea. However, one car blocked a small bridge on the downstream side of the town, causing considerable blockage by debris and leading to a significant increase in the water elevations and flood risk upstream. This led to the HRC refining the model to assess the flood hazard risk to people and vehicles for extreme flood events, as typified by this flood event and many others occurring frequently in other parts of the world. In this model, empirical relationships between water depths and corresponding critical velocities for children and adults, developed by previous researchers (Foster and Cox, 1973; Abt et al., 1989; Keller and Mitsch, 1993; Lind et al., 2004; Ishigaki et al., 2005; Jonkman and Penning-Rowsell, 2008; and Russo et al. 2013), are used to assess the degree of people safety (Xia et al., 2014; and Kvocka et al. 2016), and new incipient velocity formulae are derived to evaluate the degree of vehicle safety for unidirectional flow and for various vehicles (Xia et al., 2011b). The developed model is then applied to two case studies, including: Glasgow and Boscastle in the UK. The analysis of model predictions shows that: (i) simulated results for the Glasgow flood highlight that children would be in danger of standing in the flooded streets in a small urban area; and (ii) simulations for the Boscastle flood indicate that vehicles in the car park would be flushed away by the high velocity flow, confirming the predictive accuracy of the incipient formula for vehicles.

2 MODEL DETAILS

The core numerical model used for predicting the governing flood hydrodynamic parameters (namely elevations, inundation extent and velocities) in the studies reported herein was based on the DIVAST–TVD model. This model is an extension of the original DIVAST (Depth Integrated Velocities and Solute Transport) model, which includes a shock capturing algorithm for maintaining sharp gradients – a feature particularly relevant for modelling flood propagation through short steep river basins. The DIVAST-TVD model combines a symmetric total variation diminishing (TVD) term with the standard MacCormack scheme. The MacCormack scheme is a numerical method ideally suited to solving the time-dependent Reynolds Averaged Navier-Stokes equations, and is a variation of the original Lax-Wendroff scheme. Full details of the original scheme are given in Liang et al. (2006),with the predictor-corrector scheme, defined as (Mingham et al., 2001):

Predictor step:
$$u_i^{\overline{n+1}} = u_i^n - a\frac{\Delta t}{\Delta x}(u_{i+1}^n - u_i^n) \quad [1]$$

Corrector step:
$$u_i^{n+1} = \frac{1}{2}\left[u_i^n + u_i^{\overline{n+1}} - a\frac{\Delta t}{\Delta x}\left(u_i^{\overline{n+1}} - u_{i-1}^{\overline{n+1}}\right)\right] \quad [2]$$

where u is a “provisional” variable value, *n* is the time level, *Δt* is the time step and *Δx* is the spatial step. The first step (the predictor step) calculates a rough approximation of the desired variable(s), whereas the second step (the corrector step) refines the initial approximation. Equation [1] shows that forward difference is employed in the predictor step, while Equation [2] shows that backward difference is employed in the corrector step.

The MacCormack scheme has second-ordered accuracy and, according to Godunov’s theorem (Godunov, 1959), all schemes of accuracy greater than one will generate spurious oscillations in the vicinity of large gradients. The common approach for resolving these discontinuities is the shock-capturing method. There are two key groups of shock-capturing schemes used in computational fluid dynamics. One group of schemes is based on the Godunov method, which solves the Riemann problems at the interfaces of grid cells, while the other group is based on an arithmetical combination method of the first- and second-order upwind schemes. The DIVAST-TVD model belongs to the second group and has proven to be a useful tool for analysing storm surges, dam-break flows, flash floods etc. that all involve rapid changes in the hydrodynamic conditions. Detailed information about model development, model structure, and extensive and quantitative verifications can be found in (Liang et al., 2006; 2007; 2010) with the model being used herein to solve the general 2-D depth integrated Shallow Water Equations (SWEs) for free surface flows, as given in Xia et al. (2010).

3 FLOOD MODELLING AND HAZARD ASSESSMENT APPLICATIONS

3.1 Introduction

Following development of the shock capturing model and the growing challenges of predicting the impact of extreme flood events, occurring in the UK with increasing frequency, the model was then applied to a number of site specific scenarios to investigate the accuracy and scope of the model. The model was first tested against a dyke break experimental study, undertaken at TU Delft. The model was then refined to include the porous media equation, to study flood seepage into buildings, with the model being extended to investigate flooding of an urban area in Glasgow, with the buildings replaced with a porosity parameter.

The model was also applied to a well monitored extreme flood event in Boscastle, UK, where one of the best recorded flood events occurred in 2004. For this case, the flooding was exacerbated due to a car being moved by the flood and then blocking a river bridge. This led to an appreciation of the lack of knowledge in understanding the incipient velocity of vehicles and a series of laboratory experiments were undertaken to establish the incipient velocity for a range of vehicles. This work has been subsequently extended to develop new formulae to represent the stability of a person (i.e. a child or adult) in flood waters and for both horizontal and sloping channel beds. The flood hazard formula was included in the original numerical model, together with a proposed and improved model for flood hazard risk assessment, with the mechanics based approach being compared to the accuracy of a widely used experimentally based formula. In the most recent study, comparisons have been made of the flood hazard assessment for the safety of people in an extreme flood passing through a small, but steep, river basin in Wales. These studies are briefly summarized below.

3.2 Dyke break experiment

In the first of a series of tests undertaken to investigate the effect of including shock capturing in the two-dimensional DIVAST model, comparisons were undertaken of the predictions both with and without shock capturing. In the first instance, simulations were undertaken and compared for DIVAST-ADI and DIVAST-TVD for a sudden dam break failure, for a retention level in the reservoir of 10 m and with a downstream elevation of 5 m. The model simulations were undertaken with a viscosity of $10^{-6}m^2$/sand with the corresponding simulations showing extreme non-physical oscillations for the ADI scheme, whereas the TVD algorithm gave smooth solutions for the domain extent downstream.

In the second dam break study, simulations were undertaken of an experimental set-up studied in the Fluid Mechanics Laboratory, at Delft University of Technology. The experiment was carried out in a flume, hence all boundaries could be treated as reflective boundaries in the model. The flume had dimensions of 31.4 x 8 m, with a wall extending across the width of the flume, separating the headwater depth of 0.6 m and the tailwater depth of 0.05 m. A 0.4-m-wide sluice gate was located at the center of the separating wall, which was raised at a speed of 0.16 m/s. Since the sluice gate was opened slowly, special treatment of this process was required in the simulations (Liang et al., 2006). The Manning roughness coefficient was set to be $0.012m^{-1/3}s$ across the computational domain, which was the same as that used by other researches (Stelling and Zijlema, 2003). The grid size was 0.1 m and the time step was 0.02 s. Figure 1 shows the simulation of the propagating wave in the experimental flume and a comparison of the measured and predicted results at the end of the flume. The corresponding comparisons showed good agreement between the predicted and measured results, highlighting the accuracy of the model in predicting extreme (supercritical) flood flows,

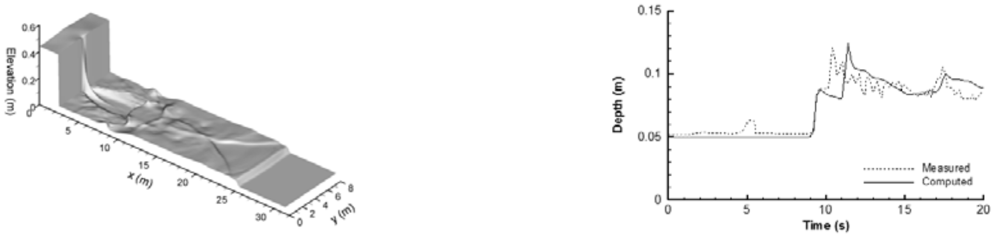

(a) Water surface prediction (b)Depth comparison downstream of gate

Figure 1. Dyke experiment simulations showing: (a) water surface predictions after 18 s and (b) comparisons between predicted and measured depths at 13 m downstream of gate.

3.3 Refined treatment of buildings

In modelling extreme flood events in urban areas, it is often desirable to evaluate the impact of buildings on flood elevation and inundation extent and hazard assessment, with such numerical model simulations

  / ISSN 1562-6865 (Online) - ISSN 1063-7710 (Print)

generally being undertaken by blocking out the buildings, i.e. by removing grid cells mapped onto buildings. However, this does not generally represent accurately the fluid flow processes involved as flood water can penetrate into a building – particularly commercial buildings, such as supermarkets –and it is therefore, more realistic to treat a building as a porous structure. In progressing such a concept studies, the model was refined to include the Darcy porous media flow equation, instead of the Navier Stokes equations, where buildings were sited. This meant replacing the buildings with either an increased roughness parameter or a hydraulic conductivity parameter.

In considering this concept, a symmetric dam-break case was considered in an idealised channel (Liang et al., 2007). The basin consisted of a 200 m wide and 400 m long flat-bed channel, bounded by solid walls and with a dam separating a reservoir from the floodplain. A square building with the side length of 10 m was located in the middle of the domain. Initially, the water depth in the reservoir was 2 m and the floodplain was dry. A 20 m wide breach was simulated in the middle of the dam, while the other parts of the dam remained intact. The interaction of the flood wave with the building was studied after the breach, both with the building included and with the building replaced by the Darcy equation and appropriate hydraulic conductivity parameters. The Manning's roughness value was taken to be 0.011 $m^{-1/3}s$ across the domain and the grid size and time step were 2 m and 0.2 s, respectively. A typical set of results are shown in Figure 2. With a calibrated and low value for the hydraulic conductivity, i.e. typically K = 1 m/s, the results have confirmed that flooding around the building was accurately simulated in comparison to treating the building as a solid object. This concept was subsequently applied to predict the flood elevations, inundation extent and hazard assessment for an urban area in Glasgow, U.K. The results proved to be accurate compared to including the buildings as solid blocks and further research is currently in hand to study pollutant seepage into buildings and using this approach.

(a) Water surface prediction (b) Depth comparisons downstream

Figure 2. Dam break failure simulations with the building modelled as a porous media, showing: (a) water surface predictions after the breach and (b) time changes in elevation for various hydraulic conductivities.

3.4 Boscastle flood event

To investigate further the capabilities of the model in predicting extreme flood events, efforts were then made to predict the propagation of an extreme flood, which occurred in August 2004, and which had a devastating impact on the village of Boscastle, U.K. The coastal village of Boscastle has a short river basin, with steep valleys and catchments, as shown in Figure 3. The river basin and village are particularly vulnerable to localized high rainfall events and flash flooding. Rainfall is efficiently channeled from the surrounding moors into a series of streams, where the flow then propagates rapidly to the nearby sea, through the River Valency.

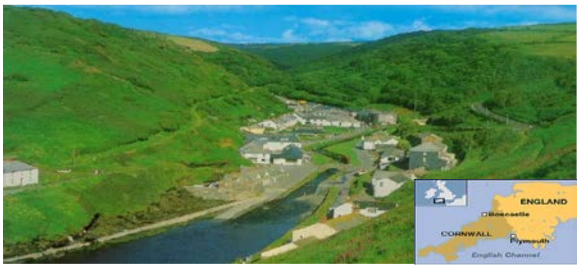

Figure 3. Aerial photo of Boscastle, showing the steep characteristics of the river basin.

The particular extreme flood event that occurred in 2004 was caused by the combination of heavy rain, saturation of the soil due to the previous two weeks receiving well above average rainfall, and the steep nature of the river basin and catchments. Over 200 mm of rainfall fell in a period of approximately 5 hours, resulting in a 1 in 400 year flood event. The total peak discharge of the flood was estimated to be 180 m^3/s (Roca and Davison, 2010). The Boscastle flood is one of the best recorded extreme flood events in the UK in recent years. The local Environment Agency reported that millions of pounds of damage resulted from the flood and about 116 vehicles were picked up in a car park just upstream of the village and washed away to sea. During this flood event, some vehicles and other large-size debris were caught under a local bridge, blocking the main flow passage and finally causing the bridge to collapse. Based on the above examples, it can be concluded that flash floods often lead to serious loss of human life and loss of vehicles, especially in densely populated urban areas. Therefore, it was clear from this flood that it is desirable to be able to predict accurately the peak flood wave elevations, the maximum inundation extent and the degree of safety to people and the risk of vehicles being picked up and moved by the flood. To investigate these effects further, in a series of numerical model simulations, the most recent study involved predicting and comparing the elevations and flood inundation extent with measured wrack marks and field observations for three different types of models.

The Boscastle flash flood was therefore simulated using three different flood prediction model structures, including: (i) the shock-capturing flood model (i.e. the TVD case), (ii) the regular ADI-type flood model (i.e. the ADI case), and (iii) the regular ADI-type flood model with no inertia terms (i.e. referred to as the NI case). All three models were compared for the same set of boundary conditions and comparisons were made with wrack marks and field observations. The model extended through the village and started at the upstream end of the River Valency, which enters the study domain from the east. The eastern boundary of the domain was set as an inflow boundary for the River Valency, i.e. the peak discharge value was specified as the upstream boundary. The downstream boundary was set to mean sea level, where the River Valency is governed by the tides in the coastal region. According to Wallingford (2005), the actual tide level at the peak of the flood was approximately 0.8 m AOD, whereas the highest tide level of around 3.5 m AOD was measured approximately one hour after the peak of the flood had passed through the domain. Neither the actual tide level at the peak of the flood, nor the high tide level, had any effect on the actual flood levels in the center of the village (Wallingford, 2005), therefore it was not deemed necessary to include a time varying tide in the model. Thus, the prescribed water level, which was fixed during the numerical simulations for all three models, was specified as the downstream boundary. The resulting predictions of the predicted and observed water elevations and wrack marks are shown in Figure 4, with the corresponding flood inundation extents shown in Figure 5.

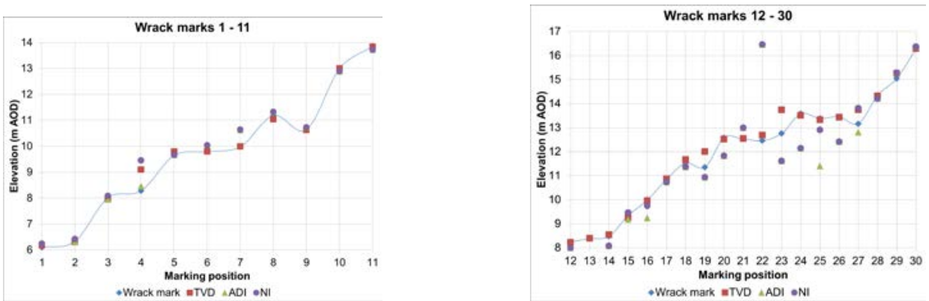

(a) Western side of flood path (b) Eastern side of flood path

Figure 4. Comparison of predicted and observed wrack elevations for the TVD, ADI and NI models, for wrack marks on the: (a) western side and (b) eastern side of the flood pathway.

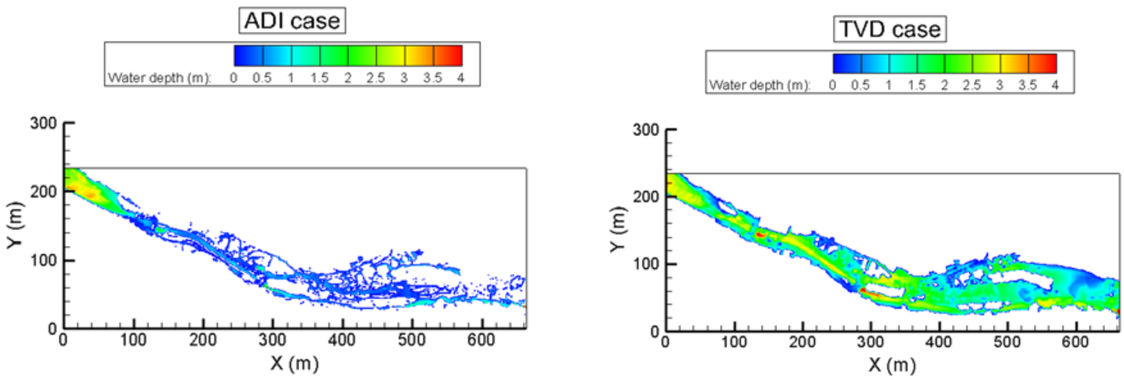

Figure 5. Predicted maximum water depths for ADI and TVD simulation cases, respectively.

From Figure 4, it can be seen that results for the TVD simulation case generally fitted the post-flood surveyed wrack marks better than either of the other two models. At marking positions 4 and 27, the TVD simulation case slightly over-predicted the flood levels, but according to the comments made by observers the maximum flood levels at these marked positions were thought to be higher than those recorded, which would be consistent with the TVD predictions. The results also showed that the ADI and NI simulation cases generally under and overpredicted the peak flood levels, respectively. The inaccuracy in the ADI approach was as expected, since as discussed previously this scheme leads to the generation of spurious numerical oscillations for such numerical schemes, and with the oscillations being particularly pronounced where sharp gradients exist in the true solution (Liang et al., 2007). Hence, it can be concluded for such a case study then the ADI simulation results are numerically inaccurate and can lead to erroneous flood inundation maps.

With regard to the inaccuracy in the NI simulation case, this result was as expected, since the diffusion wave concept is too basic for simulating extreme flood events. The inertia terms can be neglected without any major influence on the predicted water levels if the Froude number is well below 0.5, whereas at flows with higher Froude numbers then discontinuities and errors frequently start to appear. Hence, overall and based on a statistical analysis of the comparisons, the TVD simulation case results were found to reproduce the wrack marks most accurately than the other schemes considered (Kvocka et al., 2015).

The difference between the simulation results becomes more pronounced when the water depths and flood inundation extents were compared for all three test cases. Figure 5 illustrates a comparison of the results for the ADI and TVD schemes only, with the predicted depths being compared in meters. These comparisons show significant differences in the spatial variation of the depths and with the TVD case more accurately predicting the flood depths than either the ADI or the NI simulation cases. As stated previously, ADI-type models inaccurately predict the main hydrodynamic parameters for such trans-critical flows, due to the fierce spurious numerical oscillations predicted for such flood events as Boscastle. These results again confirm the initial findings, in that ADI-type models are inappropriate for simulating flash flood scenarios and where the local Froude number exceeds about 0.5.

3.5 Flood hazard assessment for vehicles and people

Following the Boscastle flood studies, outlined above, and the exacerbation of the impacts of the 2004 flood due to cars being picked up by the floodwaters and then causing a key bridge to become blocked, experimental and numerical model studies were undertaken to investigate the characteristics of the incipient velocity for a range of typical vehicles, followed by a similar analysis and experimental studies on model people.

Existing studies on the stability criteria of vehicles in floodwaters are limited. Gordon and Stone, (1973) investigated the stability of a Morris Mini car with the two back wheels being locked to prevent any movement. The vehicle stability condition was obtained when the horizontal force was just balanced by the product of the measured vertical reaction force and the coefficient of friction. In this approach, it was important to estimate the appropriate value of the friction coefficient for sliding. Gordon and Stone, (1973) indicated that the friction coefficient ranges from 0.3 to 1.0. Keller and Mitsch, (1993) conducted a theoretical investigation into the stability conditions for idealized cars, and developed a simple method for estimating the forces exerted on a stationary vehicle in floodwaters and an incipient velocity formula for a partially submerged vehicle. In the latest report by Shand et al. (2010), existing guidelines and recommendations for the limits of vehicle stability were compared with experimental and analytical results, with a marked difference being obtained between these two sets of results. Therefore, interim criteria for stationary vehicle stability were proposed for three vehicle classes, including small passenger and large passenger vehicles, as well as 4WD (four-wheel drive) vehicles. More recently, Martínez-Gomariz et al. (2016) published a review of the key studies relating to the stability criteria for flooded vehicles.

In the initial phase of an on-going study, different forces acting on partially submerged vehicles were analyzed, with a simplified version of the equation for these forces being given as:

$$U_c = \alpha \left(\frac{h_f}{h_c}\right)^{\beta} \sqrt{2gl_c \frac{\rho_c}{\rho_f}\frac{h_c}{h_f} - R_f} \quad [3]$$

where l_c =vehicle length; $R_f = h_c\rho_c/(h_k\rho_f)$ in which h_k= critical water depth at which the vehicle starts to float. The values of α and β are related to the shape of a vehicle, the tyre type and the roughness of the road surface, which are determined in this study by the experimental studies using die-cast model vehicles in a flume. A key assumption made in this analysis was that the inside space of a prototype vehicle would not be filled quickly by floodwaters and the vehicle would start to float when the outside water depth exceeded a specified depth. Approximately 100 runs of flume experiments were conducted to obtain a series of empirical relationships between water depth and the fluid velocity when the vehicle was at the threshold of instability. Three 1:18 scale die-cast typical model vehicles were considered, with the incipient velocities for partially submerged prototype vehicles in floodwaters then being estimated using two different approaches, including the predictions obtained from the model scale ratios and computations, based on the derived formula. Also, since these model experiments followed the principles of geometric, kinematic and dynamic similarity, the incipient velocity obtained under a specified water depth for a model vehicle could be directly used to estimate the critical conditions for the corresponding prototype vehicle according to the scale ratios. A typical vehicle in the flume, together with a corresponding relationship between the mean velocity and flume depth is given in Figure 6 (Xia et al., 2011b).

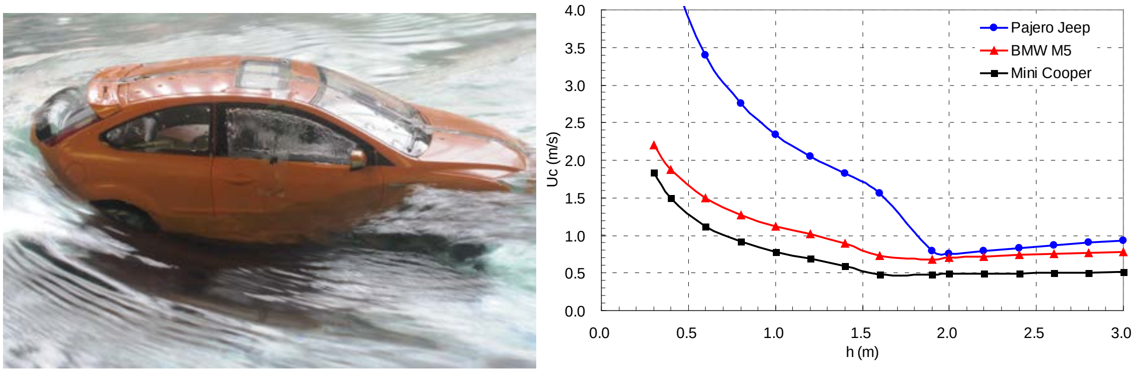

Figure 6. Partially submerged model car in a flume and incipient velocity relationships for three vehicles.

In a similar manner, the safety of people in floodwaters was investigated both by undertaking experiments on geometrically scaled models, and by developing mechanics based formulae for the stability of people relating to both the mechanisms of sliding and toppling. In the development of a mechanics based formula for toppling, the moment on a person standing in floodwaters was considered, including the forces of buoyancy, drag, gravity, and normal reaction (Chanson, 2004; Xia et al., 2014). A new revised formula also takes into account the effect of a non-uniform upstream velocity profile on the stability of a person standing in a floodwater, and also considers the impact of the body buoyancy for rapidly varying water depths. The corresponding equation for toppling is given as:

$$U_c = \alpha \left(\frac{h_f}{h_p}\right)^{\beta} \sqrt{\frac{m_p}{\rho_f h_f^2} - \left(\frac{a_1}{h_p^2} + \frac{b_1}{h_f h_p}\right)(a_2 m_p + b_2)} \qquad [4]$$

where U_c is the incipient velocity, h_f is the water depth (m), h_p is the height of a person (m), m_p is the weight of a person (kg), ρ_f is the density of water (kg/m^3), α and β are empirical coefficients and a_1, a_2, b_1 and b_2 are coefficients based on the characteristics of a human body. Further details on these parameters are given in Xia et al. (2014).

Finally, the degree of flood hazard assessment for each instability mechanism can be quantified with the following expression:

$$HR = MIN\left(1, \frac{U}{U_c}\right) \qquad [5]$$

where HR is the flood hazard rating, U is the velocity of the flow and U_c is the incipient velocity, e.g. the velocity at which a person loses stability in floodwater. The main difference between the majority of empirically derived flood hazard formulae (Ramsbottom et al., 2003; Ramsbottom et al., 2006) and this mechanics based and experimentally calibrated method is in the way the formulation takes into account the forces induced by the flow conditions. In Equation [4], it can be seen that the incipient velocity and the overturning force on the body are proportional to the water depth times the velocity squared (i.e. hv^2), whereas for the empirically based formula, widely used by regulatory authorities, the overturning force on the body is proportional to the water depth times the velocity only (i.e. hv). This means that the mechanics based and experimentally calibrated method is much more variable for higher velocities and momentum, with such conditions frequently occurring for extreme flood events. This being the case, the mechanics based method is highly adaptable to abrupt changes in the flow regime and can rapidly and more accurately assess the degree of flood hazard in a short time period, a characteristic which is particularly important for flood hazard assessment of extreme flood events.

The refined numerical model was then applied to a number of real case studies to assess the flood hazard risk to vehicle mobility and people, including for example: (i) an urban conurbation in Glasgow, U.K., (ii) the Boscastle flood of 2004, and (iii) the Malpasset dam failure in France. According to the model predictions, the following conclusions were drawn from these studies: (i) the model results for the Glasgow flood showed that children would be in danger of standing in the flooded streets in the region; (ii) for the Boscastle flood, the model results predicted that all vehicles in the village car park would be picked up and transported by the flood (as occurred), and which indirectly testified to the predictive accuracy of the incipient velocity formulae for vehicles; and (iii) for the Malpasset dam failure flood model the results showed that the adopted method for the assessment of people safety was applicable, and some local people living below the dam would have been swept away, which corresponded well with the report of casualties. Therefore, the enhanced model can be used to evaluate the flood hazard degree of safety prediction for vehicles and people in flash floods and these predictions can be used with some degree of confidence in flood risk management.

An example of these study simulations is given for urban flooding in part of Glasgow, U.K. The study domain comprised a rectangular area, 1.0 km by 0.4 km, with dense urban development either side of two main streets and a topologically complex network of minor roads. Flooding in this area was caused partly by a small stream that enters near the northeast corner of the domain and almost immediately enters a culvert that runs under the entire site. Flooding has been observed to occur here as a result of the discharge exceeding the capacity of the culvert and spilling into the street network. The stream responds very rapidly to heavy rainfall, with typical flood events being less than 1 hour duration. In this case study, the domain and flow conditions adopted were the same as those reported in Hunter et al. (2008). The domain was divided into about 48,000 equilateral triangular cells. The western boundary of the domain was specified as a free outflow boundary, and the south and north edges were specified as closed boundaries. The open boundary, with an assumed discharge hydrograph, was located near the northeast corner. A constant time step of 0.1 s and a constant Manning's roughness of 0.020 $m^{-1/3}s$ were used in the simulations. In addition, all the buildings of the city were treated as solid blocks, through which no flow could pass.

Simulations were undertaken to predict the maximum flood hazard risk for a range of different vehicles and people groups, including typical children and adults. The results are shown in Figure 7 where it can be seen that a Pajero Jeep vehicle parking at any location would be safe, while a Mini Cooper would slide in the zone near the inflow boundary. According to results for children and adults, the predictions indicate that children would be in danger if standing in the two main streets, while adults would be safe across most of the domain, with the exception of being near the inflow location. In addition, temporal variations of hazard degree for people and vehicles at different points across the domain are given in Xia et al. (2011a). These results identify a zone of shallow, high-velocity flow, in the middle of a road section that receives water from a single direction (east) and over which the complete flood wave passes during the simulation period, while further downstream an area of permanent ponding is identified at the end of the simulation period. Further simulations showed that whilst the flooding period just lasted about 20 minutes, it would lead to danger for a child standing near the inflow location, due to a high velocity of greater than 1.2 m/s and a shallow depth of less than 0.2 m. Further into the domain, a child standing in the floodwaters would be in danger due to the relatively large water depth towards the end of the simulation period. It can therefore be concluded from these simulations that flash floods occurring in this small urban area could cause significant risk to children standing in the streets, but vehicles parked on the streets would be safe over most of the study domain. Therefore, child safety during a flash flood occurring in such a small urban area needs to be emphasised, particularly in the context of flood risk management.

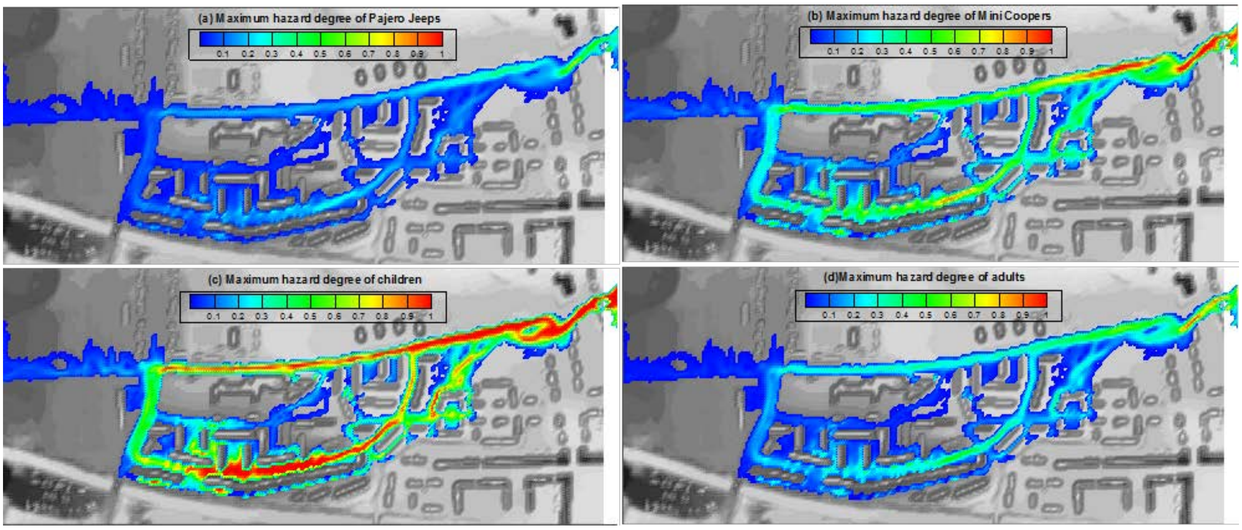

Figure 7. Distribution of maximum flood hazard risk for: (a) a Pajero Jeep (top left), (b) a Mini Cooper (top right), (c) a child (bottom left), and (d) an adult (bottom right).

More recent research studies, currently under publication review, have been undertaken to investigate the threshold value of the bed slope to establish when it is desirable to include a shock capturing algorithm and under what conditions for the stability of people in floods, a mechanics based flood hazard formula (i.e. a function of: depth x mean velocity^2) becomes more accurate, giving significantly different results from an empirically based formula (i.e. a function of: depth x velocity). These two different flood hazard assessment criteria were used to predict flood hazard indices for two different test cases, i.e. a flood wave propagating along an idealized river basin, and a flash flood event in a short and steep river basin in Wales, UK. The corresponding results obtained suggest that for river basins with a bed slope greater than approximately 1% (i.e. flashy river basins or catchments), then the flood hazard indices should be predicted using the mechanics based criteria, which include the hydrodynamic forces associated with the flow. The findings of this more recent research are consistent with the findings of Chanson et al. (2014), in that the instability thresholds for real-life flood situations should be much lower than the instability thresholds based on the criteria derived from empirical data.

4 CONCLUSIONS

In this paper, the authors have examined the type of flood hydrodynamic models and hazard assessment tools that are commonly used for predicting flood inundation extent and hazard risk assessment for rivers where flash flooding frequently occurs. A shock capturing algorithm is first developed and compared to simulations using a traditional ADI scheme and a non-inertia kinematic model. This is applied to the well-publicized 2004 Boscastle flood in the U.K. with the results showing that the TVD shock capturing model gives closer predictions of the water elevations, in comparison with observed and recorded wrack marks. More recently, studies have shown that for an idealized test channel, the shock capturing algorithm gives stable and accurate results when the bed slope exceeds about 1% and when the ADI scheme begins to exhibit numerical instabilities. The shock capturing model is also extended to include a porous media groundwater algorithm and studies are undertaken to compare the prediction of the flood wave passing a building from a dam break failure. The results show that with an appropriate hydraulic conductivity value, the removal of building could be removed and treated as a porous media, with this approach enabling accurate predictions to be made of the free surface. This approach offers considerable scope for planning a city, or city region, and furthermore offers scope for predicting pollutant transport fluxes into semi-permeable buildings.

Two flood hazard risk assessment methodologies are then studied for a range of scenarios. In the first instance, a mechanics based formula is developed for the incipient velocity of vehicles in floods, and the sliding and toppling of people, including adults and children. These mechanics based formulae are supported with experimental studies to establish typical values for a range of empirical parameters, such as the shape of the vehicle and human body etc. In the second instance, a widely used empirical formula is considered, where the hazard risk parameter is a function of the depth x velocity, as compared to the mechanics based formula, which is a function of the depth x velocity^2. The results from a comparison of these two formulae for a range of sites suggest that in urban areas, where flash flooding can be common place, then the flood hazard risk assessment should be based on using a mechanics based approach. Although the differences between both formulae are found to be relatively small for low Froude number flows, it is also observed that when the Froude number exceeds about 0.5, then the hazard risk assessment across the floodplains etc. is considerably different and particularly as the Froude number is increased further.

Finally, the studies have shown the need to improve our knowledge and modelling capabilities of flash flooding processes and flood hazard assessment in areas prone to extreme flood events, or for high Froude number flows. Also, more could be done on raising the awareness of the importance of using appropriate flood hazard assessment models, particularly by developing a more unified approach and with the flood hazard assessment being based on a more rigorous mechanics based analysis.

ACKNOWLEDGEMENTS

The research reported herein is funded through a number of research contracts, including: the UK Engineering and Physical Sciences Research Council (EPSRC), particularly the Flood Risk Management Research Consortium, the Royal Academy of Engineering, the EPSRC Water Informatics: Science and Engineering Centre for Doctoral Training, two EPSRC Impact Acceleration grants, High Performance Computing (HPC) Wales, Fujitsu, the European Regional Development Fund. The bathymetric and flow data for many of the site specific studies are provided by the Environment Agency, Natural Resources Wales and HR Wallingford.

The authors are also grateful for the support and input from a number of colleagues and past research students, including, in particular: Prof Binliang Lin, Dr Reza Ahmadian, Dr Fang Yenn Teo and Dr Brian Boye.

REFERENCES

Abt, S.R., Wittler, R.J., Taylor, A. & Love, D.J. (1989). Human Stability in a High Flood Hazard Zone. AWRA *Water Resources Bulletin,* 25(4), 881-890.

Chanson, H. (2004). *The Hydraulics of Open Channel Flow: An Introduction*. Elsevier Butterworth-Heinemann, Oxford, UK.

Chanson, H., Brown, R. & McIntosh, D. (2014). Human Body Stability in Floodwaters: The 2011 Flood in Brisbane CBD. *Proceedings of 5th International Symposium on Hydraulic Structures: Engineering Challenges and Extremes.* Brisbane, Australia.

Department of Energy, Food and Rural Affairs, (Defra). (2016). National Flood Resilience Review. https://www.gov.uk/government/publications/national-flood-resilience-review

Foster, D.N. & Cox, R.J. (1973). *Stability of Children on Roads used as Floodways,* Report of Water Research Laboratory, Australia.

Godunov, S. (1959). A Difference Scheme for Numerical Solution of Discontinuous Solution of Hydrodynamic Equations. *Matematicheskii Sbornik,* 47**,** 271–306.

Gordon, A.D. & Stone, P.B. (1973). *Car Stability on Road Floodways,* the University of New South Wales, Water Research Laboratory, Technical Report 73/12.

Hunter, N.M., Bates, P.D., Neelz, S., Pender, G., Villanueva, I., Wright, N.G., Liang, D., Falconer, R.A., Lin, B., Waller, S., Crossley, A.J. & Mason, D. (2008). Benchmarking 2D Hydraulic Models for Urban Flood Simulations. *Proceedings of the Institution of Civil Engineers, Water Management*, 161(1), 13-30.

Ishigaki, T., Baba, Y., Toda, K. & Inoue, K. (2005). Experimental Study on Evacuation from Underground Space in Urban Flood. *Proceedings of 31st IAHR Congress,* Seoul, 1116-1123.

Jonkman, S.N. & Penning-Rowsell, E. (2008). Human Instability in Flood Flows. *Journal of the American Water Resources Association,* 44(5), 1208-1218.

Keller, R.J. & Mitsch, B. (1993). *Safety Aspects of Design Roadways as Floodways: Urban Water Research Association of Australia. Melbourne, Australia,* Research Report No. 69.

Kvocka, D., Falconer, R.A. & Bray, M. (2015). Appropriate Model Use for Predicting Elevations and Inundation Extent for Extreme Flood Events. *Natural Hazards*. 79(3), 1791-1808.

Kvocka, D., Falconer, R.A. & Bray, M. (2016). Flood Hazard Assessment for Extreme Flood Events. *Natural Hazards,* 84(3), 1569-1599.

Liang, D., Falconer, R.A. & Lin, B. (2006). Comparison between TVD-MacCormack and ADI-type Solvers of the Shallow Water Equations. *Advances in Water Resources,* 29(12), 1833-1845.

Liang, D., Falconer, R.A. & Lin, B. (2007). Coupling Surface and Subsurface Flows in a Depth Averaged Flood Wave Model. *Journal of Hydrology,* 337(1-2), 147-158.

Liang, D., Wang, X., Falconer, R.A. & Bockelmann-Evans, B.N. (2010). Solving the Depth-Integrated Solute Transport Equation with a TVD-MacCormack Scheme. *Environmental Modelling & Software,* 25**,** 1619-1629.

Lind, N.D., Hartford, D. & Assaf, H. (2004). Hydrodynamic Models of Human Instability in a Flood. *Journal of the American Water Resources Association,* 40(1), 89-96.

Martínez-Gomariz, E., Gómez, M., Russo, B. & Djordjevic, S. (2016). Stability Criteria for Flooded Vehicles: A State-of-the-Art Review. *Journal of Flood Risk Management,* In Press.

Mingham, C.G., Causon, D.M. & Ingram, D. (2001). A TVD MacCormack Scheme for Transcritical Flow. *Proceedings of the Institution of Civil Engineers: Water and Maritime Engineering,* 148**,** 167-175.

Ramsbottom, D., Floyd, P. & Penning-Rowsell, E. (2003). *Flood Risks to People: Phase 1, R&D Technical Report FD2317*, Department for the Environment, Food and Rural Affairs (DEFRA).

Ramsbottom, D., Wade, S., Bain, V., Hassan, M., Penning-Rowsell, E., Wilson, T., Fernandez, A., House, M. & Floyd, P. (2006). *Flood Risks to People: Phase 2. R&D Technical Report FD2321/IR2*, Department for the Environment, Food and Rural Affairs (DEFRA).

Roca, M. & Davison, M. (2010). Two Dimensional Model Analysis of Flash-Flood Processes: Application to the Boscastle Event. *Journal of Flood Risk Management,* 3**,** 63-71.

Russo, B., Gomez, M. & Macchione, F. (2013). Pedestrian Hazard Criteria for Flooded Urban Areas. *Natural Hazards,* 69(1), 251-265.

Shand, T.D., Cox, R.J., Blacka, M.J. & Smith G.P. (2010). *Appropriate Safety Criteria for Vehicles (Report Number: P10/S1/006),* Australian Rainfall and Runoff, 28.

Stelling, G.S. & Zijlema, M. (2003). An Accurate and Efficient Finite-Difference Algorithm for Non-Hydrostatic Free-Surface Flow with Application to Wave Propagation. *International Journal for Numerical Methods in Fluids,* 43, 1-23.

Stelling, G.S., Wiersma, A.K. & Willemse, J.B.T.M. (1986). Practical Aspects of Accurate Tidal Computations. *Journal of hydraulic Engineering,* 112, 802-817.

Wallingford, H.R. (2005). *Flooding in Boscastle and North Cornwall, August 2004 (Phase 2 Studies Report),* Report EX 5160. Wallingford.

Xia, J., Chen, Q., Falconer, R.A., Deng, S. & Guo, P. (2016). Stability Criterion for People in Floods for Various Slopes. *Proceedings of the Institution of Civil Engineers, Water Management,* 169(WM4), 180-189.

Xia, J., Falconer, R. A., Wang, Y. & Xiao, X. (2014). New Criterion for the Stability of a Human Body in Flood Waters. *Journal of Hydraulic Research,* 52(1), 93-104.

Xia, J., Falconer, R.A., Lin, B. & Tan, G. (2011a). Numerical Assessment of Flood Hazard Risk to People and Vehicles in Flash Floods. *Environmental Modelling and Software,* 26(8), 987-998.

Xia, J., Lin, B., Falconer, R.A. & Wang, G. 2010. Modelling Dam–Break Flows over Mobile Beds using a 2D Coupled Approach. *Advances in Water Resources,* 33(2), 171-183.

Xia, J., Teo, F.Y., Lin, B. & Falconer, R.A. (2011b). Formula of Incipient Velocity for Flooded Vehicles. *Natural Hazards,* 58(1), 1-14.

UNESCO WATER SECURITY INITIATIVES FOR ENHANCED RESILIENCE AND 2030 AGENDA DELIVERY IN ASIA AND THE PACIFIC REGION

SHAHBAZ KHAN[(1)]

[(1)]United Nations Educational, Scientific and Cultural Organization (UNESCO)
Jl. Galuh 2 No. 5, Kebayoran Baru, Jakarta Selatan, Jakarta 12110, Indonesia
s.khan@unesco.org

ABSTRACT

2030 Agenda provides both the vision and the commitment to address and resolve the big issues of our time, including: poverty eradication, peace and security, safe and sufficient food, sustainable energy, pollution prevention and control, water and environmental resources management, disease control, mobility, natural and man-induced disasters, population growth, urbanization and sustainable/livable cities. The development of solutions to these key global challenges and the overall transition towards a green economy will need to be based on sound science, technology and innovation. Water plays a key role in almost all the global challenges and therefore water related SDG 6 is an enabling goal for the 2030 Agenda. In Asia and the Pacific region, there are many challenges that modern society is facing in terms of water management. The poorest people, mostly women, are suffering the greatest scarcity and deterioration of water quality. This situation is exacerbated by factors such as climate change, the increasing intensification of farming and agriculture, as well as increasing demand on water as a result of population growth and changing lifestyles. On the other hand, in many instances water management policies and practices have ignored the needs of the people who in a daily routine have to face water scarcity, and therefore must design new adaptive strategies to meet their needs. One of the targets of the MDGs is to halve the proportion of the population without sustainable access to safe drinking water between 2000 and 2015. We are still facing several barriers to reach this objective. One of the handicaps is the dissemination of paradigms and technologies developed under differing socio-cultural setting in developed countries to solve water challenges in the developing countries. As a result, these are not always accepted or fully incorporated, and even sometimes they become a source of conflict or produce negative effects on the target groups and their ecosystems.

Keywords: 2030 Agenda; SDGs; Asia-Pacific; challenges.

1 INTRODUCTION

The Asia-Pacific region is extremely dynamic, undergoing rapid urbanization, economic growth, industrialization, and extensive agricultural development. Although these are desirable trends in many ways, they also represent drivers that are affecting the region's capacity to meet its socio-economic water development needs. The region is extremely diverse, with seven of the world's most populous countries and many of its smallest nations, several of which are located in the Pacific. Between 1987 and 2007, the region's population grew from just under 3 billion to about 4 billion people. Average population density, at 111 people per km2, is the highest in the world. China and India alone recorded almost half of world's progress, with increases of 457 million and 522 million, respectively since 1990. This is not surprising, however, since the inhabitants of these two countries represent 46% of the developing world's population. Of note are the impressive gains in Eastern Asia, which added 23 percentage points, and the small decline in coverage in the Caucasus and Central Asia and in Oceania.

Water security, however, remains the key challenge for many countries coping with complex water issues that cut across economic sectors in the region. Population growth and economic development have placed unprecedented pressures on water. Estimates show that with current practices, the world will face a 40% shortfall between forecasted demand and available supply of water by 2030 (UNWATER 2016). Today, 70% of global water withdrawals are for agriculture. Feeding 9 billion people by 2050 will require a 60% increase in agricultural production and a 15% increase in water withdrawals. As a result, groundwater reserves are under increasing pressure around the world, with many being over-exploited. Moreover, the world will need more water for energy generation even as 1.3 billion people still lack access to electricity. The world's fast-growing urban regions such as Asia and the Pacific are also consuming more water for both domestic and industrial use. As a result of these multiple pressures, by 2025, about 1.8 billion people will be living in regions or countries with absolute water scarcity.

2 WATER CHALLANGES

Box-1 Key water challenges

The 2030 Development Agenda needs to respond to new global water realities, which indicate that humanity is facing numerous unprecedented and inter-connected socio-economic and environmental sustainability challenges further complicated by an intensifying hydrological cycle under global change. The most pressing water challenges of the 21st century include:

- Intensifying water efficiencies in food production
- Failing access to water and sanitation
- Stressed aquatic ecosystems and biodiversity loss
- Increasing conflicts on water rights
- Degrading water quality
- Ever increasing human water foot prints
- Unsustainable groundwater abstractions
- Frequent hydrologic extreme events causing floods and droughts
- Water privatization leading to inequalities in water access
- Closed rivers and over exploited aquifer systems leading to water stress for all uses
- Unplanned urban growth threatening water balances
- Inadequate human and institutional capacities to deal with the above challenges

2.1 Complexities and inter-relatedness of water challenges

These water-related global challenges are hugely complex with strong inter-connections. For instance, ensuring food security for a rapidly growing world population depends on availability of water, land and energy, and on scientific breakthrough in enhancing production. Current food production methods, however, are highly polluting, causing eutrophication, greenhouse gas emissions, biodiversity loss and water stress. In addition, climate change and extreme weather events lead to massive crop damage, and pose a growing threat to agriculture yields and food security. The task to address the above water challenges is phenomenally complex, and therefore science has to play a major role in helping to understand the complexities and multi-dimensional character of sustainable development.

2.2 Ensuring water as a human right

On 28 July 2010, through Resolution 64/292, the United Nations General Assembly explicitly recognized the human right to water and sanitation and acknowledged that clean drinking water and sanitation are essential to the realization of all human rights. Water democracy comes from political democracy enabling the availability of water, making possible that the water is "everybody's business". This is a matter of right to water and life. There is a need to understand economic and legislative aspects of providing water and sanitation as a human right in different hydrogeographical and societal settings. The human right to water has to entitle everyone to sufficient, safe, acceptable, physically accessible and affordable water for personal and domestic uses. A rights-based approach is needed to prioritize non-discriminatory access to water, promote inclusive participation in all decision-making mechanisms and ensure accountability and legal obligations of public institutions.

2.3 Water security beyond water supply and sanitation goals

MDG 7, Target 7c, focused on the importance of providing safe drinking water and sanitation. But, there are additional water issues beyond Target 7c that also need attention. Water is the main limiting factor preventing increased food production, water quality deterioration affects biodiversity, and many people (especially children) die from water borne disease. It is estimated that over 90% of all climate change impact is water related; we need better flood forecasting, community preparedness, and adaptation measures. The rivers and groundwater systems are becoming increasingly polluted; this creates challenges to society at large for aquifer and river restoration and integrated water resources management. There is an urgent need to go beyond MDG Target 7c, by understanding ecological impacts of water projects, including for drinking water supply, and also for industrial water use, irrigation, and dams and dikes on water quantity, quality and related environment links.

2.4 More crop per drop

More than 70% of all water use globally goes to food production. To secure sufficient food production for an estimated 9 billion people in 2050, we need to consider a paradigm shift in the way we produce food. There are medium (3 to 5 years) and longer term (beyond 5 years) challenges to achieve societal benefits through more crop per drop in water stressed regions. These objectives can be summarized as below:

- Medium term: improve efficiencies (drought resistant crops, high yield/low water use varieties via biotech; efficiency of irrigation systems etc.)
- Longer term: new ways of food production with full water and nutrient recycle (on the extreme end of the scale, there is the option to produce meat in factories).

2.5 Water culture a sound basis for water management

Water is life because, "there is no life without water", and the existence of every society is about the existence of a determined culture of water. There is no society or social group without water culture, every community has its own water values. Every society and every social group has developed a unique water culture, allowing them to live in their territory. Moreover, if we want to change a culture of water into another, this requires necessary restructuring of the modes of perception, the belief systems and the ways to perceive, to believe, to know, to organize, to live and to plan a common future. We have to build bridges with the past and the present to build better water futures. It is from culture that we can produce a real process of change towards a sustainable development.

2.6 Adaptive water management for better coping with extremes

Climate change affects both the quality and availability of water resources. The consequences are significant. Water-related natural disasters, such as flooding, drought, and landslides, are becoming more frequent and more severe. Rising temperatures, causing increased evaporation and glacial melt, are reducing the reliability and quality of water supplies. Responsible management of water must take into account the real danger of physical water renewability, which not only depends on global climate change (which affect the water cycle in quantitative terms), but also of the local regional and global water management practices. In many parts of the world, both the quantity and good-quality water are on substantial decline. The main pollutants of groundwater are nitrates that are generated primarily by intensive farming and agricultural fertilizers and pesticides. Adaptive water management is needed to adjust practices in accordance with anticipated climate change impacts on water resources, to use the limited water efficiently and manage the agriculture water productivity effectively by making every drop counts for social, economic and environmental benefits to society and nature.

2.7 Inclusive and relevant water technologies to avoid unintended consequences

Imported and exclusive technological models which are elaborated under different environmental and cultural conditions can sometimes have negative impacts on both environment and society. For example, reservoirs that apart from having a huge impact at social and environmental level can have a limited life because they rapidly accumulate sediments if constructed in unstable watersheds. 100% of the public water supply is treated to make it drinkable, while the drinking, food cooking and water washing uses account for less than 35%. This means that 65% of the work and energy used is not necessary. Another example is the use of chlorine. This is used to prevent microbes from proliferating along the way in the supply network, but at the same time it creates new health concerns, producing several toxic compounds, some of them recognized as carcinogenic. Besides, the toxicity of chlorine requires a lot of energy to be produced. In some areas, the impact of the exploitation of underground aquifers is usually gradual and "invisible". The rate of exploitation of aquifer systems is unsustainable in most areas and can cause irrecoverable land subsidence. The excessive exploitation of coastal aquifers is causing sea water intrusion. There is a need for new forms of technology and innovation as well as improved applications for using different sources of water (such as rain water harvesting, untreated river water, grey water reuse) fit for a purpose.

2.8 Paradigm shift in urban water management

Urbanization is keeping domestic water use on an upward trend. Today, an average person uses more than double the water than a hundred years before. Domestic water use represents on average 11% of total water withdrawal worldwide and is used to supply towns, cities and rural communities (the vast majority of domestic water consumption is linked to hygiene). The natural hydrological processes are significantly changed by newly built environments. In addition, rainwater collects chemicals and other concentrated forms of pollutant (such as zinc and lead), which are then carried directly into streams and rivers. Rainwater is discharged with no prior treatment, especially in emerging and the least developed regions. In developing countries, more than 80% of wastewater is currently discharged into the environment in an untreated state, polluting rivers, lakes and coastal areas. There is a need for formulating sound policies through learning alliances at different levels aimed at incorporating reduce, recycle, reuse and redesign concepts in water-intensive foods and goods systems to reduce human water foot prints.

2.9 Management needs to be in the hands of women

Women are often the primary users of water in domestic consumption, subsistence agriculture, health and sanitation. Women in many cases also take the primary role in educating children, in child and family health including sanitation and in caring for the sick. They also spend a disproportionate number of hours on laborintensive, time-consuming and unpaid domestic tasks such as fetching water and firewood, washing clothes and dishes and preparing meals. Too often, women and girls are disproportionately affected by the lack of access to water and, although women carry out most of the water related tasks, play a key role in food production, especially in subsistence farming, their participation in decision making processes on water and food management remains very low. This does not only result in biased and misinformed decision-making, but it also jeopardizes the achievement of women's human rights, reducing their opportunities to education, decent work and political engagement, and perpetuate the intergenerational transfer of poverty and disempowerment. Understanding gender roles can help plan water interventions and policies which are based on the knowledge of how and why people make the choices they do in water use in order to meet their needs.

2.10 Towards a new hydro-diplomacy for crossing water boundaries

It is well known that water is not distributed equally among different sectors of society and across geopolitical boundaries. The problem of water is vital in all communities; no life or production is possible without water. The use of water whether it is abundant or not, entails the real possibility of confrontations between social sectors. Consequently, before we deal with water, it is necessary to picture the set of tensions that could be generated around it while crossing boundaries. The source of stress may be at local, regional, national or international level. This is due to different positions adopted by individuals based on their subjectivity, which is the result of their cultures and their own relationship with water. The water sharing and use proposals have to include all agents in a major and constructive role. It is necessary to remember that all positions are worthy of consideration and if there is a real interest in establishing communication channels, it will be possible to converge and complement each other. Trying to put yourself in someone else's place and looking through their worldview, trying to discover how others perceive the situation, is the first step in a process to reach water agreements.

2.11 Corporate social responsibility of the water businesses

In countries where many people lack access to safe water, the growth in bottled water consumption is dramatic, for example by 50% a year in India. The global bottled water business is in the hands of a few multinational companies. The fact that a few companies can exploit very high-quality water for their own benefit, while leaving behind social and ecological issues is questioned. Only a few companies own safe drinking water technologies that a local municipality can hardly assume. Also the water extraction, which is often done in the higher parts of the mountains, in places of great natural value and landscape, creates a huge environmental impact as well as ecological impacts of associated packaging. In addition, bottled water requires transportation, which includes developing infrastructures such as roads, hence increasing fuel consumption and emission of greenhouse gases. In meeting the drinking water challenges, there is a need for greater corporate and social responsibility of the private sectors especially the multinational companies.

2.12 Increasing human capacities in all water management areas

The key objective of Integrated Water Resources Management (IWRM) is to re-establish water quality and ecosystem functions through improved storm water management, human and industrial waste management, flood loss reduction, sedimentation and pollution control, improvement of water quality, recreation, education and introduction of natural or manmade cropping systems tailored to deliver solutions at the river basin level. This needs to be set in a human rights-based approach aimed at achieving 'sufficient, safe, acceptable, and affordable water for personal and domestic uses' for all. Locally appropriate based IWRM formal and informal education at all levels is needed to address water supply and sanitation-related exclusion issues that are commonly rooted in weak governance, power inequality and poverty, rather than sheer physical availability of water.

3 CONCLUDING REMARKS

UNESCO and wider UN System are working on integrated approaches for achieving water security under SDG 6 of 2030 Agenda (UNESCO 2009, Speed at al 2013, WWAP 2009). However, implementation at the river basin and country levels remains the greatest challenge in achieving water security. These impediments include lack of political commitment and awareness, true stakeholder identification and engagement, capacity and management information and communication. Sound monitoring systems, communications strategies, formal communication and stakeholder engagement mechanisms can facilitate improved information sharing to support action. It is critical that these types of barriers are recognized and addressed during the development of the water security plans for timely implementation. 2030 Agenda implementation may be further supported by:

- understanding the institutional landscape associated with delineated activities at the river basin and country levels
- identifying implementing institutions and champions, and getting them onboard, for real stakeholder engagement
- agreeing to hanging fruit solutions that can start immediately in order to generate momentum

- Initiating targeted social marketing, broad promotion and awareness-building through public-private partnerships
- Twining of river basins facing similar issues for national and international cooperation.

REFERENCES

Speed R., Li Y., Le Quesne T., Pegram G. & Zhiwei Z. (2013). Basin Water Allocation Planning. Principles, procedures and approaches for basin allocation planning. *UNESCO*, Paris.

UNESCO (2009). IWRM Guidelines at River Basin Level Parts 1, 2, 3 and 4.

UNWATER (2016) Monitoring Water and Sanitation in the 2030 Agenda for Sustainable Development World Water Assessment Program (2009) Integrated Water Resources Management in Action

BED SHEAR STRESS AND TURBULENCE CHARACTERISTICS UNDER SOLITARY WAVES

PENGZHI LIN(1), HAIJIANG LIU(2), DANDAN CHEN(3), FANG HE(4), XIAOCHUN TANG(5) & XIZENG ZHAO(6)

(1,3,5) State Key Laboratory of Hydraulics and Mountain River Engineering, Sichuan University, China
(2) College of Civil Engineering and Architecture, Zhejiang University, China
(6) Ocean College, Zhejiang University, China
cvelinpz@126.com

ABSTRACT

Bed shear stress and turbulence under waves are of fundamental importance to understand sediment transport and bed morphology in coastal waters. In this study, the experiments were conducted to reveal the characteristics of bed shear stress and turbulence under solitary waves. Three cases corresponding to laminar and turbulent boundary layers respectively were investigated. A 2D Laser-Doppler-Velocimetry (LDV) was used to measure the velocity profiles across the water depth and the information of turbulence kinetic energy was extracted from the measured velocities for turbulent case. A new method of finding the wave-induced bed shear stress over a smooth bed from the measured velocities within or near the viscous sub-layer was developed. The experimental data of velocities, bed shear stress, and turbulence kinetic energy were compared to the available theories and the numerical results obtained from a Reynolds-Averaged Navier-Stokes (RANS) equations model with a BSL $k-\omega$ turbulence closure. The relationship between the bed shear stress and turbulence was discussed.

Keywords: Bed shear stress; solitary wave; viscous sub-layer; LDV, BSL $k-\omega$ model.

1 INTRODUCTION

The bed shear stress induced by coastal waves is closely related to the sediment motion and beach morphology. In laboratory studies, the bed shear stress can be obtained by the direct and indirect methods. The direct methods consist of two main categories, namely, hot-film method and shear plate method. The former method uses a calibrated hot-film sensor attached on the bottom to find the bottom shear stress from the electrical voltage information (*e.g.,* Jensen et al., 1989). The latter finds the shear force by measuring the displacement of a shear plate mounted on the bottom and converts the shear force to the shear stress (*e.g.,* Barnes et al., 2009; Guard et al., 2011). Pujara and Liu (2014) improved the shear plate technique by considering the presence of pressure gradients across the plate. The indirect method refers to the method that extracts the information of bed shear stress by using the measured velocities above the bed and it includes the log-law fitting method and momentum integral method. The near bottom velocities can be obtained by using Laser Doppler Velocimetry (LDV) and Particle Image Velocimetry (PIV) (*e.g.,* Van der A et al., 2011; Yuan and Madsen, 2014).

A solitary wave is often used to represent leading tsunami and it has the unique feature of simple wave form maintaining the positive free-stream velocities while its near-bed flow acceleration can be both positive and negative. Ippen and Mitchell (1957) used a shear plate to measure the time histories of bottom shear stress under solitary waves. Keulegan (1948) and Tanaka et al. (1998) derived analytical solutions to the velocity distribution and bed shear stress under a solitary wave. Such analytical solutions were later used as the reference for many numerical models (*e.g.,* Lin and Zhang, 2008; Vittori and Blondeaux, 2008; Suntoyo and Tanaka, 2009). In recent years, people used non-intrusive apparatus in the experimental studies of solitary wave-induced boundary layer characteristics. For example, Liu et al. (2007), Sumer et al. (2010), Lin et al. (2015b), and Lin et al. (2016) used PIV to measure the detailed flow structure near bottom, from which the bed shear stress was extrapolated by using log-law or momentum integral method.

The aim of the present study is to develop a new way of finding the bed shear stress under a solitary wave over a smooth bed by using the measured velocities within or very near to the viscous sub-layer. Three experiments will be conducted to represent both laminar and turbulent boundary layer. The LDV will be used to measure the velocities down to the bottom. The turbulence kinetic energy information will be extracted from the measured data in order to better understand the correlation between the turbulence and bed shear stress. In the meantime, a numerical model using the BSL $k-\omega$ turbulence closure will be employed for simulation of detailed flow and turbulence structures in and outside of the boundary layers. The experimental data and numerical results will be compared to theories and discussed.

2 Experimental Setup

2.1 Experiment setup

The experiments were conducted in a 28.0 m long, 1.2 m wide and 1.0 m deep wave tank in the State Key Laboratory of Hydraulics and Mountain River Engineering at Sichuan University. The wave tank has glass sidewalls and waves were generated with a piston-type wave maker at one end of the wave tank. The wave gage was located 10.0 m away from the wave maker, with the sampling frequency of 100 Hz and the precision of 0.15 mm (Figure 1a). The TSI 2D LDV was deployed at the same cross section as the wave gauge, with the precision of 0.5 mm/s in this study (Figure 1b). The focal length of the laser probe is 144.0 mm, and the distance between the probe and the side wall is about 10.0 – 20.0 mm. For the LDV measurements, the lowest point was 0.3 mm above the glass bottom, with the spacing between two adjacent measuring points being 0.05 mm for laminar boundary layer and 0.1 mm for turbulent one (Figure 1c).

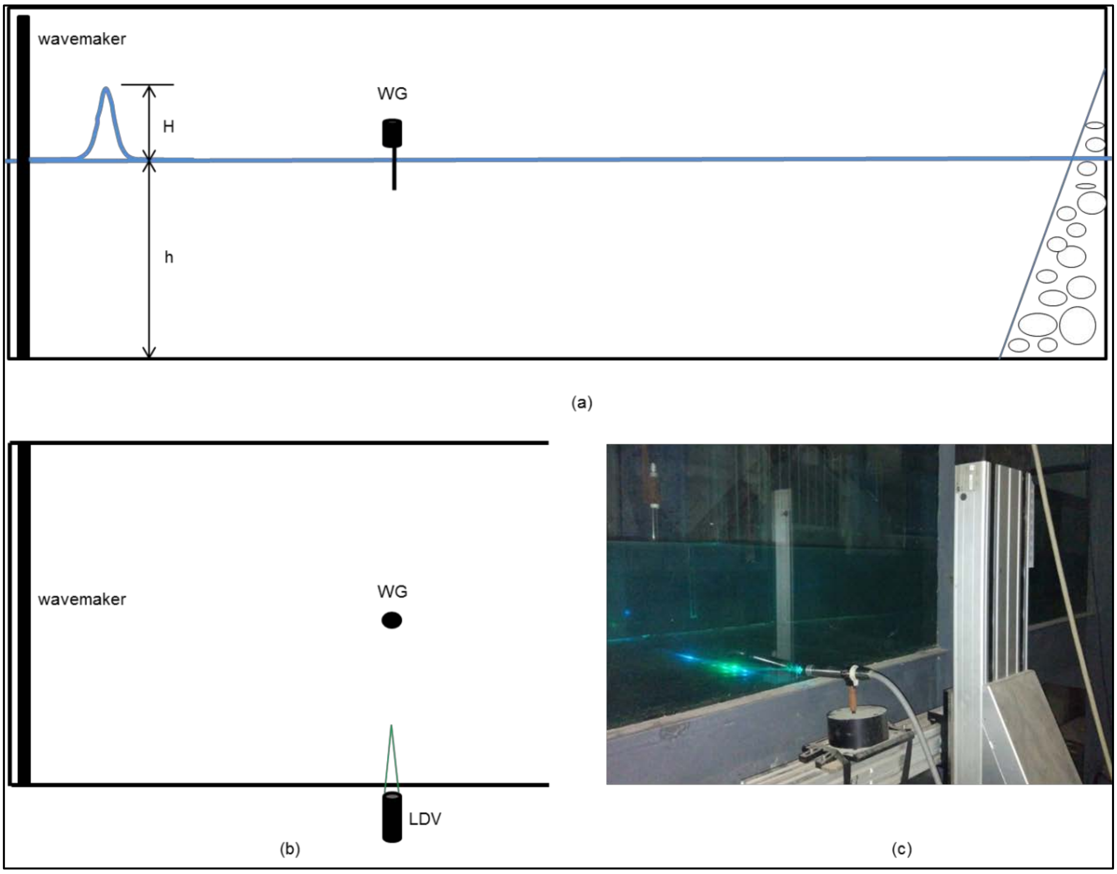

Figure 1. (a) Side view of the wave tank and the arrangement of wave gauge, (b) top view of the wave tank and the arrangement of LDV probe, (c) Photo of tank and LDV probe.

Three cases were investigated with different combinations of water depth (h), wave height (H), and bed material (Table 1). Also shown are the maximal free stream velocities, U_c and U_m calculated from two different theories, which will be explained in Section 4.1. While the first two cases were conducted above the smooth glass bottom, the last one was on a rough bed consisting of gravels with the diameter of d_{50} = 20.0 mm. From the experimental results, cases S-1 and S-2 are associated with laminar boundary layer, while S-3 the turbulent boundary layer.

Table 1. Parameters in three experimental cases.

Case	h (m)	H (m)	U_c (m/s)	U_m (m/s)
S-1	0.25	0.04	0.269	0.224
S-2	0.25	0.09	0.657	0.449
S-3	0.30	0.10	0.660	0.462

3 NUMERICAL METHODS

3.1 Governing equations and turbulence model

The 2D numerical model is based on Reynolds-Averaged Navier-Stokes (RANS) equations:

$$\frac{\partial u_i}{\partial x_i} = 0 \qquad [1]$$

$$\frac{\partial u_i}{\partial t} + u_j \frac{\partial u_i}{\partial x_j} = -\frac{1}{\rho}\frac{\partial p}{\partial x_i} + g_i + \frac{1}{\rho}\frac{\partial \tau_{ij}}{\partial x_j} \qquad [2]$$

where $x_i (i = 1,2)$ is the Cartesian coordinate, u_i denotes the *i*-th component of the velocity vector, t the time, ρ the density of the water, p the pressure, g_i gravitational acceleration in the *i*-th direction, and τ_{ij} the shear stress given as:

$$\tau_{ij} = \rho\left(\nu + \nu_t\right)\frac{\partial u_i}{\partial x_j} \qquad [3]$$

in which ν_t is the eddy viscosity. In the following computations we adopt the values of $\rho = 1.0 \times 10^3 kg/m^3$ and $\nu = 1.0 \times 10^{-6} m^2/s$ for water at 20 °C and under one atmospheric pressure.

The two-equation BSL $k - \omega$ model proposed by Menter (1994) is used for turbulence closure.

$$\frac{\partial k}{\partial t} + u_j \frac{\partial k}{\partial x_j} = \frac{\tau_{ij}}{\rho}\frac{\partial u_i}{\partial x_j} - \beta^* k\omega + \frac{\partial}{\partial x_j}\left[\left(\nu + \sigma_k \nu_t\right)\frac{\partial k}{\partial x_j}\right] \qquad [4]$$

$$\frac{\partial \omega}{\partial t} + u_j \frac{\partial \omega}{\partial x_j} = \gamma \frac{\omega}{k}\frac{\tau_{ij}}{\rho}\frac{\partial u_i}{\partial x_j} - \beta\omega^2 + \frac{\partial}{\partial x_j}\left[\left(\nu + \sigma_\omega \nu_t\right)\frac{\partial \omega}{\partial x_j}\right] + 2\left(1 - F_1\right)\sigma_{\omega 2}\frac{1}{\omega}\frac{\partial k}{\partial x_j}\frac{\partial \omega}{\partial x_j} \qquad [5]$$

$$\nu_t = \frac{k}{\omega} \qquad [6]$$

The blending function F_1 is defined as:

$$F_1 = \tanh\left(\arg_1^4\right) \qquad [7]$$

where,

$$\arg_1 = \min\left(\max\left(\frac{\sqrt{k}}{0.09\omega y};\frac{500\nu}{y^2\omega}\right);\frac{4\rho\sigma_{\omega 2}k}{CD_{k\omega}y^2}\right) \qquad [8]$$

in which y is the distance to bed, and:

$$CD_{k\omega} = \max\left(2\rho\sigma_{\omega 2}\frac{1}{\omega}\frac{\partial k}{\partial y}\frac{\partial \omega}{\partial y};10^{-20}\right) \qquad [9]$$

The model is a combined model of standard $k - \omega$ model of Jones and Launder (1972) and $k - \omega$ model of Wilcox (1988), the value of F_1 changing gradually from one to zero in the desired region, retaining the accurate formulation of the Wilcox $k - \omega$ model in the near wall region, while returning to $k - \omega$ model outside of the boundary layer. The detailed discussions for the model constants, β^*, σ_k, γ, β, σ_ω, $\sigma_{\omega 2}$, are referred to Menter (1994).

3.2 Boundary conditions and numerical method

The no-slip condition is applied at the bed, where the velocities and turbulent kinetic energy are $u = v = k = 0$, and the specific dissipation rate (ω) is given as:

$$\omega = \begin{cases} \lim\limits_{\Delta y \to 0} \dfrac{6\nu}{\beta^* \Delta y^2} & , \quad k_s^+ < 3.3 \\ \dfrac{u_*^2}{\nu} S_R & , \quad k_s^+ \geq 3.3 \end{cases} \tag{10}$$

where k_s^+ is the bed roughness Reynolds number, which is defined as $k_s^+ = k_s u_*/\nu$, $u_* = \sqrt{\tau_b/\rho}$ is the friction velocity, τ_b is bed shear stress. S_R is related to k_s^+:

$$S_R = \begin{cases} \left(50/k_s^+\right)^2 & , \quad k_s^+ < 25 \\ 100/k_s^+ & , \quad k_s^+ \geq 25 \end{cases} \tag{11}$$

At the free surface, the gradients of velocity, turbulent kinetic energy and specific dissipation rate are equal to zero, *i.e.,* at $y = \eta$, $\partial u/\partial y = \partial k/\partial y = \partial \omega/\partial y = 0$.

The above governing equations were solved by the projection method (Lin and Xu, 2006). In order to obtain the adequate resolution near the bottom, the grid spacing was increased exponentially from bottom to free surface, with the minimum grid size near the bed in y direction being $\Delta y = 0.1\ mm$, fine enough to capture the viscous sub-layer.

4. RESULTS AND DISCUSSIONS

4.1 Free surface elevation and velocity distribution

According to Grimshaw (1971) and Liu et al. (2007), the free surface elevation and horizontal velocity distribution outside of boundary layer of a solitary wave are:

$$\frac{\eta}{H} = s'^2 - \frac{3}{4}\varepsilon' s'^2 q'^2 + \varepsilon'^2\left(\frac{5}{8}s'^2 q'^2 - \frac{101}{80}s'^4 q'^2\right) \tag{12}$$

$$\begin{aligned} \frac{u}{\varepsilon'\sqrt{gh}} = {} & s'^2 - \varepsilon'\left[-\frac{1}{4}s'^2 + s'^4 + \left(z'+1\right)^2\left(\frac{3}{2}s'^2 - \frac{9}{4}s'^4\right)\right] \\ & - \varepsilon'^2\left[\begin{aligned} & \frac{19}{40}s'^2 + \frac{1}{5}s'^4 - \frac{6}{5}s'^6 + \left(z'+1\right)^2\left(-\frac{3}{2}s'^2 - \frac{15}{4}s'^4 + \frac{15}{2}s'^6\right) \\ & + \left(z'+1\right)^4\left(-\frac{3}{8}s'^2 + \frac{45}{16}s'^4 - \frac{45}{16}s'^6\right) \end{aligned}\right] \end{aligned} \tag{13}$$

in which $\varepsilon' = \dfrac{H}{h}$; $z' = z/h$; $s' = \operatorname{sech}\left[\dfrac{\beta'}{\mu'}\left(x' - c_3' t'\right)\right]$; $q' = \tanh\left[\dfrac{\beta'}{\mu'}\left(x' - c_3' t'\right)\right]$; $\mu' = \dfrac{h}{l_0}$; $\beta' = \sqrt{\dfrac{3\varepsilon'}{4}}\left(1 - \dfrac{5}{8}\varepsilon' + \dfrac{71}{128}\varepsilon'^2\right)$; $x' = x/l_0$; $t' = \sqrt{gh}\,t/l_0$; $c_3' = \sqrt{1 + \varepsilon' - \dfrac{1}{20}\varepsilon'^2 - \dfrac{3}{70}\varepsilon'^3}$, and l_0 is a horizontal length scale that is taken as h for convenience of computation.

Tanaka et al. (1998) proposed the following analytical expression for horizontal velocity within laminar boundary layer under a solitary wave as:

$$\frac{u}{U_c} = \sec h^2(\xi) - \frac{2}{\sqrt{\pi}} \int_0^\infty \sec h^2 \left(\xi + \left(\frac{\beta' z}{\alpha} \right)^2 \right) e^{-\alpha^2} d\alpha \quad [14]$$

where $\xi = act$, $a = \sqrt{3H/4h^3}$, $c = \sqrt{g(h+H)}$, $U_c = cH/h$, and $\beta' = \sqrt{ac/4\nu}$.

Comparisons of free surface elevation between the computational results, experimental measurements and analytical solution for cases S-1 and S-2 are shown in Figure 2. Reasonably good agreements are obtained for S-1, with the discrepancy increased for S-2 with larger wave height. The mean velocity profiles at different phases for cases S-1 and S-2 are shown in Figure 3, together with the numerical results and analytical solution Equation (14). In normalization of velocity, the maximal free stream velocity (U_m) is used and calculated from Equation (13) at bottom. It is also noted that Equation (14) would overestimate u if we use the expressions of c and U_c in the same equation. For this reason, the calculated u was re-scaled by multiplying U_m/U_c before it was plotted. Outside of the boundary layer, the agreement among the theories, numerical results and experimental data is generally good, with the deviation from the theories increasing for larger wave height and during the decelerating phase. Inside the boundary layer while the numerical results stay together with the experimental data in most instants, their differences from the theories are relatively large during the deceleration phase, especially for case S-2 with high nonlinearity of $H/h = 0.36$.

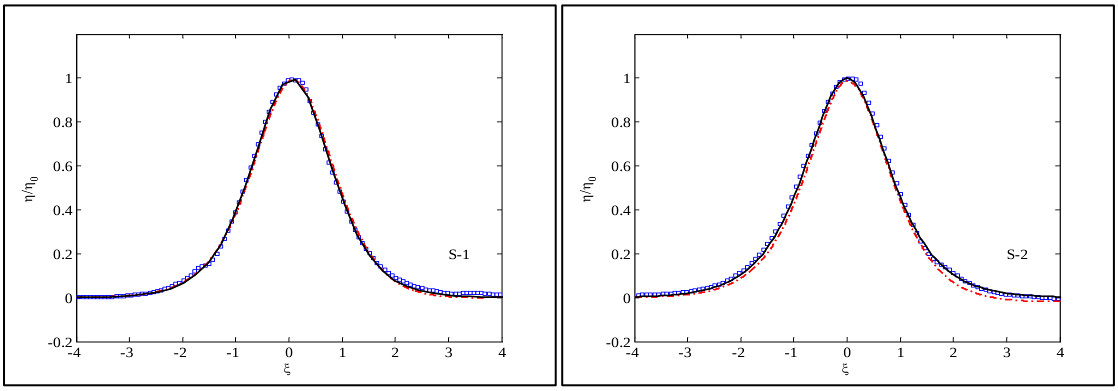

Figure 2. Comparison of the free surface elevation among experimental data (squares), numerical results (dashed-dotted lines) and analytical solution (solid lines) for case S-1 (left) and case S-2 (right).

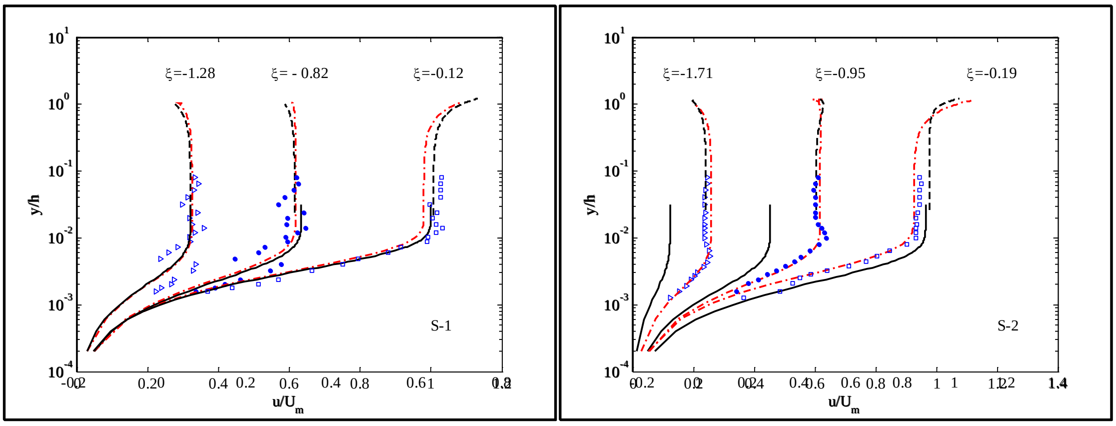

Figure 3. Comparison of horizontal velocity profiles among experimental data (symbols), numerical results (dashed-dotted lines) and analytical solutions (dashed lines for Grimshaw's solution and solid lines for Tanaka et al.(1998) solution) for cases S-1 (left) and S-2 (right).

4.2 Bed shear stress

In this study, we introduce a new method of calculating the bed shear stress by using the measured velocities in the vicinity of viscous sub-layer. It is well-known that for flows above a smooth bottom, there exists a viscous sub-layer inside of which the viscous effect predominates and the following relationship holds:

$$u^+ = y^+ \quad [15]$$

where $u^+ = u/u_*$ and $y^+ = yu_*/\nu$) with u_* being the frictional velocity. For steady flows, this viscous sub-layer has $y^+ \leq 5$, while for unsteady flows this threshold may vary. This implies that if we can manage to get the measurement point down to the viscous sub-layer, the bed shear stress can be simply obtained by using a single point measurement as:

$$\tau_w = \rho u_*^{\ 2} = \frac{\rho u(y)\nu}{y} \qquad [16]$$

Here, let's first re-plot near bottom velocities for S-1 by using the left vertical axis for real dimension and right axis expressed as y^+. It is found that during the entire stage, the value of $y^+$for the lowest measuring point (0.3 mm above the bottom) is smaller than six, while the lowest three measuring points maintaining nearly linear and stayed together with rather low level of scattering. This observation inspires us to derive a simple method of using the lowest three points to best fit the line of Equation (15), except for the phase of near bed velocity reversing (Figure 4d), for which the lowest two points had oppisite velicities and thus only the lowest point velocity is used to calculated the bed shear by using Equation (16).

The fitted lines are plotted in Figure 4 together with the numerical results. It is interesting to observe that although the detailed profiles between the numerical results and experimental data exhibit differences within this very thin region (1.0 mm), the extrapolated velocity gradients from the experimental data seem to agree with the numerical computation rather well, in all stages.

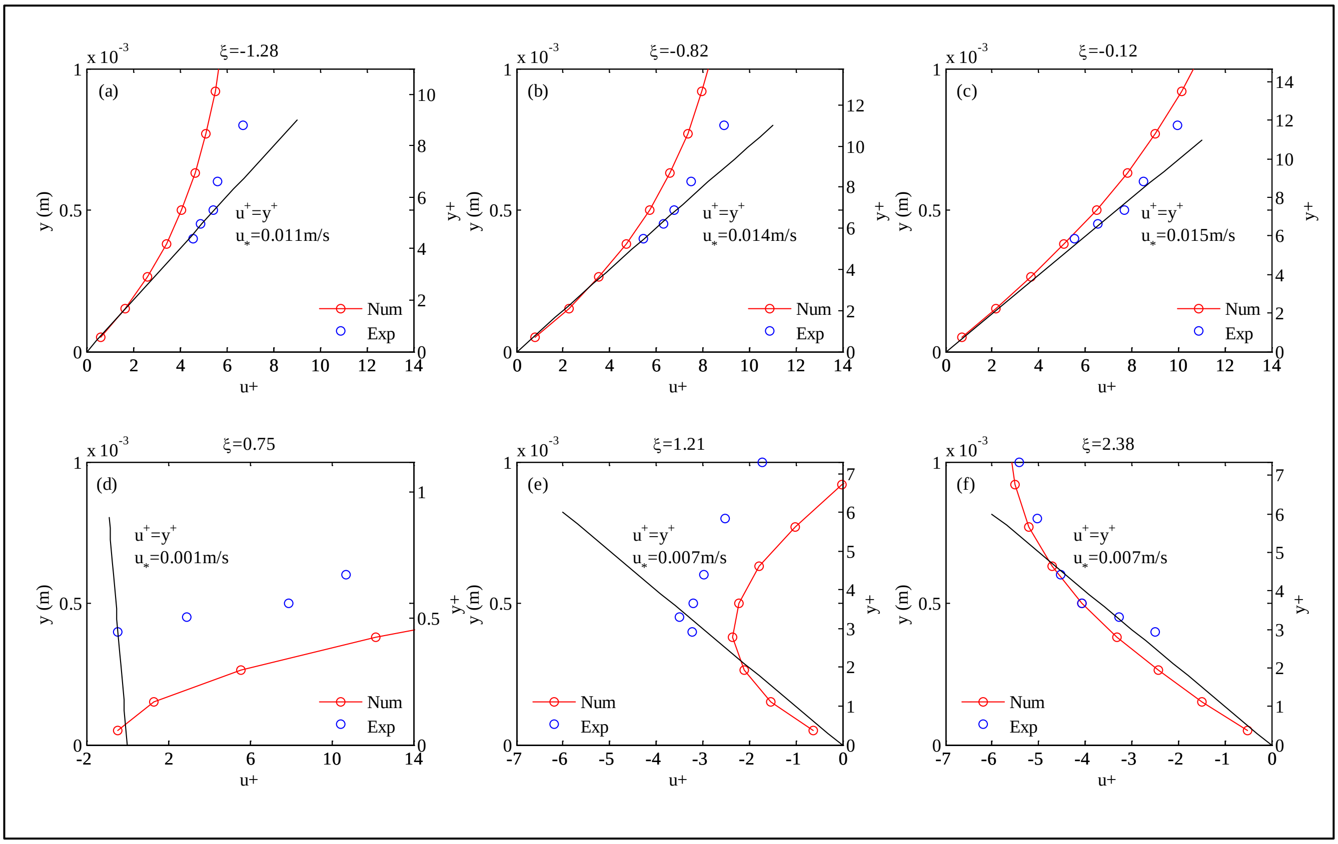

Figure 4. Illustration of how the bed shear stress is calculated by using the lowest three points of measured velocities near the viscous sub-layer for S-1.

This encourages us to practice further validation of the methods by comparing the calculated shear stress to the theories as well. According to Tanaka et al. (1998), the bed shear stress (τ_w) of the laminar boundary layer flow under a solitary wave is:

$$\tau(\xi)' = \frac{\tau_w}{\rho}\frac{\sqrt{\pi}}{4U_c\sqrt{ac\upsilon}} = \int_0^\infty \sec h^2\left(\xi+\alpha^2\right)\tanh\left(\xi+\alpha^2\right)d\alpha \qquad [17]$$

Figure 5 shows the comparison of the experimentally found bed shear stress with the numerical results and the theoretical solutions from Equation [18]. Similar to Figure 3, the calculated τ_w is re-scaled by multiplying $U_m{}^2/U_c{}^2$. It is found, a bit surprisingly, from Figure 5 that for both cases the numerical results agree rather well with the experimental data at all times, although the comparisons of velocities profiles in Figure 3 and Figure 4 are not that perfect. Apparent phase differences are observed for both cases when compared to the theoretical solutions and the actual arrival time of the peak is delayed. Besides the phase differences, the magnitude also exhibits differences. These findings agree with those by Suntoyo and Tanaka (2009) who numerically simulated boundary layer flows under solitary waves with different Reynolds numbers and compared their computations to the theories.

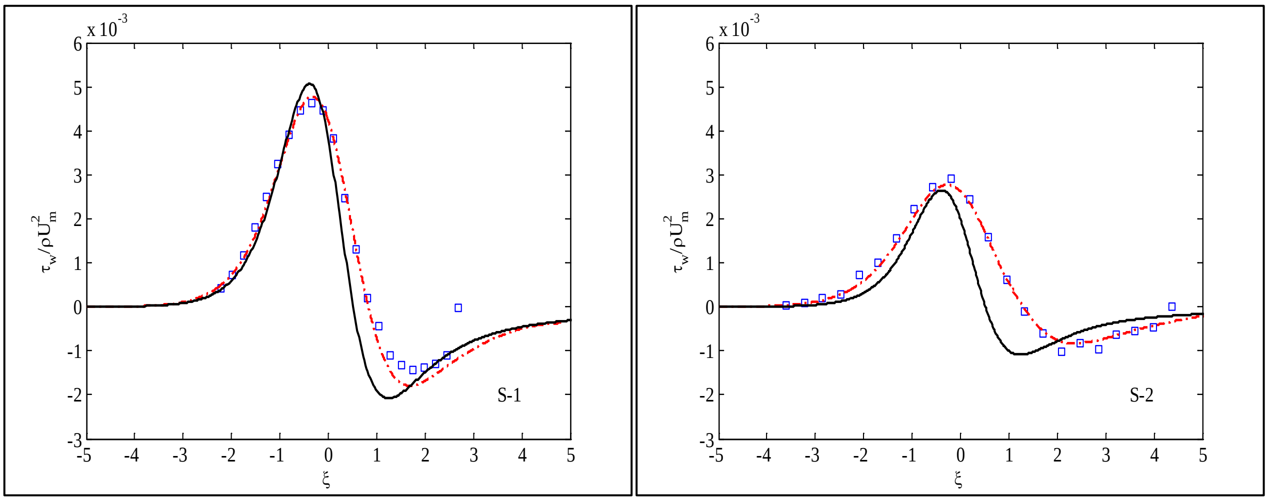

Figure 5. Comparison of bed shear stress among experimental data (square), numerical results (dashed-dotted lines) and analytical solutions (solid lines) for case S-1 and case S-2.

4.3 Turbulence characteristics

For case S-3, as the bed is rough and the boundary layer is turbulent, the measured velocities are further analyzed to extract the turbulence kinetic energy. The bed shear, however, cannot be obtained using the method proposed in this study because the viscous sub-layer is lower than the bed roughness. Figure 6 gives the comparisons of free surface displacement, together with the bed shear stress. While the free surface profiles are well predicted by the theory and simulated by the numerical model, the numerical results of bed shear stress is much larger than theoretical solutions based on laminar flow assumption. In addition, the phase difference between the bed shear stress and free surface elevation becomes smaller.

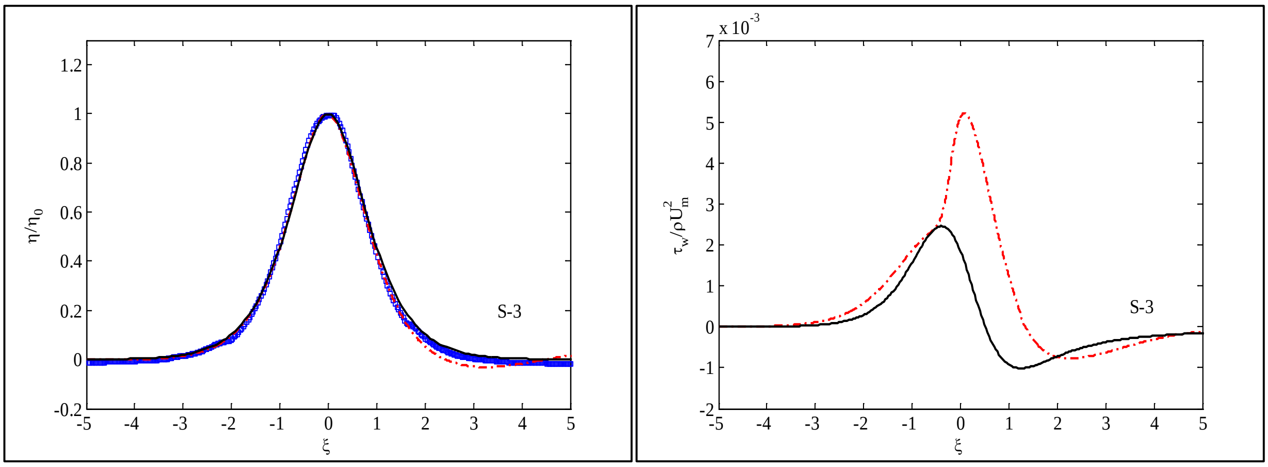

Figure 6. Comparison of the free surface elevation and bed shear stress among experimental data (square), numerical results (dashed-dotted line) and analytical solution (solid line) for case S-3.

In order to better understand why the bed shear is significantly changed for S-3, we also plot out the velocity profiles in Figure 7 and turbulence kinetic energy in Figure 8. It is seen from Figure 7 that as compared to S-1 and S-2, the boundary layer is elevated for S-3 due to turbulence mixing, which causes a larger value of bed shear stress and smaller phase difference from the main stream velocity. The numerical results agree well with the experimental data during the accelerating phase, while the differences increase during the initial stage of decelerating phase. From Figure 8, it is seen that the turbulence level stays low during the accelerating phase, and it becomes significant during the decelerating phase. The numerical model predicts the same trend of turbulence growth and decay as those of experimental data, although the magnitude does not agree perfectly and the boundary layer thickness is underestimated by the numerical model. Figure 8 also shows the simulated eddy viscosity, a key parameter for understanding turbulence mixing inside the turbulent boundary layer. From this plot, it is seen that the simulated eddy viscosity has a close correlation with the simulated turbulence kinetic energy during its growth stage until $\xi = 1.24$. However, after the passage of wave crest accompanied by the decay of turbulence kinetic energy, the eddy viscosity still keeps a rather high level of over 10 times of molecular viscosity, implying that the vertical mixing process has a much longer life span than the turbulence kinetic energy itself.

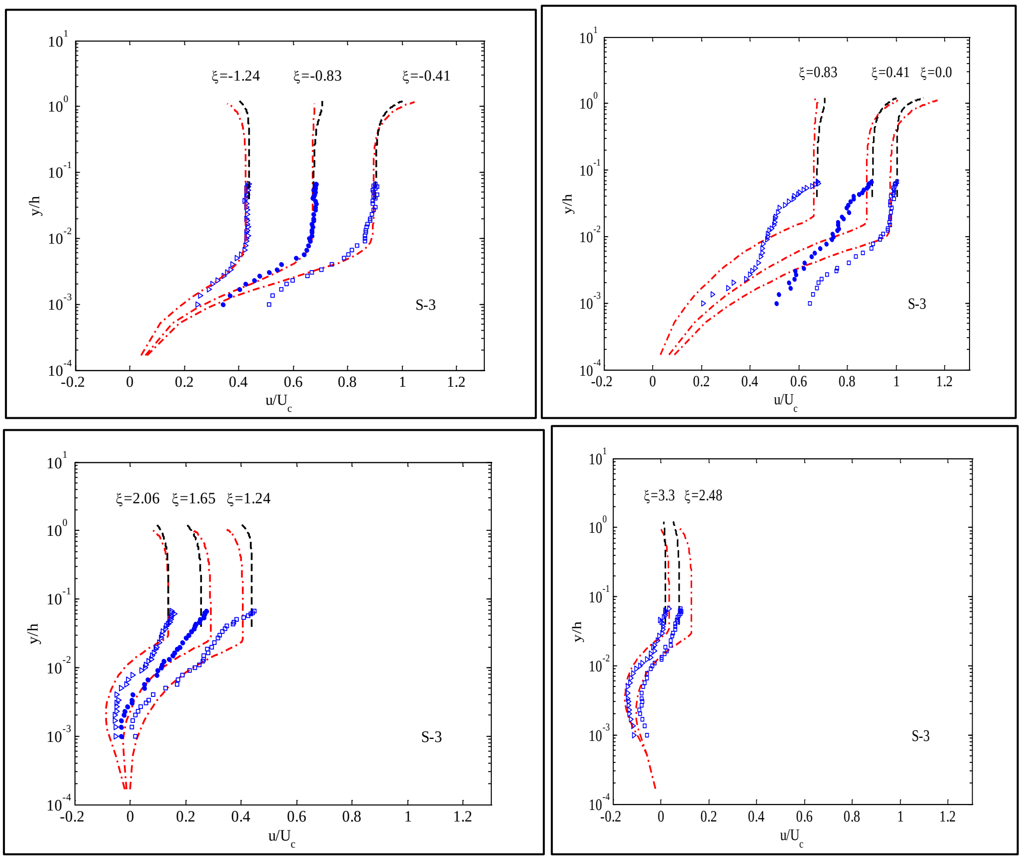

Figure 7. Comparison of velocity profiles among experimental data (symbols), numerical results (dashed-dotted lines) and analytical solution (dashed lines) for case S-3.

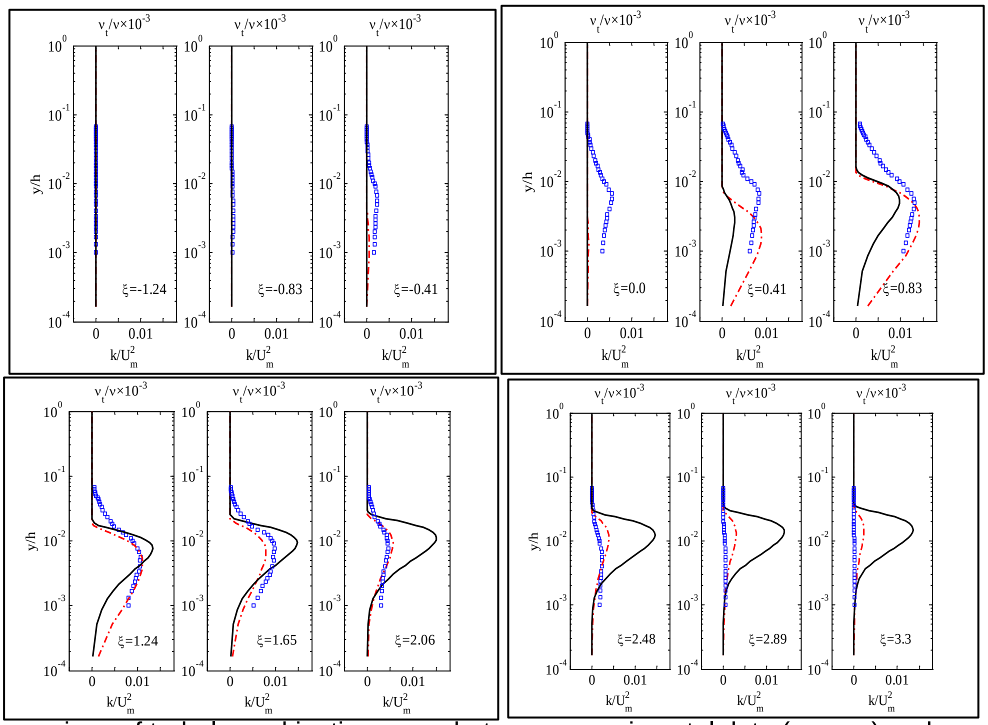

Figure 8. Comparison of turbulence kinetic energy between experimental data (square) and numerical results (dashed-dotted lines) for case S-3; solid lines represent calculated eddy viscosity.

5 CONCLUSIONS

In this study, we proposed a new way of finding wave-induced bed shear above a smooth bed by using velocity measurements within or in close vicinity of viscous sub-layer. The least-square method was used with the lowest three measured velocities to find the time-varying bed shear stress. The method is suitable to a wide range of unsteady flows with both laminar boundary layer and turbulent boundary layer over a smooth bed. Three experiments of solitary propagation over flat beds were conducted to represent both laminar and turbulent boundary layers, and the velocities were measured by using LDV. The bed shear stresses found from the experiments were compared to the numerical results and the theories. For laminar boundary layer cases, the numerical results of bed shear stress agreed well with the experimental data and both of them exhibit a phase lag when compared to the theories, possibly due to their relatively large Reynolds number, close to transitional flow regime. For turbulent boundary layer, the numerical results of bed shear is much larger than the theoretical solution and its phase difference from the main stream velocity is also much reduced.

Further analysis and discussions were made for turbulence characteristics inside the turbulent boundary layer above a rough bed under a solitary wave. The experimental data and numerical results were compared and it was found that the turbulence level stayed low during the accelerating phase and started to grow near the transitional stage from accelerating to decelerating. The trend of turbulence growth and decay predicted by the numerical model and measured in experiments was similar but the magnitude was not the same at all times. The calculated eddy viscosity inside the turbulent boundary layer showed that it was 10 times greater than the molecular viscosity during the decelerating stage and it caused a strong mixing and thicker boundary layer thickness, which in turn affected the velocity profiles and bed shear stress.

ACKNOWLEDGEMENTS

The works were supported, in part, by the Natural Science Foundation of China (No. 51479126, 51609211, 51479175, and 51679212) and Natural Science Foundation of Zhejiang Province, China (No. LR14E090002 and LR16E090002).

REFERENCE

Barnes, M.P., O'Donoghue, T., Alsina, J.M. & Baldock, T.E. (2009). Direct Bed Shear Stress Measurements in Bore-Driven Swash. *Coastal Engineering*, 56(8), 853-867.

Grimshaw, R. (1971). The Solitary Wave in Water of Variable Depth. Part 2. *Journal of Fluid Mechanics*, 46(03), 611-622.

Guard, P.A., Nielsen, P. & Baldock, T.E. (2011). Bed Shear Stress in Unsteady Flow. *Coastal Engineering Proceedings*, 1(32), 8.

Ippen, A.T. & Mitchell, M.M. (1957). *The Damping of the Solitary Wave from Boundary Shear Measurements,* (No. TR23). Massachusetts Inst of Tech Cambridge Hydrodynamics Lab.

Jensen, B. L., Sumer, B. M. & Fredsøe, J. (1989). Turbulent Oscillatory Boundary Layers at High Reynolds Numbers. *Journal of Fluid Mechanics*, 206, 265-297.

Jones, W.P. & Launder, B. (1972). The Prediction of Laminarization with a Two-Equation Model of Turbulence. *International journal of heat and mass transfer*, 15(2), 301-314.

Keulegan, G.H. (1948). Gradual Damping of Solitary Waves. *Journal of Research of the National Bureau of Standards*, 40(6), 487-498.

Lin, C., Yu, S.M., Wong, W.Y., Tzeng, G.W., Kao, M.J., Yeh, P.H. & Tsai, C.P. (2016). Velocity Characteristics in Boundary Layer Flow Caused by Solitary Wave Traveling over Horizontal Bottom. *Experimental Thermal and Fluid Science*, 76, 238-252.

Lin, C., Yu, S.M., Yeh, P.H., Yu, M.H., Tsai, C.P., Hsieh, S.C. & Raikar, R. (2015). Characteristics of Boundary Layer Flow Induced by Solitary Wave Propagating over Horizontal Bottom. *Journal of Marine Science and Technology*, 23(6), 909-922.

Lin, P. & Xu, W. (2006). NEWFLUME: A Numerical Water Flume for Two-Dimensional Turbulent Free Surface Flows. *Journal of Hydraulic Research*, 44(1), 79-93.

Lin, P. & Zhang, W. (2008). Numerical Simulation of Wave-Induced Laminar Boundary Layers. *Coastal Engineering*, 55(5), 400-408.

Liu, P.L.-F., Park, Y.S. & Cowen, E.A. (2007). Boundary Layer Flow and Bed Shear Stress under a Solitary Wave. *Journal of Fluid Mechanics*, 574, 449-463.

Menter, F.R. (1994). Two-Equation Eddy-Viscosity Turbulence Models for Engineering Applications. *AIAA journal*, 32(8), 1598-1605.

Pujara, N. & Liu, P.L.F. (2014). Direct Measurements of Local Bed Shear Stress in the Presence of Pressure Gradients. *Experiments in fluids*, 55(7), 1767.

Sumer, B.M., Jensen, P.M., Sørensen, L.B., Fredsøe, J., Liu, P.L.F. & Carstensen, S. (2010). Coherent Structures in Wave Boundary Layers. Part 2. Solitary Motion. *Journal of fluid mechanics*, 646, 207-231.

Tanaka, H. (2009). Numerical Modeling of Boundary Layer Flows for a Solitary Wave. *Journal of Hydro-environment Research*, 3(3), 129-137.

Tanaka, H., Sumer, B.M. & Lodahl, C. (1998). Theoretical and Experimental Investigation on Laminar Boundary Layers under Cnoidal Wave Motion. *Coastal Engineering Journal*, 40(01), 81-98.

Van der A, D.A., O'Donoghue , T., Davies, A.G. & Ribberink, J.S. (2011). Experimental Study of the Turbulent Boundary Layer in Acceleration-Skewed Oscillatory Flow. *Journal of Fluid Mechanics,* 684, 251-283.

Vittori, G. & Blondeaux, P. (2008). Turbulent Boundary Layer under a Solitary Wave. *Journal of Fluid Mechanics*, 615, 433-443.

Wilcox, D.C. (1988). Reassessment of the Scale-Determining Equation for Advanced Turbulence Models. *AIAA journal*, 26(11), 1299-1310.

Yuan, J. & Madsen, O. S. (2014). Experimental Study of Turbulent Oscillatory Boundary Layers in an Oscillating Water Tunnel. *Coastal Engineering*, 89, 63-84.

SOME LIKE IT HOT: STRATIFICATION, CIRCULATION AND TURBULENCE IN A SHALLOW, TROPICAL RESERVOIR

STEPHEN G. MONISMITH(1), EDMOND LO(2), XING ZIKUN(3), YANG PEIPEI(4), JAMES L. HENCH(5) & DEREK A. FONG(6)

(1,6) Department of Civil and Environmental Engineering, Stanford University, Stanford, California, USA, monismith@stanford.edu; dfong@stanford.edu

(2,4) Department of Civil and Environmental Engineering, Nanyang Technological University, Singapore, cymlo@ntu.edu.sg; yangpp@ntu.edu.sg

(3) Country Garden Holdings Company Limited, Tianjin, People's Republic of China, zkxing0010@gmail.com

(5) Duke University Marine Laboratory, Duke University, Beaufort, North Carolina, USA, jim.hench@duke.edu

ABSTRACT

In this paper we give an overview of field and computational work that we have carried out over the last decade in Kranji Reservoir (Singapore), studying the fundamental hydrodynamics of the reservoir. This includes studies of the basic circulation dynamics of the reservoir including motions generated by wind stresses, inflows, and by surface heat fluxes. A key feature of the reservoir is that there is nearly as much variation in temperature in one week as there is in one year. As a consequence, there are no discernible seasonal variations in stratification, and thus diurnal stratification variations play a central role in the hydrodynamics of the lake. For example, wind stresses force complex baroclinic motions that are not seiching because internal seiche periods are generally longer than the time over which stratification develops due to heating and then decays due to surface cooling. Inflow events, which are short-lived, usually lasting a few hours, and intense, bring relatively large volumes of colder water into the reservoir, creating the most stable and long-lived stratification. Because winds are generally relatively weak on the reservoir, flows driven by cooling of shallow regions may be an important mechanism for transporting materials from the shallow areas away from the dam, towards the deeper waters near the dam. Because the practical motivation for our work was concern over nutrient-driven eutrophication, particularly involving the cyanobacteria *Microcystis Aeruginosa*, much of our effort is focused on quantifying rates of vertical turbulent mixing using temperature microstructure profiling. While the near-surface structure of turbulent mixing (turbulent kinetic energy, dissipation rates, etc.) is well described by the existing concepts of surface mixed layer dynamics, more complicated and variable rates of mixing are observed below the mixed layer depending on the nature of the flows generated by cooling and by inflows. Nonetheless, consistent with observed stratification variations, vertical mixing is sufficiently rapid to ensure nearly complete vertical mixing throughout the water column every day, suggesting that given a very shallow photic zone, positively buoyant phytoplankton like *Microcystis* may be able to effectively compete with negatively buoyant ones like most diatoms. Overall, flows and the temperature structure in the reservoir appear to be quite three dimensional, suggesting that modeling transport processes in the lake requires a 3d model.

Keywords: Lakes; reservoirs; mixing; circulation; turbulence.

1 INTRODUCTION

For the most part, the study of lakes and reservoirs has focused on systems found at temperate latitudes. These are systems that generally have seasonal cycles of temperature stratification and thus exhibit motions and patterns of mixing that are best described as perturbations of the seasonal structure (Imberger and Patterson, 1990). In contrast, tropical lakes, especially ones that are shallow, have received substantially less attention despite their importance to water supplies throughout Asia as well as being important to ecosystems in their own right (Talling and Lemoalle, 1998; MacIntyre et al., 2002). The dynamics of these systems may differ substantially from temperate ones in that the forcing can be very different, e.g. intense tropical storms that generate large, intermittent and short-lived inflows, or the lack of a cold winter period to form cold bottom water. Notably, because primary production rates for many types of phytoplankton vary exponentially with temperature (Robarts and Zohary, 1987), many of these reservoirs, notably the large lake like Taihu in China (Paerl and Paul, 2002), experience significant water quality problems due to cyanobacteria blooms.

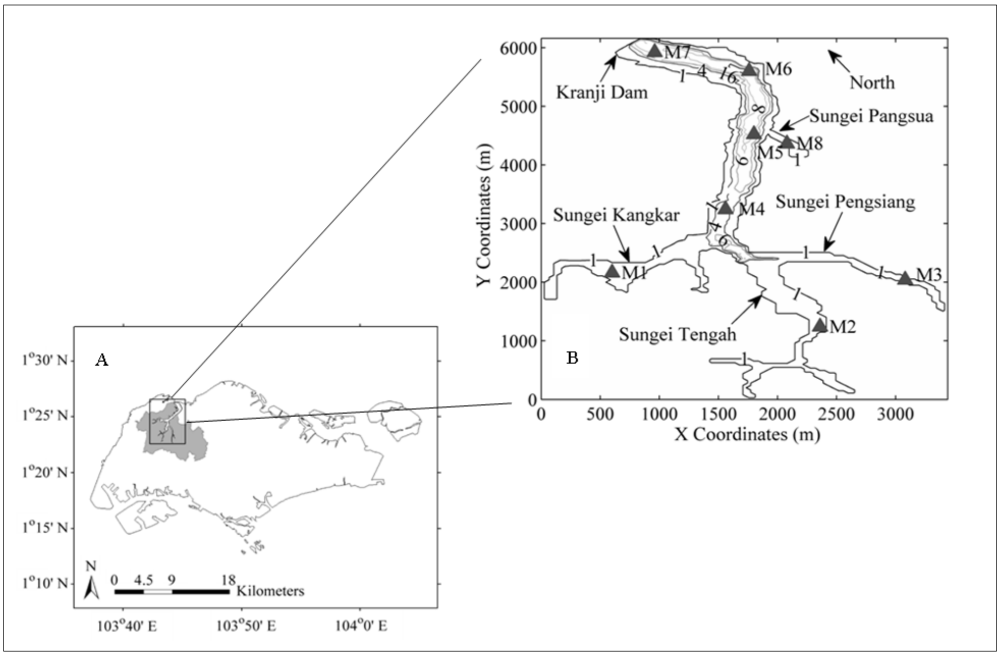

Figure 1: Kranji Reservoir location and instrument layout for 2006-2007 experiments (taken from Xing et al. 2014 –used w. permission of ASLO).

In this paper we focus on a shallow water supply reservoir, Kranji Reservoir, in Singapore (1° 25.155'N, 103° 44.223'E – figure 1) that has experienced episodes of high increase in cyanobacteria (principally *Microcystis Aeruginosa*) biomass since it went into operation (Xing et al., 2014a). The reservoir, which was created by damming of a small coastal inlet on the Strait of Johor, has a catchment that includes both light agriculture and dense urban areas typical of Singapore. Management of the reservoir by the Singapore Public Utilities Board (PUB) has included significant efforts to reduce nutrient inputs to the reservoir from the catchment as well as the operation of a system of aerators. As part of these management efforts, PUB initiated a series of studies of water quality improvement strategies for the reservoir using the ELCOM-CAEDYM coupled with 3D hydrodynamic-water quality models which was developed by the Centre for Water Research (CWR) in Western Australia (Romero et al., 2004; Xing, 2011; Xing et al., 2014a). Particular interest in modeling was shown due to the transport and fate of phosphorus entering the reservoir from inflows into several shallow upstream arms, and the role of stratification in the development of cyanobacteria blooms. Early examination of model results and comparison of limited temperature time series, suggested that flows in Kranji were complex and that stratification varied substantially on a daily time scale such that the usual conceptual models of reservoir dynamics, e.g. wind-generated internal seiching (Spigel and Imberger, 1980), were not applicable to Kranji. Thus, in an effort to improve model predictions and to aid in development of effective reservoir management strategies, a series of observational studies of currents, temperatures, and turbulent mixing was initiated in 2006 that continued through 2012. This work is described in Xing (2011) and Yang (2015), as well as in Xing et al. (2012; 2014b) and Yang et al. (2015). Here, we primarily use our spring 2006 study to illustrate the important aspects of the behavior of Kranji reservoir in response to heating, cooling winds, and inflows.

2 SITE AND METHODS

Kranji reservoir is about 3km long from the dame to the upstream end where three shallow arms join to the main body of the reservoir. It has an average depth of 5m and a maximum depth of nearly 20m, a surface area of 3 x 10^6m^2, and a volume of 1.6 x 10^7m^3 (Xing, 2011). Time series of temperature at multiple depths in the deepest part of the reservoir were acquired using various systems, including the CWR/ Precison Measurement Engineering (PME) Lake Diagnostic System, between 2004 and 2012 (Xing, 2011; Yang, 2015). These data show that seasonally variable average temperatures in the reservoir range between 27 (January) and 31 degree celcius (May), with the cooler "winter" period temperatures reflecting the effects of the cooler, wetter, and windier weather experienced between December and March due to the Northeast Monsoon (Xing, 2011; Figure 2). In general temperature stratification, varied between 0 and 4 degree celcius over the entire depth, where only in a few instances (spring, 2007) did stratification persist for more than a day. As seen in the long-term temperature time series as well as the shorter time variability we showed below, stratification due to diurnal heating was confined to the upper 2m of the water column due to the relative large shortwave radiation extinction coefficients (e.g. typically 2 to 4m^{-1}).

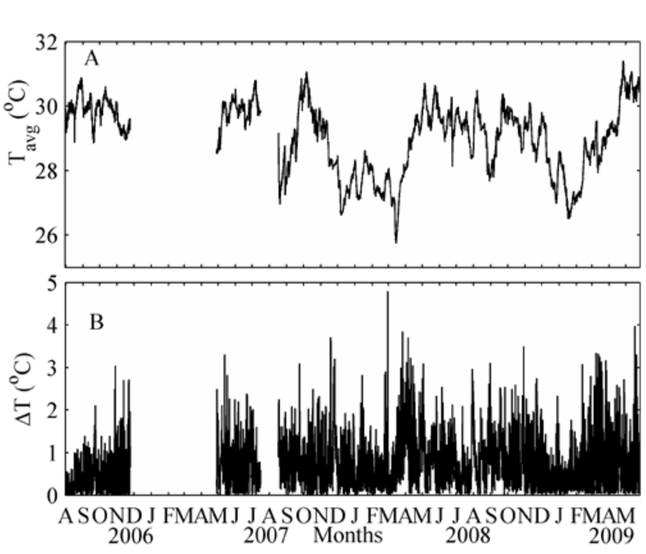

Figure 2. Depth averaged temperature and temperature stratification in the center of Kranji Reservoir 2006-2009 (taken from Xing 2011).

Four major field experiments were carried out: March-May 2006; April to June 2007; Sept. to Nov. 2011; and, July 2012. Details are given in Xing (2011) and Yang (2015). In each study different combinations of current meters and temperature recorders were deployed at stations along the axis of the lake and in the shallow side arms. For example, in the 2006 experiment, a 1 MHz Nortek Acoustic Doppler Profiler (ADP) was deployed near the center of the lake (sta. M5 in Figure 1) with Seabird SBE 39 thermistor loggers at 6 depths and a 2 MHz Nortek ADP with 4 SBE 39 loggers near the junction of the side arms and the main body of the reservoir (sta. M4). During experiments in 2007, 2011 and 2012, we also used several 1200 KHz Teledyne RDI Acoustic Doppler Current Profilers (ADCPs) and considerably more temperature loggers, including the newer Seabird SBE 56 loggers. In the 2007 experiment currents and temperatures were measured in the 3 upstream side arms using Nortek Vector Acoustic Doppler Velocimeters and SBE 39 temperature loggers. In all except the 2006 study, we also deployed a Campbell Scientific meteorological station on a raft on the lake, recording wind speed, wind direction, air temperature, humidity, and up and down-going short and long wave radiation.

In addition to mean flow measurements, on several occasions (23/24 April 2006; 22/23 and 29/30 Sept. and 5/6 Oct 2011; 11/12, 18/19, and 25/26 July 2012) for continuous 24 hour periods, we carried out turbulent microstructure profiling at the center of the lake using a PME Self Contained Microstructure Profiler (SCAMP – see MacIntyre et al., 2002). Rising at 10cm/s through the water column, SCAMP measures mm-scale variations in water properties including in particular, temperature. In this application, temperature was used to measure turbulence in several ways: (1) Direct computation of the rate of temperature variance dissipation, χ, from small-scale temperature gradients (Ruddick et al., 2000); (2) Fitting of temperature gradient spectra computed for ca. 0.5 to 1m data segments to the theoretical Batchelor spectrum to derive estimates of ε, the rate of turbulent kinetic energy dissipation (Luketina and Imberger, 2001); (3) Computation of the overturning (Thorpe) scale by rearrangement of observed "unstable" temperature profiles (Dillon, 1982).

3 DIURNAL TEMPERATURE VARIABILITY

The general variability of the temperature field in the reservoir throughout several week periods is seen in Figure 3, a plot of the vertically variable temperature near stations M5 and M4 during the 2006 study. Key features seen in Figure 3 that exemplify the behavior we have seen in all 4 studies are: (1) the formation of shallow diurnal stratification and (2) significant cooling of the reservoir due to a short-lived (ca. 1 day) cold inflow that started on day 105.

Comparing Figures 2 and 3, it is clear that distinct periods of heating and cooling over a few days produce nearly the full range of temperatures seen over the entire year. No doubt this only reflects the small annual temperature range experienced by Singapore as a whole.

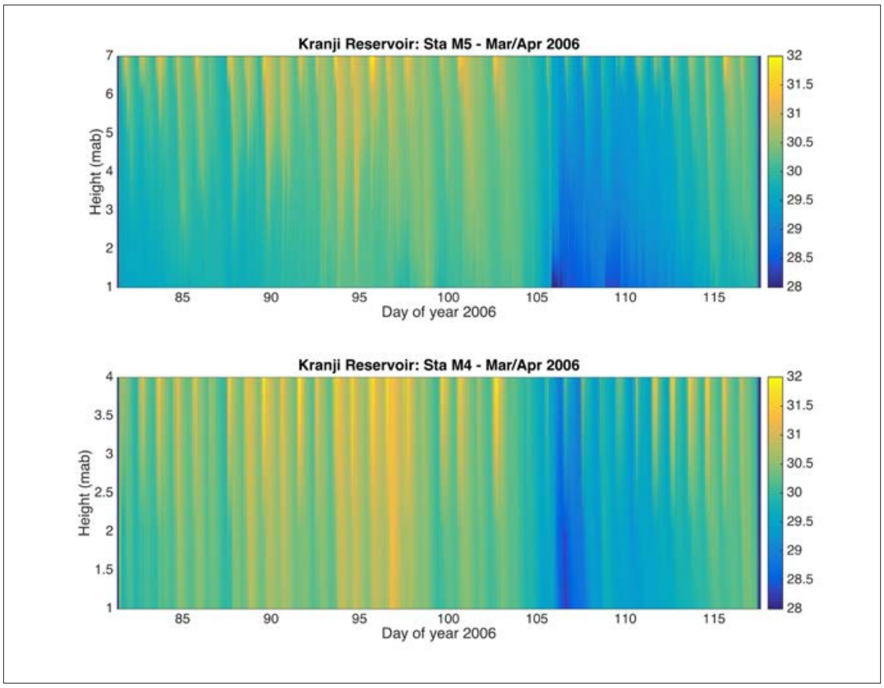

Figure 3. Temperatures in the water column during the 2006 Kranji study.

The shallowness of the near-surface mixed layer and its variability was best illustrated by examining one day in detail using the SCAMP temperature profiles since these offer far higher spatial resolution (Figure 4). Taken on approximately 15 minute intervals, these show the development of a 0 to 2m deep surface mixed layer from the morning through the late afternoon, that then was mixed down in the evening as the surface cools (Anis and Singhal, 2006). Interestingly, the water column appears not to be mixed completely, since at the end of the night, there remains a ca. 0.1 deg C temperature difference between the bottom and the surface. This behavior was somewhat different from the mixed layer dynamics of a temperate reservoir described in Imberger (1985), where a strong seasonal thermocline remains below the diurnal mixed layer throughout much of the year.

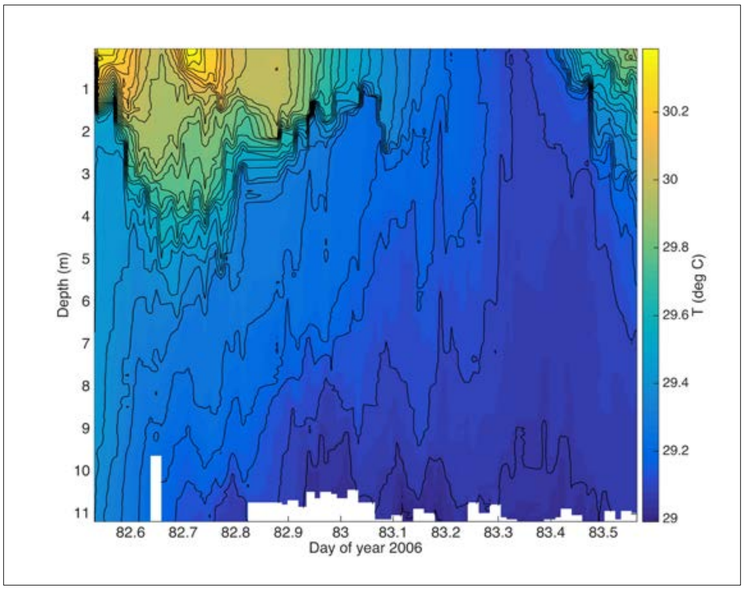

Figure 4. SCAMP-derived temperature variability over one 24 hour period.

An important aspect of the temperature field was that it also varies horizontally as well as vertically. Indeed horizontal temperature differences, particularly at the surface, were generally comparable to vertical ones (Figure 5; see also Xing et al., 2014b), suggesting that temperature driven flows might be an important feature of circulation in Kranji reservoir (Xing et al., 2014b; Yang 2015), as previously reported for the Wellington Reservoir in Western Australia (Monismith et al., 1990).

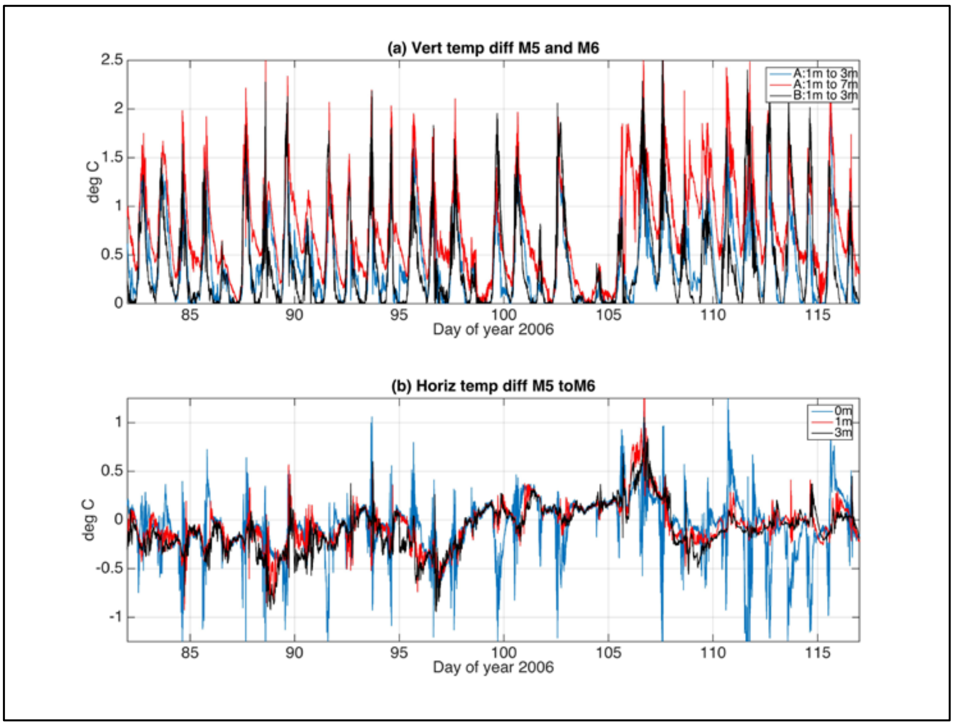

Figure 5. Vertical and horizontal temperature differences during the 2006 study.

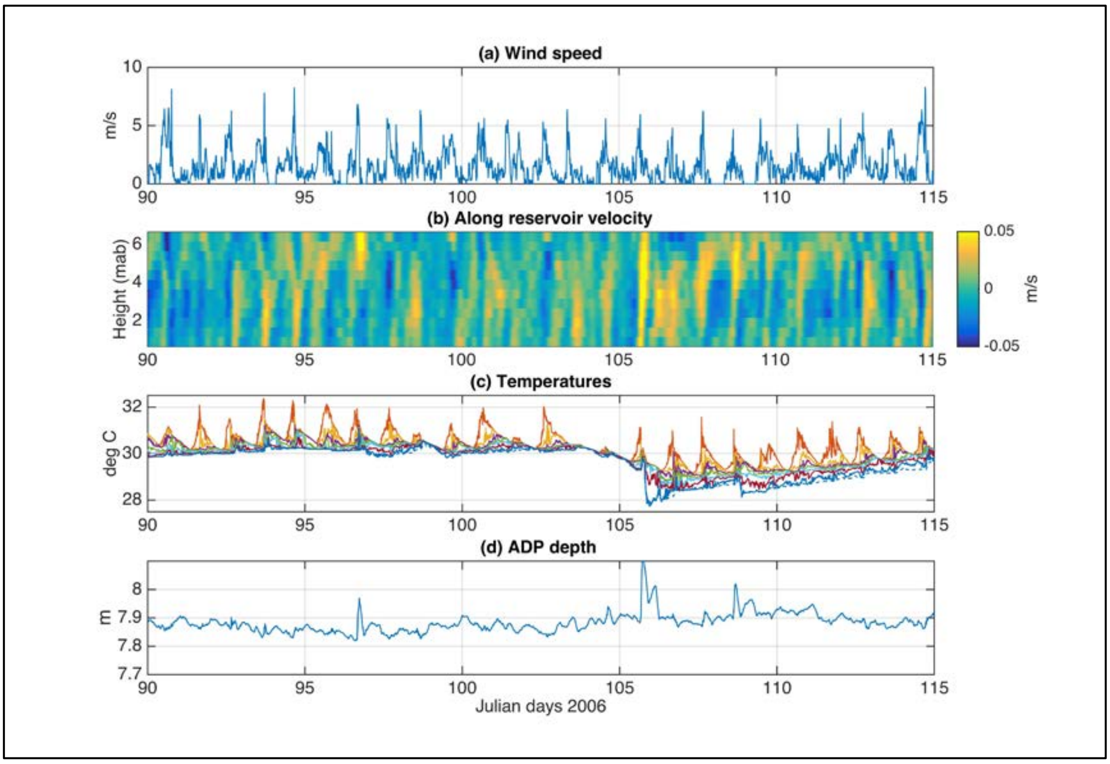

Figure 6. Winds, along reservoir velocities, temperatures, and depth near station M5 during 2006 study.

4 FLOWS

Flows observed during the 2006 study largely varied diurnally, albeit in a complex way (Figure 6). In part this was due to the fact that the stratification evolves on a time scale comparable to or even shorter than the first mode internal seiche period. The first mode seiche period can be calculated as (Spigel and Imberger, 1980)

$$T_i = \frac{2L}{\sqrt{\frac{g'h_1h_2}{H}}} \quad [1]$$

where L is the length of the reservoir, g' is reduced gravity based on the difference in density between two layers having thicknesses h_1 and h_2, and $H = h_1 + h_2$. In the present case L ≈ 3000m, a maximal value of g' ≈ 3 x 10^{-3}m^2/s, h_1 ≈ 2m and h_2 ≈ 6m, giving a lower bound on T_1 ≈ 90,000s (26h). Thus, seiching should not be part of the response of the reservoir to winds since the stratification develops and was eliminated on a timescale that was comparable to be shorter than the seiche period. Nonetheless, for winds that start suddenly and then are maintained, the maximum baroclinic velocity response in the center of the reservoir was expected to be at t ≈ Ti/4 ≈22,000s (6.5h), and so the initial response may resemble as derived by Spigel and Imberger. This can be seen in our velocity data, where the diurnal winds, which typically blow from the dam to the back of the reservoir (Xing, 2011), force near-surface flows away from the dam, also producing a flow towards the dam at depth, but there was generally no subsequent oppositely directed flow as expected for seiching. Spectral analysis of these velocities (not shown) confirms the existence of forced motions at diurnal frequencies and weaker responses at periods of 3 days and 12 hours, the former possibly representing the effects of weekly variations in weather.

A second striking feature was strong towards the dam flow seen near day 105/106. This represents a strong, cold inflow that dropped the reservoir temperatures overall by nearly 2 degrees and raised the water level by 10cm. Unlike inflow events in many temperate reservoirs, which can persist for days, or in the case of reservoirs fed by spring snow melt weeks, inflow events like that seen in Figure 6, for Kranji typically last only a few hours, and thus were more directly affected by diurnal surface forcing than their temperate counterparts (Xing et al., 2014; Yang, 2015). Note that the water level also dropped immediately afterwards due to reservoir gate operations that released water from the reservoir. As shown in Xing et al. (2012), data from our 2007 study, ADCP/ADP derived velocities can be used in conjunction with measured depths to infer reservoir water balances. Temperature measurements including thermal energy balances can also be carried out to assess the accuracy of measured and computed surface heat fluxes. This event also points to an important challenge with respect to long-term predictive modeling of reservoirs like Kranji. While inflow temperatures had a large effect on reservoir temperature, and watershed models can produce reasonably accurate values of inflows from precipitation, there does not appear to be any way currently to predict inflow temperatures of tropical reservoirs. In the present case, analysis of the 2007 study data, a case for which inflow temperatures, high frequency, local meteorological data, and catchment precipitation were all available, failed to show any obvious relationship between inflow temperatures and meteorological conditions.

As discussed by Xing et al. (2014), i.e., as seen in several of our Kranji studies, the overall response to inflows and surface forcing appears to depend on two parameters,

$$I_{IW} = \frac{Bh}{u_*^3 A_s} \quad I_{WB} = -\frac{u_*}{(B_s h)^{1/3}} \quad [2]$$

where B and B_s are the buoyancy fluxes associated with inflows and surface heating, A_s is the surface area of the reservoir, u_* is the wind stress, and h is the reservoir depth. For example, when $I_{IW} > 0.4$, the reservoir dynamics is dominated by the effects of cold inflows, whereas when $I_{IW} < 0.4$ (weak inflows) and $I_{WB} < 1$ (winds are weak), the primary response is the development of a near surface mixed layer. When $I_{WB} > 1$, circulation in the reservoir includes upwelling and relatively strong horizontal temperature gradients.

5 TURBULENT MIXING AND STRATIFICATION

A key measure of the stability of the reservoir water column is the gradient Richardson number,

$$Ri = N^2 / S^2 \quad [3]$$

where N^2 is the buoyancy frequency and S = ∂U/∂z is the vertical velocity shear. In general, in order for the flow to be turbulent, Ri should be < 0.25 (Turner, 1973), a result that was well supported by various direct numerical simulations of stratified shear turbulence (Holt et al., 1990). The temperature and velocity data shown in Figure 6 can be combined to calculate Ri at the measurement station, a result that was conveniently shown in terms of cumulative distribution functions (Figure 7). Examination of the variability of Ri shows that for much of the time, most of the water column at the measurement station was stable, i.e., even near the surface Ri was less than its critical value of 0.25 at 30% of the time. This suggests that in general vertical mixing in the reservoir was relatively weak, especially below the surface mixed layer. For example in the middle of the water column (z = 4.75 mab) Ri < 0.25 was only about 15% of the time. As discussed in Huisman et al. (1999), these were conditions that are ideal for dominance of cyanobacteria like *Microcystis*.

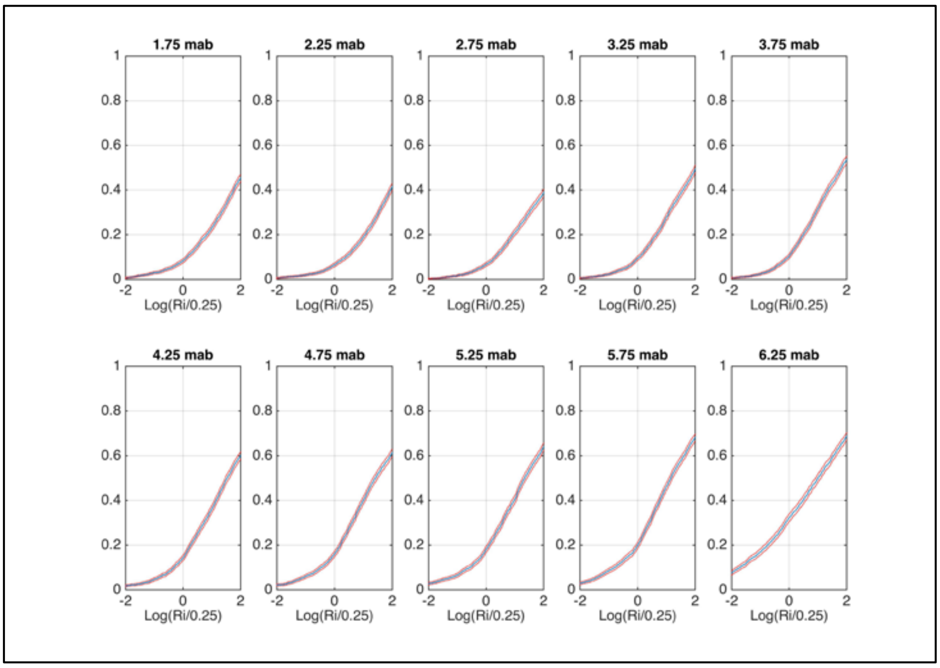

Figure 7. Cumulative distributions of Ri (fraction < specified value of Ri) near station M5.

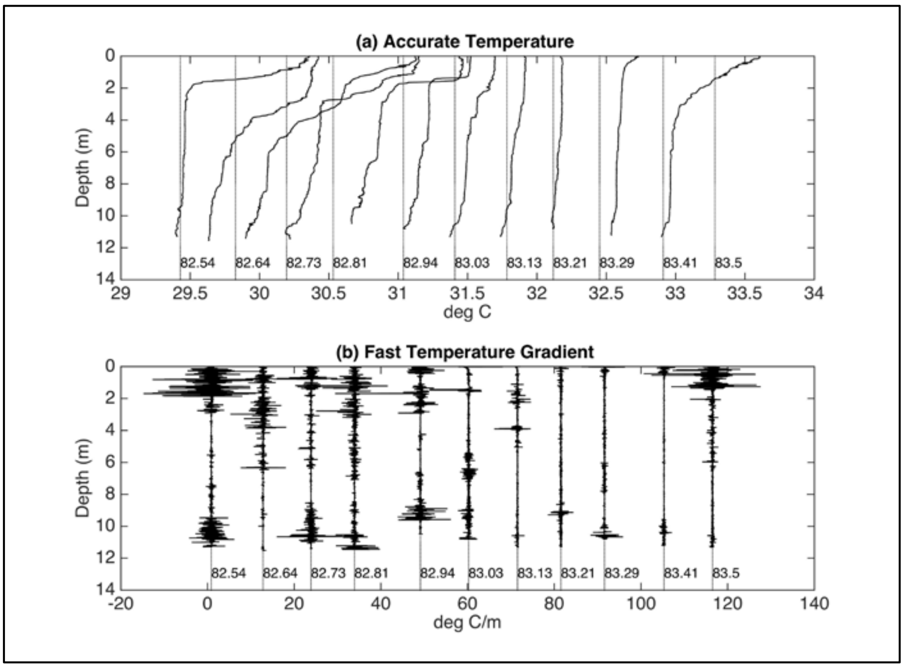

Figure 8. Microstructure-derived temperature and fine-scale temperature gradients during 2006 study. In panel (a), the vertical lines mark a temperature of 29.4 deg C for each profile (at times as indicated); in panel (b) the vertical lines mark $\partial T/\partial z = 0$.

It should be noted that since Ri is based on shear, it does not capture the effects of convection, as is observed at night. To better examine turbulence behavior, it was useful to examine the turbulence microstructure data. SCAMP profiles of temperature and temperature gradient (Figure 8), the latter an excellent indicator of turbulence, show the presence mid day (82.54) of a shallow mixed layer near the surface separated from the rest of the water column by a relatively strong thermocline. In this shallow layer, turbulence was active whereas below this layer in mid column, the flow was only intermittently turbulent. Rates of turbulence dissipation (e), derived from the SCAMP profiles (Figure 9) reinforce this view, with generally small values (O(10^{-9}) W/kg) below the surface mixed layer. In contrast, once convection was active over the entire depth, elevated dissipation rates (O(10^{-6}) W/kg) were seen throughout the water column. As noted in Yang et al. (2015), these elevated dissipation rates were consistent with other observations of convection (Anis and Singhal. 2006) with $\varepsilon \approx 0.6$ ($B_s h$).

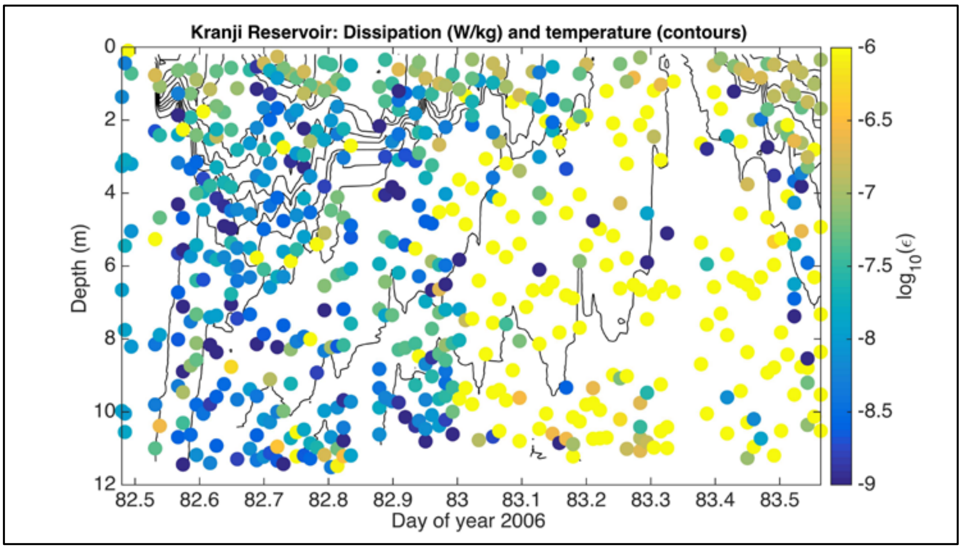

Figure 9. Microstructure derived turbulence dissipation rates during 2006 study. Temperature contours in 0.1 deg. increments between 29 and 30.3 deg. C are also shown.

6 THREE-DIMENSIONAL CIRCULATION MODELING

Observations of the thermal structure of Kranji show considerable spatial as well as temporal variability, such that a 1D model of thermal structure like DYRESM (Imberger and Patterson, 1990) would not be appropriate. Model runs were done with the 3D hydrodynamic code, ELCOM (Hodges et al., 2000), with various resolutions between 40m x 40m x 0.5m (x-y-z) to 10m x 10m x 0.2m (Yang, 2015). Examination of the 3D modeling showed that the flows at any section in the reservoir vary considerably across the width of the reservoir, with the appearance at times flows towards the dam along the western shore and towards the three-arm junction along the eastern shore (Figure 10).

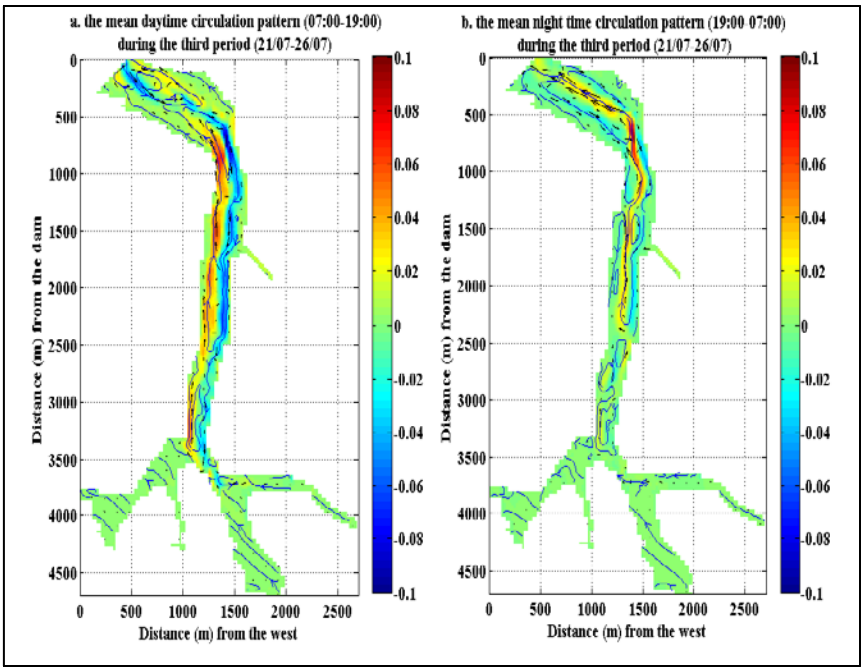

Figure 10. Depth-averaged flows computed for the 2012 study (Yang 2015).

In this regard, a particularly striking example of the importance of including three dimensions, and the ability of the model to capture complex variability, is shown in Figure 10. A comparison of the cross-sectional velocity variation was recorded by transecting with an ADCP mounted on a boat as a model output. In order to properly capture the weak currents, the ADCP transect took several hours, so velocity fields computed for different times must be used for the comparison. Remarkably, the model shows the same transverse structure as observed, in the concentration of flow towards the dam along the western shore of the reservoir with behavior that must represent similar variability in the temperature field.

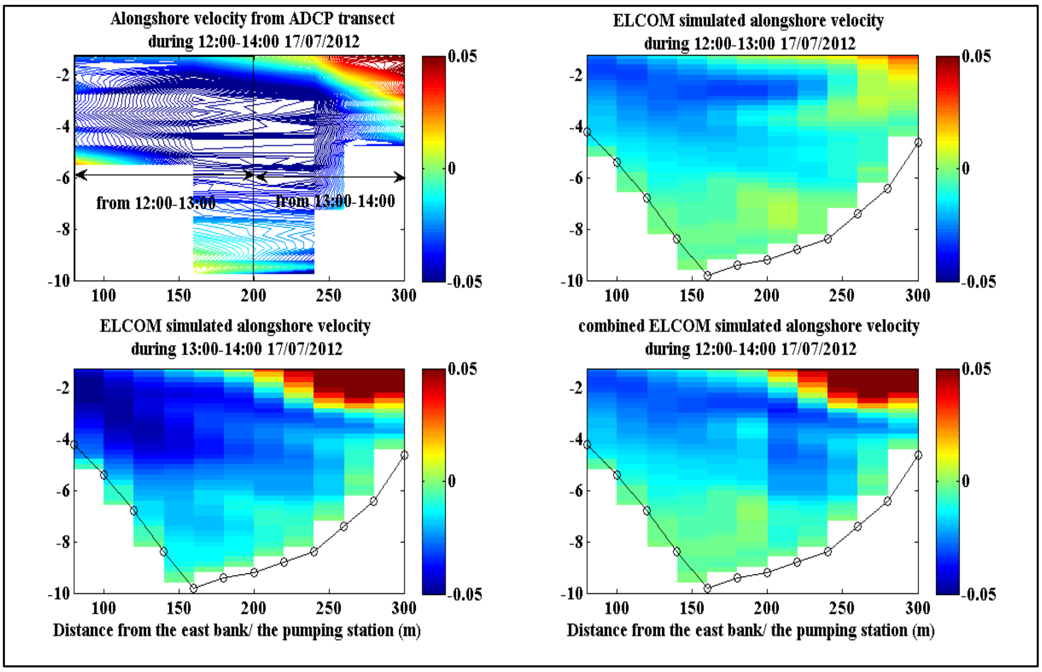

Figure 10. Cross-sectional variations in along-axis velocities from 2012 study and as modeled by ELCOM (taken from Yang, 2015). Velocities given in m/s.

As expected, increasing resolution improved the skill with which the model reproduced in observed flows. Temperature predictions were generally better than those for velocities, with correlation coefficients for computed and observed horizontal temperature differences. A measure of the combined effects of flows and surface forcing was being generally quite high with ca. 0.9, whereas correlation coefficients for velocities in the center of the reservoir were ca. 0.7. In part this may reflect the fact that the bathymetry data used for the model was of uncertain quality, having been derived from topographic maps of the reservoir area before filling. It also may reflect the limitations of the meteorological data where from experience it was clear that winds in the area around the three-arm junction were generally different than winds measured near the dam. On the other hand, a comparison of measured and computed velocities using empirical orthogonal functions (EOFs – c.f. Thompson and Emory 2000) was more encouraging in sense of structures, time variability and variances represented by the first 3 model and the observed EOFs were quite similar, suggesting that the model was capturing much of the essential physics of the reservoir flows.

7 CONCLUSIONS

In this paper we have presented an overview of the complex temperature, velocity and turbulence behavior we have observed in a series of studies of Kranji Reservoir in Singapore. These observations make clear that flows and temperature variability, where turbulent mixing differ somewhat from what is observed in temperate lakes. In particular, stratification formation and destruction takes place largely on a daily basis, with no formation of a seasonal thermocline. Short-lived intense inflows can also have a far more dramatic effect on reservoir structure and flows than in reservoirs where stratification varies seasonally. One caveat in this regard is the extent to which Kranji's polymictic behavior is primarily an effect of the shallowness of the reservoir (Rueda et al., 2003), as opposed to being an effect of the weakness of seasonal variations in surface heat fluxes. Thus, a comparison study of a temperate lake with similar dimensions, e.g. Pinto Lake, California (Kudela, et al., 2015) would be ideal.

From the practical engineering standpoint of predicting water quality in systems like Kranji, two things stand out from our work on Kranji Reservoir: (1) Three dimensional modeling with sufficient resolution must be used to resolve those flow structures responsible for horizontal materials within the reservoir and proper forcing data are also necessities; (2) Even then, observations of flows and temperatures are also needed to assess model fidelity, and thus to establish confidence and to define the uncertainty in model predictions. Moreover, an important open question is that of what sets reservoir inflow temperatures for inflows associated with the intense convective storms seen in places like Singapore.

ACKNOWLEDGEMENTS

This work was supported by the Singapore Stanford Partnership, and was made possible by the generosity of the Public Utilities Board (PUB) of Singapore who provided access to the reservoir as well as logistic support during equipment deployment and retrieval. Various students from NTU and Stanford helped with the field work, including Vamsi Sridharan, Kristen Davis, Steve Davis, and the students in SSP 262e class. The authors would also like to thank the laboratory technicians at the Hydraulics Laboratory of the School of Civil and Environmental Engineering, Nanyang Technological University, for their help in building mooring hardware.

REFERENCES

Anis, A. & Singhal, G. (2006). Mixing in the Surface Boundary Layer of a Tropical Freshwater Reservoir. *Journal of Marine Systems*, 63(3), 225-243.

Dillon, T.M. (1982). Vertical Overturns: A Comparison of Thorpe and Ozmidov Length Scales. *Journal of Geophysical Research,* 87(C12), 9601-9613.

Emery, W.J. & Thomson, R.E. (2001). *Data Analysis Methods in Physical Oceanography*. Elsevier Press.

Holt, S.E., Koseff, J.R. & Ferziger, J.H. (1992). A Numerical Study of the Evolution and Structure of Homogeneous Stably Stratified Sheared Turbulence. *Journal of Fluid Mechanics*, 237, 499–539.

Hodges, B.R. (2006). Numerical Error Assessment and a Temporal Horizon for Internal Waves in a Hydrostatic Model. *Ocean Modelling*, 13(1), 44-64.

Huisman, J., van Oostveen, P. & Weissing, F. (1999). Critical Depth and Critical Turbulence: Two Different Mechanisms for the Development of Phytoplankton Blooms. *Limnology and Oceanography*, 44(7), 1781-1787.

Imberger, J. (1985). The Diurnal Mixed Layer. *Limnology and Oceanography*, 30(4), 737-770.

Imberger, J. & Patterson, J.C. (1989). Physical Limnology. *Advances in Applied Mechanics,* 27, 303-475.

Kudela, R.M., Palacios, S.L, Austerberry, D.C., Accorsi, E.K., Guild, L.S. & Torres-Perez, J. (2015). Application of Hyperspectral Remote Sensing to Cyanobacterial Blooms in Inland Waters. *Remote Sensing of Environment*, 167, 196-205.

Luketina, D.A. & Imberger, J. (2001). Determining Turbulent Kinetic Energy Dissipation from Batchelor Curve Fitting. *Journal of Atmopheric and Oceanic Technology*, 18(1), 100-113.

MacIntyre, S., Romero, J.R. & Kling, G.W. (2002). Spatial-Temporal Variability in Surface Layer Deepening and Lateral Advection in an Embayment of Lake Victoria, East Africa. *Limnology and Oceanography*, 47(3), 656-671.

Monismith, S.G., Imberger, J. & Morison, M.L. (1990). Convective Motions in the Sidearm of a Small Reservoir. *Limnology and Oceanography*, 35(8), 1676-1702.

Paerl, H.W. & Paul, V.J. (2012). Climate Change: Links to Global Expansion of Harmful Cyanobacteria. *Water Research*, 46(5), 1349-1363.

Robarts, R.D. & Zohary, T. (1987). Temperature Effects on Photosynthetic Capacity, Respiration, and Growth Rates of Bloom-Forming Cyanobacteria. *New Zealand Journal of Marine and Freshwater Research*, 21(3), 391-399.

Romero, J.R., Antenucci, J.P. & Imberger, J. (2004). One- and Three-Dimensional Biogeochemical Simulations of Two Differing Reservoirs. *Ecological Modelling*,174(1), 143-160.

Ruddick, B., Anis, A. & Thompson, K. (2000). Maximum Likelihood Spectral Fitting: The Batchelor Spectrum. *Journal of Atmospheric and Oceanic Technology*, 17(11), 1541-1555.

Rueda, F.J., Schladow, S.G., Monismith, S.G. & Stacey, M.T. (2003). Dynamics of Large Polymictic Lake. I: Field Observations. *Journal of Hydraulic Engineering*, 129(2), 82-91.

Spigel, R.H. & Imberger, J. (1980). The Classification of Mixed-Layer Dynamics in Lakes of Small to Medium Size. *Journal of Physical Oceanography,* 10(7), 1104-1121.

Talling, J.F. & Lemoalle, J. (1998). *Ecological Dynamics of Tropical Inland Waters*. Cambridge University Press.

Turner, J.S. (1973). *Buoyancy Effects in Fluids*. Cambridge University Press.

Xing, Z. (2011). Thermal Structure and Hydrodynamics of a Shallow Tropical Reservoir. *PhD Thesis*, School of Civil and Environmental Engineering, Nanyang Technological University.

Xing, Z., Fong, D.A., Tan, K.M., Lo, E.Y.M. & Monismith, S.G. (2012). Water and Heat Budgets of a Shallow Tropical Reservoir. *Water Resources Research* 48(6)**,** doi:10.1029/2011WR011314.

Xing, Z., Chua, L. & Imberger, J. (2014a). Evaluation of Management Scenarios for Controlling Eutrophication in a Shallow Tropical Urban Lake. *International J. of Environmental Pollution and Remediation*, 2(2), 66-72.

Xing, Z., Fong, D.A., Lo, E.Y.M. & Monismith, S.G. (2014b). Thermal Structure and Variability of a Shallow Tropical Reservoir. *Limnology and Oceanography,* 59(1), 115-128.

Yang, P. (2015). Vertical Mixing and Flow Patterns in a Tropical Shallow Lake. *PhD Thesis*, School of Civil and Environmental Engineering, Nanyang Technological University.

Yang, P., Xing, Z., Fong, D.A., Monismith, S.G., Tan, K.M. & Lo, E.Y.M. (2015). Observations of Vertical Eddy Diffusivities in a Shallow Tropical Reservoir. *Journal of Hydro-environment Research*, 9(3), 441-451.

A SMART CITY WITHOUT SMART WATER IS ONLY A PIPE DREAM!

DRAGAN SAVIC[1]

[1] Centre for Water Systems, University of Exeter, North Park Road, Exeter, EX4 4QF, United Kingdom,
d.savic@exeter.ac.uk

ABSTRACT

More than half of the world's population lives in a city, and this proportion is projected to grow over 70 percent by 2050. Critical infrastructure systems, including water, energy and transport systems, are essential in ensuring the wellbeing of the population. Protecting critical infrastructure and ensuring continued and efficient operation is and will be an important part of future sustainable cities and 'Smart City' ecosystems. However, water infrastructure systems are often overlooked when 'Smart City' initiatives are considered. This may be due to several factors, including the centralised 'top down' approach to provision of water services by an 'invisible utility', disengagement of citizens who often feel that their individual actions are insignificant compared with actions of the utility, or simply our inability to properly harness the power of new technologies to better manage urban water systems. This paper addresses some of those Smart City issues, provides a summary of important information and communication technologies and how they fit with the 'smart water' infrastructure concepts. Illustrative examples of some smart water technologies and their use in water system management are also shown. The initially slow uptake of smart water technologies is changing due to the shift in attitudes of people in charge of urban water management, better understanding of the potential of these new technologies to improve water service delivery and emergence of new water industry leaders trained in hydroinformatics. The role of hydroinformatics is identified in increasing understanding (knowledge) of both utility managers (top down) and citizens (bottom up) and in developing and applying modelling tools that support integrated decision-making and citizen engagement.

Keywords: Smart cities; smart water; infrastructure; hydroinformatics; management.

1 INTRODUCTION

In 1900, only 15 percent of the world's population lived in cities (Spence et al., 2008). However, the pace of urban population growth accelerated rapidly in the 1950s so that about 100 years later over half of the world's people lives in cities. Critical infrastructure, including water, energy and transport systems, is essential in ensuring the wellbeing of that population. Infrastructure provision is also related to ensuring that human settlements are environmentally sustainable and resilient, socially inclusive, safe and violence-free, and economically productive (Habitat, 2016). Therefore, protecting critical infrastructure and ensuring continued and efficient operation is and will be an important part of making future cities sustainable.

Nowadays, the use of information and communication technologies (ICT) and the emergence of the Internet of Things (IoT) could support a much more 'symbiotic' relationship between city governments, citizens and businesses. The assumption is that digital sensors, home appliances, smart phones and wearable smart devices, which form the backbone infrastructure of IoT, will encourage collaboration between various city stakeholders and engagement of citizens. Availability and use of open data - that anyone can access, use or share – will also increase opportunities for collaboration and engagement. These prospects have contributed to the rise of the 'Smart City' concept, where ICT (and IoT) are used to enhance a city's liveability, workability and sustainability (Smart Cities Council, 2017). Although there is no universally agreed definition of a Smart City, the idea is in line with the 2030 agenda for the UN Sustainable Development Goal 11 (SDG 11) to make cities and human settlements inclusive, safe, resilient and sustainable (UN, 2017).

It is not surprising, then, that ICT infrastructure is the focus of most Smart City initiatives. Various predictions for growth in the IoT and machine-to-machine markets have been staggering. Considering that 4.9 billion IoT devices were in use in 2015, the estimates for 2020 range from 20.8 billion to 75 billion (Hosain, 2016)! Following on from the IoT infrastructure as the key enabler, transport and economic development have been identified as top ranked challenges by city governments, as reported by Alizadeh (2017). He conducted a survey of 130 urban governments involved with IBM's Smart Cities Challenge to understand their main areas of interests. Smart mobility and transport have been on the agenda of most governments as they affect numerous aspects of the Smart City, impact on citizens' quality of life and involve all stakeholders expecting benefits from the Smart City implementation (Benevolo et al., 2016). Like IoT and transport, smart energy has been one of the dominant topics for Smart Cities. According to Schwarz (2012) energy in a Smart City relies on a smart, sustainable and resilient energy system built in an integrated planning approach for energy planning, active buildings, smart grids, smart supply technologies with inclusion of regional renewable sources, and sustainable mobility. This complexity and interconnectivity with transport systems makes energy provision a significant challenge for future Smart Cities.

Although part of urban critical infrastructure, water and wastewater systems are often overlooked when Smart Cities are considered or discussed, there may be quite a few reasons for that, but one probable reason is the so-called ‘Big Water’ phenomenon, a term coined by Sofoulis (2005). It indicates the dominant sociotechnical system for municipal water supply and wastewater disposal. This is a system that involves a centralised public or corporatised utility, which assumes almost complete responsibility for the supply of drinking quality water and for disposal of wastewater. Because of that, there is a lack of public concern and awareness of responsibility for managing water resources, which is also reflected in low engagement with the utility and an unwillingness to pay for water services. Water utilities, by their own nature, are also designed to be ‘invisible’ – ‘out of sight, out of mind’. This is emphasised by citizens, on average, spending very little time in direct contact with utility staff, with this generally being either concerning billing issues or following a problem with their service. The disengagement is also attributed to actions at an individual citizen level being insignificant as compared to actions on the utility side when, for example, maintaining infrastructure to fix leaks (Energy Saving Trust, 2015).

Hydroinformatics (also known as Water Informatics or Water Information Engineering) has grown rapidly in recent years and seeks to take full advantage of the proliferation of remotely sensed information from space and ground based sensors with increasing capabilities in terms of spatial, temporal and spatial resolution. Hydroinformatics is not only aimed at increasing understanding (knowledge) of utility managers, but also that of citizens and at developing and applying modelling tools that support integrated decision-making and citizen engagement. This paper addresses first the place of smart water management in the context of Smart Cities, including water supply/distribution and wastewater/urban drainage systems. It then introduces some of the key ICT technologies relevant to smart water systems, followed by examples of smart water and wastewater applications. Finally, discussion and conclusions are also provided.

2 SMART WATER MANAGEMENT IN SMART CITIES

The basic premise of a smart water utility, as defined by Ingildsen and Olsson (2016), is a simple framework which suggests that water utilities must embrace the “MAD” approach to enable smart water management. The acronym stands for ‘measure’ (M), ‘analytics’ (A) and ‘decision-making’ (D). The framework emphasises that the focus should be: (i) having good spatial and temporal data via field measurements; (ii) understanding and analysing the data collected; and (iii) using those findings for sound decision-making. To be an active part of a Smart City, a water utility has also to re-engage with its citizens as water users. This is contrary to a ‘perfect utility’ doctrine, which is achievable only if it and its activities are ‘invisible’ to the users.

This section deals with the two main areas of the urban water cycle: (i) water supply and distribution (so called ‘clean’); and (ii) wastewater and urban drainage (so called ‘dirty’) systems. The key issue discussed in the reminder of the paper, which applies to both areas of the water cycle, is the capacity of urban infrastructure systems to provide services at a required quality level. Although space limitations prevent providing an exhaustive list of smart water issues and technologies, the paper will identify some of the key elements of smart water management systems. This inevitably means that some of the equally important areas will be missing. For example, the paper focuses only on smart technologies for centralised (as opposed to distributed) provision of water/wastewater services, does not deal explicitly with smart technologies for water quality management in the urban water cycle and does not cover all elements of the cycle, such as water and/or wastewater treatment, where substantial potential for smart management can also be achieved.

2.1 Water supply and distribution systems

Providing capacity to satisfy demand for water is the key to sustainable water management and to satisfying urban water needs now and in the future. Supply-side and/or demand-side management are the two approaches at the opposite ends of water management options. The former focuses on making more water resource available for use, while the latter involves water conservation and increased water use efficiency, thus reducing the need for new resources.

Demand Management – Supply-side water management has been dominating water management strategies in cities. As population changes, climate variability and accelerated urbanisation start to increase pressure on water resources, meaning fewer opportunities for large infrastructure projects to provide more resources. Additionally, more stringent regulation will also mean that fewer resources will be available for consumption, thus requiring more work being done on demand-side management. Smart water systems have traditionally been focusing on smart water utility networks, which are a set of products, solutions and systems that enable utilities to remotely and continuously monitor and diagnose problems, prioritize and manage maintenance issues and use data to optimize all aspects of the water distribution network (Sensus, 2017). Until recently, this definition has appeared to focus on supply-side management. This also means that it excludes citizens, *i.e.*, even when customer meters are available, they are read only once or twice per year, or at best monthly, thus not allowing for users’ engagement with the water utility. This is in line with smart monitoring (involving devices that allow continuous electronic reading, transmittal and display of the water consumption) traditionally having been focused on the supply side, *i.e.*, at major facilities and input points to the system with the main aim of monitoring leakage in the distribution system or billing bulk customers, rather than on the demand side, at the user's premises (Savić et al., 2014). The recent trend of introducing smart water metering brings the opportunity for domestic customers to better understand their consumption and for utilities to get a better handle on household water demand. Smart City ICT will provide an opportunity not only for the water utilities to better manage their systems, but also a prospect of engaged citizens becoming fully aware of the value of water and their own role in urban water management.

Energy Management - A report by the UK Energy Saving Trust (2013) indicates that, of all the CO_2 emissions in the country, 6% are from water use. The majority (89%) come from heating water in homes, while the remaining 11% come from pumping and treating water as part of the supply and sewage network. A similar split between utility and household contributions to greenhouse gas emissions has been reported in the USA (Griffiths-Sattenspiel and Wilson, 2009), where heating water in homes amounts to 58% of the total country's energy usage, while 21% is attributed to water utilities. However, most of the research on smart water systems has been focusing on how to manage energy usage in water utility networks. For example, Mala-Jetmarova et al. (2017) provide a review of over a hundred publications on improving pump operation that appeared in research literature, whereas domestic energy usage for heating water (for activities such as baths, showers, washing up and water-using electrical appliances), has been largely neglected. Understanding water demand in households and how managing demand can help reduce its energy usage is, therefore, equally if not more important than how to reduce energy usage in smart water networks.

Water Loss (Leakage) Management - Leakage is an important element of water 'demand' in water supply distribution systems. It is estimated that about 45 billion litres of water are lost through leakage, which according to the World Bank report (Kingdom et al., 2006), costs utilities approximately $14 billion per annum. However, few citizens are aware that a significant proportion of the leakage occurs on customer-owned underground supply pipes. For example, around 25% of 'total leakage' reported by UK water companies is attributed to customer-side leakage. With more sensing technology being deployed in water distribution networks, together with the increased focus on smart water metering at the point of usage, the potential for smart analytics to improve water management in the effort to reduce leakage and associated costs of water loss, energy usage and active leakage control, can be significant.

2.2 Wastewater and urban drainage systems

Providing capacity to transport wastewater (sewage) from houses and commercial buildings to treatment or disposal is the main purpose of sewer systems. Combined systems also collect rainwater runoff, which together with domestic sewage and treated industrial wastewater, they are then transported to a wastewater treatment plant before releasing it back to the environment. Their structural integrity and functional efficiency are key to the continued safeguard of public health in terms of the effective conveyance and treatment of domestic and commercial effluents mixed with rainwater runoff. As with water supply and distribution systems, functional efficiency of these systems can be increased by providing more capacity or better utilisation of the existing network, which is akin to supply-side management in clean water systems. On the other hand, reducing the need for additional capacity through demand-side management represents an alternative that can also engage citizens in the urban water cycle.

Sewer Flood Management – Preventing flooding from sewers is a key activity for municipality and water utility managers around the world. When the capacity of a combined sewer system is exceeded, usually during heavy rainfall events, either or both flooding and discharge of untreated wastewater through combined sewer overflows (CSO) can occur. Therefore, providing enough capacity in wastewater systems is a key requirement for managing sewer flood risk. Sewer flooding can also happen due to failures in the wastewater network such as blocked or collapsed pipes, which points to the need for efficient and effective maintenance of these systems. However, these failures cannot be eliminated totally, which points to the need to identify the most at-risk wastewater assets and assess the risk of sewer flooding their failures may cause. Sustainable Drainage Systems (SuDS) are drainage components that can help mitigate sewer capacity problems by storing or re-using rainwater (surface water) at source and by decreasing flow rates to watercourses (Butler and Parkinson, 1997). Additionally, they can be useful for treating rainwater to improve water quality. Therefore, combined with smart ICT systems (Melville-Shreeve et al., 2016), SuDS have not only the potential to reduce the risk from sewer flooding and CSO spills, but also to integrate various Smart City sustainability activities and enhance public and environmental health.

Sewer Infiltration Management – Infiltration occurs when groundwater or sea water gets into wastewater systems through cracks and other defects in sewer pipes. This additional water in the pipes reduces their capacity for collecting, storing and transporting wastewater flows, thus increasing risk of flooding and CSO spills. Infiltration also decreases the pollutant removal efficiency of wastewater treatment plants (Karpf and Krebs, 2011) and, in the case of sea water infiltration, causes serious corrosion of pipes and production of harmful gases, such as hydrogen sulphide (Long, 1994). Groundwater and sea water infiltration, in particular, accelerates pipe degradation and increases the chance for exfiltration, thus allowing wastewater to cause additional harm to the environment. Quantifying and localising sewer infiltration is a complex problem and requires high spatial and temporal resolution of flow measurements in the system (Karpf and Krebs, 2011). Smart measurements and analytics offer an alternative approach to intensive and costly flow surveys often used to assess sewer infiltration.

3 ICT TECHNOLOGIES FOR SMART WATER MANAGEMENT IN SMART CITIES

Without attempting to be exhaustive about technological advances underpinning smart water management in Smart Cities, this section provides some of the basic ICT technologies required not only by water but also by other infrastructure systems. The technologies covered include the Internet of Things (IoT), smart sensors, machine learning, big data analytics, data visualisation, gamification and cloud computing services.

3.1 Internet of Things (IoT)

With the Internet becoming more widely available, the cost of connecting to it decreasing, and more Wi-Fi enabled products and embedded devices (such as sensors, actuators and smartphones), technology costs are going down. This has led to the proliferation of the Internet of Things devices (and associated technologies and products), which involves networks of connected machines and sensors with the ability to monitor and manage physical objects electronically (Bughin and Chui, 2017). This is highly relevant for Smart Cities, where the objective of the IoT could be seen to support added-value services for citizens and giving utilities more opportunities to innovate using the latest ICT technologies. It is natural then to envisage the use of IoT in also providing enhanced water service to citizens and engaging them more with service providers.

3.2 Smart sensors

Sensors are used widely by water and wastewater service providers in cities around the world to collect information about their infrastructure and its performance. A sensor device that possess some ‘intelligence’ (including via a Central Processing Unit), is called a “smart sensor” (Brajović and Kanade, 2004). This integration of sensing and processing can result in an adaptive sensing system that can make fully or semi-autonomous decisions with change in environmental conditions. Smart sensing is also a crucial and integral part of IoT.

3.3 Machine learning and big data analytics

Big data is normally associated with extremely large datasets that cannot be handled in tolerable elapsed time with the traditional data analytic methods (Chen and Han, 2016). The main reason for that is that big data is characterised by three main features, *i.e.,* “three Vs”: volume, variety and velocity. It is obvious that data volume is the primary attribute of big data, which is often reported in terabytes (10^{12} bytes), petabytes (10^{15} bytes) or even larger quantities. Owing to the large number and types of sensors being used for data collection, big data often comes from a great variety of sources. Availability of data in real or near real-time makes its velocity (or speed - the frequency of data generation or the frequency of data delivery) an important attribute. However, these features of big data – massive, high dimensional, heterogeneous, complex or unstructured, incomplete, noisy, and erroneous – have seriously challenged traditional statistical approaches, which are mainly designed for analysing relatively smaller samples (Berman, 2013).

Big data analytics can be viewed as advanced techniques operating on massive amounts of data to reveal hidden patterns and hard to see correlations, which in turn support decision-making or value generation. These analytic methods are closely aligned with the definition of machine learning, a multidisciplinary field of computer science, statistics, artificial intelligence and information theory, particularly suitable for exploiting information hidden in big data (Ratner, 2011). These methods include many different approaches, including but not limited to classification, regression, clustering, feature selection, dimensionality reduction, ensemble learning, network analysis, density estimation (Sugiyama, 2015).

3.4 Visualisation and gamification

Data visualisation is the presentation of data in a pictorial or graphical format, making it one of the most valuable means through which humans make sense of data - and big data, in particular. Historically, this probably started with the emergence of maps and graphs in the 17^{th} century, progressing to today’s ability to visualise large amounts of data via computing technology. Even with the advances in machine learning for big data analytics, visualisation makes analysis more approachable to most people. However, visualisation is normally accessible to a small community of scientists and data enthusiasts, which prevents it from being widely used. To engage a much broader section of citizens in a Smart City beyond only scientists, something else is needed – the entertainment element. Gamification of and provision of ‘serious games’ for water management and related issues, can be a valuable tool for engaging citizens. Serious games, which are games used for purposes other than mere entertainment, can and will make citizens and various stakeholders more aware of the socio-techno-economic issues related to managing complex water systems (Savić et al., 2016). Through an example of a serious game, Savić et al. (2016) show how a visually-rich application with an

  / ISSN 1562-6865 (Online) - ISSN 1063-7710 (Print)

intuitive user interface can help even non-experts (students, in their case) approach a solution to a water management problem only previously achieved by experts employing sophisticated optimisation tools.

3.5 Cloud computing services

The US National Institute of Standards and Technology (NIST) defines cloud computing as “a model for enabling ubiquitous, convenient, on-demand network access to a shared pool of configurable computing resources (*e.g.,* networks, servers, storage, applications, and services) that can be rapidly provisioned and released with minimal management effort or service provider interaction” (Mell and Grance, 2009). The key here is that instead of having to rely on fixed hardware resources (*e.g.,* a single or networked group of computers within an office or organisation), a user can quickly scale up to using multiple resources without the need to upgrade his/her own hardware. This ‘virtualisation’ allows for massive scalability, giving users virtually unlimited resources for much less cost.

4 EXAMPLES OF SMART WATER AND WASTEWATER APPLICATIONS

4.1 Smart water metering for demand management of household consumption

Smart meters have been widely applied and evaluated for demand management in the context of domestic energy use. Sønderlund et al. (2016) report that there is solid evidence for the efficacy of so-called smart feedback methods in managing energy use, with reductions in consumption ranging from 5 to 20%. They also show that results for smart water meters and their effectiveness in curbing water consumption vary between 2.5 and 28.6% in various studies, therefore indicating the real potential for smart-meter technology to curb domestic water use. The uptake of smart domestic metering by the water industry is lagging the energy sector. However, this is slowly changing, with water utilities in the UK having to face restrictions in water availability and increases in demand. For example, Thames Water would face a supply shortfall of 133 million litres (Ml) per day by 2020 or even 416 Ml per day by 2040 (Figure 1), if the situation with demand increases continued its trend (Thames Water, 2014). That is why they have embarked on a smart metering installation programme that will see 414,000 smart water meters installed in London by 2020, which by 2025 would mean that they will have to deal with 35 billion meter reads per year.

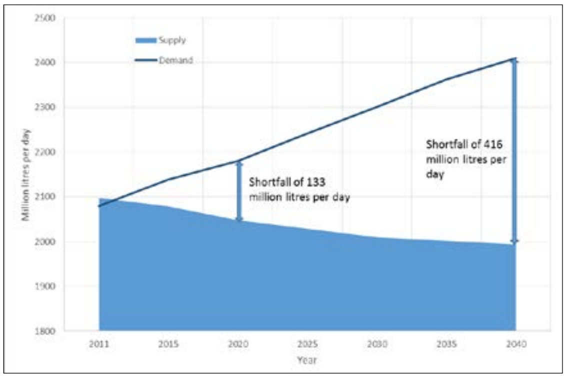

Figure 1. Forecast gap between supply and demand in London (Thames Water, 2014).

Availability of such large quantities of data invites a question of how this ‘big data’ can be best analysed for the tasks of quantifying, estimating and forecasting water consumption. Owing to the complex stochastic nature of water demands, those tasks are typically performed and models used in a deterministic context (Cutore et al., 2008). Creaco et al. (2015; 2016a; 2016b) used data obtained during the iWIDGET FP7 project (Savić et al., 2014) to develop a probabilistic household demand model at high time resolution, from 1 minute up to 15 minutes, or coarse time resolution, *i.e.,* daily demand. When properly calibrated, these models can be used to generate consistent demand associated with a single household or a group of households. Figure 2 shows a result of one of the experiments performed by Creaco et al. (2016b). The figure demonstrates how a frequency distribution of 100 synthetically generated demand series (upper and lower envelopes and the average values) fits the measured consumption data.

Spatial and temporal aggregation of the demand pulses through the “bottom-up” approach then enables proper assessment of nodal demands for water distribution network modelling, which is then used to better characterise hydraulic models used for operational purposes (Creaco et al., 2017).

The iWIDGET project (http://www.i-widget.eu/) dealt with the management and extraction of useful information from vast amounts of high-resolution consumption data, the development of customised intervention and awareness campaigns to influence behavioural change, and the integration of iWIDGET concepts into a set of decision-support tools for water utilities and consumers, applicable in differing local conditions. To meet these aims and challenges, iWIDGET investigated:

(i) how best to provide the dynamic accurate measurement and data transfer of useful information about end-user water consumption;
(ii) how best to use consumption data to improve the operation of utilities and influence end-users to modify their behaviour;
(iii) how to arrive at the best business model to convert a promising technology into a useful and cost-effective product; and
(iv) how to demonstrate and validate the new methodologies on three case studies: in the North (UK), South (Portugal) of Europe, as well as a pilot case study in Athens (Greece).

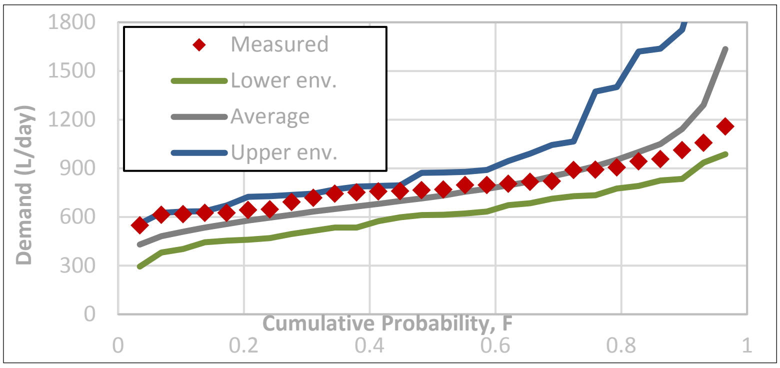

Figure 2. Generated Weibull cumulative frequencies F of daily water demand as compared to the calculated daily water demand cumulative frequency obtained from the measured data.

The iWIDGET prototype system (Kossieris et al., 2014), which has been implemented and was fully operational from September 2014 to February 2016, supports decisions at both the household and utility levels. It analyses the usage pattern of individual households and presents data, analytical results, comparisons and feedback. Screenshots of the main interface and some information provided to individual users are given in Figure 3, Figure 4 and Figure 5. The iWIDGET system provides households with information about their water (Figure 3) and energy usage (Figure 4), compares it to others (Figure 5) and offers customised suggestions on how to reduce use and take advantage of current pricing schemes, through an e-learning platform.

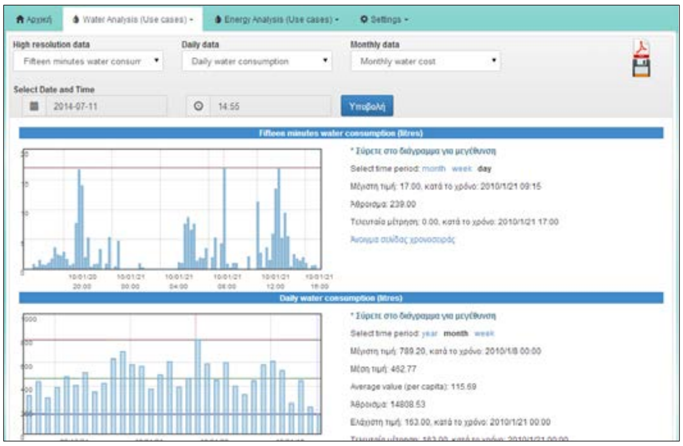

Figure 3. iWIDGET water use information for a household.

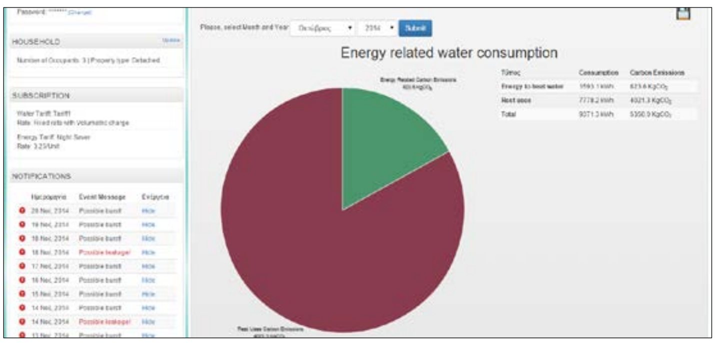

Figure 4. iWIDGET energy use information for a household.

  / ISSN 1562-6865 (Online) - ISSN 1063-7710 (Print)

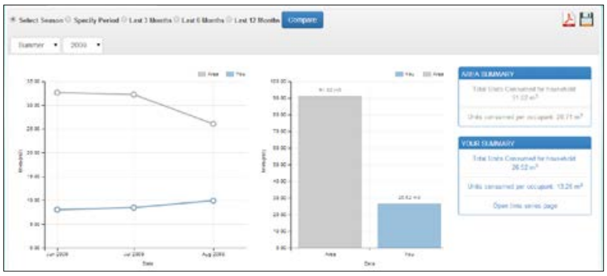

Figure 5. iWIDGET screen showing comparison of water consumption in a household with the average consumption in the area.

For the utilities, the system provides information to help with the development of water pricing, demand forecasting and demand management. It can also assist with the design of intervention options and awareness campaigns customised to the requirements of householders and utilities, taking advantage of state-of-the-art thinking on behavioural change processes in the social sciences, by applying agent-based modelling techniques.

4.2 Smart water metering for leak detection in water networks

Water lost through leakage can often be a significant component of the demand in water distribution networks. As pressure increases on water utilities to tackle water loss, there is a growing need for methods to enable fast and economic detection of pipe bursts and other anomalous flows in water systems (Romano et al., 2014a; 2014b).

Laucelli et al. (2016) demonstrated a soft computing and machine learning based system for using near real-time data (provided through hydraulic sensor technology and on-line data acquisition systems), for detection of pipe bursts in a water distribution system. The reasons why such a system has been selected are that: (i) it is a self-learning system requiring only a limited number of data/patterns and being able to deal with often patchy, poor-quality data; (ii) it can extract useful information (required for making reliable operational decisions) from the vast and often imperfect sensor data collected by modern Supervisory Control And Data Acquisition (SCADA) systems; (iii) it does not need expensive high frequency measurements; (iv) it requires limited manual or semi-manual interpretation of the results obtained; and (v) it only relies on the empirical observation of a water distribution system behaviour over time (*i.e.*, no network modelling is needed).

The burst prediction system uses the Evolutionary Polynomial Regression (EPR) strategy (Savić et al., 2009; Berardi and Kapelan, 2007; Berardi et al., 2014) to develop a data-driven prediction model of water consumption using values recorded over a few past weeks (*i.e.*, time windows), each of which is treated as a separate data set. The machine learning model returns a range of predictions for the water consumption in a distribution system given the pressure/flow measurements at a small number of points in the network. For example, Laucelli et al. (2016) demonstrate this approach on 41 weeks of flow and pressure data collected every 15 minutes at the inlet of a District Metering Area (DMA). The EPR model then returns 41 consumption predictions (ΔF) for each time step. Based on those results, a probability distribution can be developed for predictions at each time step. Figure 6 shows the results of the model application to a day when hydrant manipulation was applied to simulate a leak in a real system. The solid centre line represents the average of 41 predictions, the dotted lines represent the upper and lower limits and the circles represent actual measurements. The measured data is compared to models' prediction range to detect abnormal/unexpected changes in consumption. This approach considers the history of the water consumption habits of the customers in the DMA. The red coloured circles represent possible anomalies/pipe bursts, the yellow circles represent consumption above the expected/average value, but still no cause for alarm, while green circles represent measurements within the expected range. The approach also allows the estimation of a possible amount of water volume lost through the burst, which is an output of the methodology.

However, even with the latest developments in sensing technologies and promising results of various anomaly detection methodologies, diagnosing and locating problems in a DMA due to a burst pipe remains a challenging task due to inherent uncertainties (*e.g.*, stochastic nature of water consumption and lack of field data) (Savić et al., 2013). The Neptune Project (Savić et al., 2008) developed and tested new methodologies supporting near real-time decision-making for operators of water distribution systems dealing with a variety of anomalies (pressure and flow) with a primary focus on pipe bursts.

These methods require considerable information inflow, hence a prototype Decision Support System (DSS) was developed to analyse, process and present data efficiently, allowing the operator to reach timely, informed decisions. The DSS consists of: (i) an alarm monitor; (ii) a likelihood evaluator; (iii) an impact evaluator; (iv) an alarm ranking procedure; and (v) a visualisation interface – front end (Savić et al., 2013). The alarm monitor periodically checks for new (fresh) alarms and in the event of an alarm being generated by the pipe burst detection module, the monitor performs the necessary initialisation steps (*e.g.*, forecasting water demands, setting hydraulic model boundary conditions, etc.) before the risk assessment can be started. The Likelihood evaluator is assigning probability of pipe burst location to every pipe within a DMA where an alarm is generated (Bicik et al., 2011). To evaluate the impact of a failure of any pipe in a DMA, hydraulic and water quality simulations need to be performed to calculate several performance indicators (*e.g.*, cost of lost water, duration of low pressure impact, discolouration potential, etc.) for each of the pipes. The impact of significant failures needs to be evaluated at system level since it is likely to affect other DMAs in the network. The alarm ranking procedure then considers the likelihood and impact to rank alarms based on criticality. Finally, the front end presents an overview of the real-time state of the entire water distribution system through a prioritised list of all alarms (*i.e.*, detected anomalies) as well as through using a GIS interface (Figure 7).

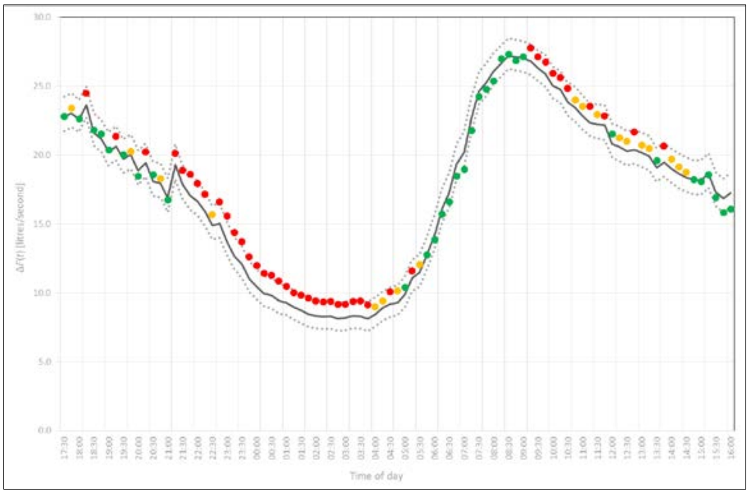

Figure 6. One day diagram representing predicted average and upper/lower limits with measured flows (Laucelli et al., 2016).

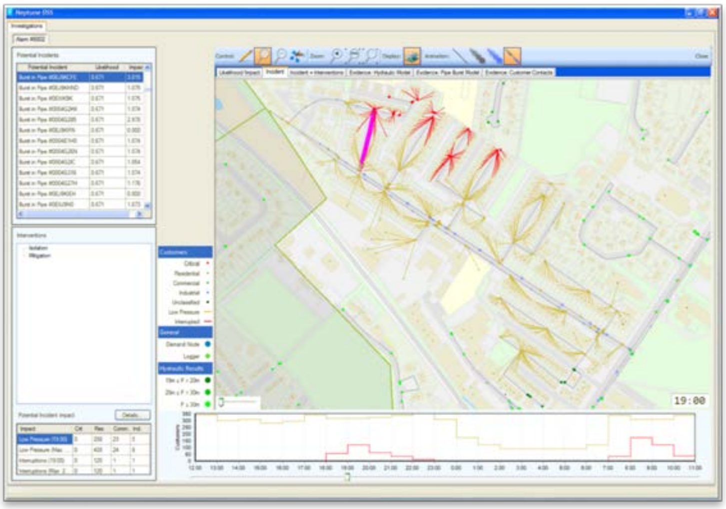

Figure 7. Neptune DSS Alarm Diagnostics user interface (Savić et al., 2013).

4.3 Early warning system for sewer flood management

Reliable models are required to predict location, severity and/or risk of sewer flooding in cities. To be used for operational purposes, these need to provide a reasonable lead-time (often measured in hours). Hydraulic models can be used to model the response of combined sewer systems to rainfall events and provide that operational information. However, for large networks, these can be slow and computationally expensive, thus not fit for purpose in case of needing near real-time response. Based on that, there are two distinct approaches that can be used to provide an early warning system for sewer flooding events, employing much more computationally efficient hydraulic models or machine learning methods. For either of those approaches further simplifications could involve disregarding complex linkages between the sewer network and the terrain above. The following two approaches have been tested and proven possible: fast overland flood modelling and data-driven (machine learning) sewer surcharge modelling.

To achieve computationally efficient overland flood modelling for urban scale problems, a two-dimensional (2D) cellular automata (CA) model, CADDIES (Cellular Automata Dual-DraInagE Simulation), was developed by Ghimire et al. (2013) and then further improved by Guidolin et al. (2016). CADDIES employ simple transition rules rather than complex Shallow Water Equations to model 2D flooding in urban areas. The simplified feature of cellular automata allows the model to be implemented in parallel environments (*i.e.*, multi-core CPUs and graphic cards GPUs), resulting in significantly improved modelling efficiency. Further refinements of the methodology show that in dense urban areas the CA model applied on regular square grids offers process speed increases between 5 and 20 times above that of the industry standard software using irregular triangular meshes, while maintaining 98 – 99% flooding extent accuracy (Gibson et al., 2016).

Duncan et al. (2011) demonstrate the use of an alternative approach, RAPIDS (RAdar Pluvial flooding Identification for Drainage System), where machine learning methodology is used to predict flooding in sewer systems. A faster surrogate method based on Artificial Neural Networks (ANN) has been developed, which enables modelling of very large networks in real-time, without unacceptable degradation of accuracy. Due to the lack of measured data of urban flooding events, the industry benchmark modelling software is used as a surrogate for providing 'real' information on urban sewer system performance at manholes, CSOs and outfalls. ANN models are then developed to predict performance at these key points of interest for any rainfall loading condition and these predictions are compared to benchmark results, which are treated as 'ground truth' for the purposes of the study.

In their study, Duncan et al. (2011) applied the approach to three catchments in the UK. The rainfall input to ANN was single-peak design storms, with a matrix of design storm events created in line with standard UK procedures. For flooding manholes, the target data were depth and flood volumes. Figure 8 compares the performance of ANN with respect to the targets as a 'confusion matrix'. It shows how many counts the ANN correctly predicts surcharge and how many times it correctly predicts flooding according to three depth categories (A = below soffit; B = between soffit and basement flood level; C = above basement flood level).

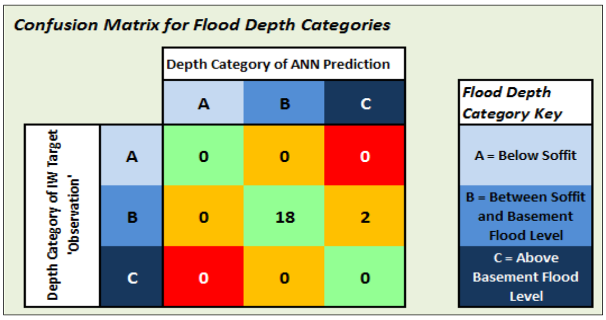

Figure 8. An example catchment confusion matrix for total of 20 sewer manholes, for depth category of peak for a 50-year return period, 1-hour duration design rainfall event (UKWIR, 2012).

4.4 Sewer infiltration management

Infiltration is an ongoing issue for water companies and detecting it can be a time-consuming and expensive activity. Walker and Savić (2017) investigated the use of a machine learning (data driven) model based on ANNs to model infiltration using measured water temperature in combined sewers. Distributed temperature sensing has been shown to produce a good indication of spatial location of infiltration and inflow sources in sewer systems (Panasiuk et al., 2016). However, although effective, their approach using fibre-optic cables is expensive for use throughout a large sewer system. An alternative is to use small self-contained temperature sensors that record time, date and temperature at user defined intervals. In the case study by Walker and Savić (2017), all loggers were set up with a logging interval of five minutes, but data were downloaded once a month.

The first part of the analysis involves the development of a benchmark model for dry-weather situations, *i.e.*, when infiltration is expected to be minimal. This model is then compared to the wet-weather situation to assess the contribution of infiltration to increased flows in sewers. However, the flow measurements are expensive, thus only pump run times (as a surrogate for flows) in the sewer have been available. The model is based on temperature and rainfall inputs as follows:

(i) rainfall for the current day;
(ii) antecedent rainfall, aggregated over the last several days; and
(iii) temperature aggregated over the current 24-hour period. Preliminary results indicate that the use of cheap temperature sensors/loggers with machine learning methods can provide a good indication of the location and amount of infiltration in sewers.

5 DISCUSSIONS AND CONCLUSIONS

The expected growth in population, sensor numbers, data volumes (particularly open data) and ICT technologies undoubtedly open a myriad of opportunities for Smart Cities to become more liveable, workable, resilient and sustainable. Critical infrastructure systems, including water, energy and transport systems, are and will be essential in ensuring the wellbeing of the urban population. Protecting critical infrastructure and ensuring continued and efficient operation is and will be an important part of future sustainable cities and Smart City ecosystems. However, water infrastructure systems are often overlooked when Smart City initiatives are considered. This may be due to several factors, including the centralised 'top down' approach to provision of water services by an 'invisible utility', disengagement of citizens who often feel that their individual actions are insignificant compared with actions of the utility, or simply our inability to properly harness the power of new technologies to better manage urban water systems. One thing is certain – water is and should be a key element of the Smart City concept.

ICT and related technologies, including IoT, smart sensors, machine learning, big data analytics, visualisation, gamification and cloud computing, have until recently been out of reach of the people involved in managing water systems in our cities. This is slowly changing due to the shift in attitudes of people in charge of urban water management, better understanding of the potential of these new technologies to improve water service delivery and emergence of new water industry leaders trained in hydroinformatics.

Hydroinformatics, which requires understanding of both water systems (including hydraulics and hydrology) and ICT technologies, can help city planners, managers and citizens take advantage of the proliferation of remotely sensed information from space and ground based sensors with increasing capabilities in terms of spatial, temporal and spectral resolution. Hydroinformatics deals with the intersection of 'big data' with 'smart technologies' to deliver more sustainable water solutions at various scales, enabling innovation through evidence-based insight. This new discipline can and should also empower citizens to engage with water service provision through a 'bottom up' approach, *i.e*., at an individual level. However, for our society to take full advantage of leading-edge technologies we need to develop a new breed of specialists: hydroinformaticians, scientists and engineers capable of working at the interface of traditionally separate informatics, science and engineering disciplines to manage effectively the information and water systems. Educational and research programmes, such as the Centre for Doctoral Training in Water Informatics: Science and Engineering (WISE CDT www.wisecdt.org) in the UK, or Hydroinformatics courses offered by institutions such as UNESCO-IHE (Delft, the Netherlands), promise to fill the skills gap by offering postgraduate courses that foster new levels of innovation and collaboration and train cohorts of engineers and scientists at the boundary of water informatics, science and engineering.

Although limited in scope and numbers, the examples of smart water and wastewater applications provided in this paper illustrate the potential of ICT technologies to help water managers keep pace with the level of data that is generated from measurement instruments in the field. They also provide opportunities to develop new ways of using data, which has not been previously possible, *e.g*., water temperature sensing for sewer infiltration assessment or 2D modelling for flood assessment at large scales. It is not just water managers and utilities that will benefit from smart technologies finding their way into Smart Cities, but also their citizens. For example, near-real-time information about household water and energy usage, instantaneous feedback and customised suggestions on how to reduce use and take advantage of current pricing schemes, empower and engage citizens in managing their own water and energy use. This is turn can help utilities better manage demand for their services and prolong the life of water infrastructure.

ACKNOWLEDGEMENTS

The author would like to acknowledge the Engineering and Physical Sciences Research Council (Grants: EP/M018865, EP/L016214, EP/H015736, EP/E003192), UK Water Industry Research and European Commission (iWIDGET project, grant: 318272) for financial support. The author is also thankful to a number of past and present colleagues and co-workers from the Centre for Water Systems at the University of Exeter for their contribution to the tools and studies presented in this paper.

REFERENCES

Alizadeh, T. (2017). An Investigation of IBM's Smarter Cites Challenge: What do Participating Cities Want?. *Cities*, 63, 70-80.

Angelidou, M. (2016). Four European Smart City Strategies. *International Journal of Social Science Studies*, 4(4), 18-30.

Benevolo, C., Dameri, R.P. & D'Auria, B. (2016). Smart Mobility in Smart City. In *Empowering Organizations,* 13-28.

Berman, J.J. (2013). *Principles of Big Data: Preparing, Sharing, and Analyzing Complex Information*. Elsevier, Morgan Kaufmann.

Bicik, J., Kapelan, Z., Makropoulos, C. & Savić, D.A. (2011). Pipe Burst Diagnostics Using Evidence Theory. *Journal of Hydroinformatics*, 13(4), 596-608.

Brajović, V. & Kanade, T. (2004). When are Smart Sensors Smart? An Example of an Illumination-Adaptive Image Sensor. *Sensor Review*, 24(2), 156-166.

Bughin, J. & Chui, M. (2017). The Internet of Things: Assessing Its Potential and Identifying the Enablers Needed to Capture the Opportunity, In *Internet of Things in the Modern Business Environment,* 111-125, IGI Global.

Butler, D. & Parkinson, J. (1997). Towards Sustainable Urban Drainage. *Water Science and Technology*, 35(9), 53-63.

Chen, Y. & Han, D. (2016). Big Data and Hydroinformatics. *Journal of Hydroinformatics*, 18(4), 599-614.

Creaco, E., Farmani, R., Kapelan, Z., Vamvakeridou-Lyroudia, L. & Savic, D. (2015). Considering the Mutual Dependence of Pulse Duration and Intensity in Models for Generating Residential Water Demand. *Journal of Water Resources Planning and Management*, 141(11).

Creaco, E., Alvisi, S., Farmani, R., Vamvakeridou-Lyroudia, L., Franchini, M., Kapelan, Z. & Savic, D. (2016a). Methods for Preserving Duration–Intensity Correlation on Synthetically Generated Water-Demand Pulses. *Journal of Water Resources Planning and Management*, 142(2).

Creaco, E., Kossieris, P., Vamvakeridou-Lyroudia, L., Makropoulos, C., Kapelan, Z. & Savic, D. (2016b). Parameterizing Residential Water Demand Pulse Models through Smart Meter Readings. *Environmental Modelling & Software*, 80, 33-40.

Creaco, E., Pezzinga, G. & Savic, D. (2017). On the Choice of the Demand and Hydraulic Modelling Approach to WDN Real-Time Simulation. *Water Resources Research,* (in review).

Cutore, P., Campisano, A., Kapelan, Z., Modica, C. & Savic, D. (2008). Probabilistic Prediction of Urban Water Consumption Using the SCEM-UA Algorithm. *Urban Water Journal*, 5(2), 125-132.

Duncan, A.P., Chen, A.S., Keedwell, E.C., Djordjevic, S. & Savic, D. (2011). Urban Flood Prediction in Real-Time from Weather Radar and Rainfall Data Using Artificial Neural Networks. Weather Radar and Hydrology, In *Proceedings of a Symposium Held in Exeter, UK, (IAHS Publ. 351, 2012)*, 568-573.

Economist (2017) Liquid Gold - Companies are Racing to Add Value to Water. http://www.economist.com/news/business/21719511-sales-bottled-water-overtook-those-soft-drinks-america-last-year-companies-are-racing, (last accessed on 12/04/2017).

Energy Research Knowledge Centre (2014). *Energy Research Challenges for Smart Cities*, European Union. https://setis.ec.europa.eu/energy-research/sites/default/files/library/ERKC_PB_Smart_Cities.pdf (last accessed on 12/04/2017).

Energy Saving Trust (2013). *At Home with Water*, Technical Report. http://www.energysavingtrust.org.uk/sites/default/files/reports/AtHomewithWater%287%29.pdf (last accessed on 17/04/2017).

Energy Saving Trust (2015). *At Home with Water 2*, Technical Report. http://www.energysavingtrust.org.uk/sites/default/files/reports/AHHW2%20final.pdf (last accessed on 17/04/2017).

Ghimire, B., Chen, A.S., Guidolin, M., Keedwell, E.C., Djordjević, S. & Savić, D.A. (2013). Formulation of a Fast 2D Urban Pluvial Flood Model Using a Cellular Automata Approach. *Journal of Hydroinformatics*, 15(3), 676-686.

Gibson, M.J., Savic, D.A., Djordjevic, S., Chen, A.S., Fraser, S. & Watson, T. (2016). Accuracy and Computational Efficiency of 2D Urban Surface Flood Modelling Based on Cellular Automata. *Procedia Engineering*, 154, 801-810.

Griffiths-Sattenspiel, B. & Wilson, W. (2009). *The Carbon Footprint of Water,* River Network Report. https://www.csu.edu/cerc/researchreports/documents/CarbonFootprintofWater-RiverNetwork-2009.pdf (last accessed on 17/04/2017).

Guidolin, M., Chen, A.S., Ghimire, B., Keedwell, E.C., Djordjević, S. & Savić, D.A. (2016). A Weighted Cellular Automata 2D Inundation Model for Rapid Flood Analysis. *Environmental Modelling & Software*, 84, 378-394.

UN-Habitat (2016). *Urbanization and Development Emerging Futures*, World Cities Report 2016. https://unhabitat.org/wp-content/uploads/2014/03/WCR-%20Full-Report-2016.pdf (last accessed on 12/04/2017).

Hanemann, M. (2005). The Value of Water. *Manuscript,* University of California at Berkeley. http://www.ctec.ufal.br/professor/vap/Valueofwater.pdf (last accessed on 12/04/2017).

Hosain, S.Z. (2016). Reality Check: 50B IoT Devices Connected by 2020 – Beyond the Hype and Into Reality. RCR Wireless News. http://www.rcrwireless.com/20160628/opinion/reality-check-50b-iot-devices-connected-2020-beyond-hype-reality-tag10 (last accessed on 12/04/2017).

Ingildsen, P. & Olsson, G. (2016). *Smart Water Utilities: Complexity Made Simple*. IWA Publishing.

Karpf, C. & Krebs, P. (2011). Quantification of Groundwater Infiltration and Surface Water Inflows in Urban Sewer Networks Based on a Multiple Model Approach. *Water Research*, 45(10), 3129-3136.

Kingdom, B., Liemberger, R. & Marin, P. (2006). *The Challenge of Reducing Non-Revenue Water (NRW) in Developing Countries: How the Private Sector Can Help: A Look at Performance-Based Service*

Contracting, Report for World Bank. https://siteresources.worldbank.org/INTWSS/Resources/WSS8fin4.pdf (last accessed on 17/04/2017).

Kossieris, P., Kozanis, S., Hashmi, A., Katsiri, E., Vamvakeridou-Lyroudia, L.S., Farmani, R.C., Makropoulos, C. & Savic, D. (2014). A Web-Based Platform for Water Efficient Households. *Procedia Engineering*, 89, 1128-1135.

Laucelli, D., Romano, M., Savić, D. & Giustolisi, O. (2016). Detecting Anomalies in Water Distribution Networks Using EPR Modelling Paradigm. *Journal of Hydroinformatics*, 18(3), 409-427.

Long, M.J. (1994). Sea-Water Infiltration: The Dramatic Corrosion of Ductile-Iron Rising Mains. *Water and Environment Journal*, 8(5), 538-545.

Mala-Jetmarova, H., Sultanova, N. & Savic, D. (2017). Lost in Optimisation of Water Distribution Systems? A Literature Review of System Operation. *Environmental Modelling & Software*, 93, 209-254.

Mell, P. & Grance, T. (2009). The NIST Definition of Cloud Computing. *National Institute of Standards and Technology*, 53(6), 50.

Melville-Shreeve, P., Ward, S. & Butler, D. (2016). Rainwater Harvesting Typologies for UK Houses: A Multi Criteria Analysis of System Configurations. *Water*, 8(4), 129.

Panasiuk, O., Hedström, A., Langeveld, J., Liefting, E., Schilperoort, R., de Haan, C. & Viklander, M. (2016). Using Distributed Temperature Sensing for Locating Infiltration and Inflow into Foul Sewers in Cold Climate. In *8th International Conference on Sewer Processes and Networks, Rotterdam,* The Netherlands.

Ratner, B. (2011). *Statistical and Machine-Learning Data Mining: Techniques for Better Predictive Modeling and Analysis of Big Data*. CRC Press, Taylor & Francis Group.

Romano, M., Kapelan, Z. & Savić, D.A. (2014a). Automated Detection of Pipe Bursts and Other Events in Water Distribution Systems. *Journal of Water Resources Planning and Management*, 140(4), 457-467.

Romano, M., Kapelan, Z. & Savić, D.A. (2014b). Evolutionary Algorithm and Expectation Maximization Strategies for Improved Detection of Pipe Bursts and Other Events in Water Distribution Systems. *Journal of Water Resources Planning and Management*, 140(5), 572-584.

Savić, D.A., Boxall, J.B., Ulanicki, B., Kapelan, Z., Makropoulos, C., Fenner, R., Soga, K., Marshall, I.W., Maksimovic, C., Postlethwaite, I. & Ashley, R. (2008). Project Neptune: Improved Operation of Water Distribution Networks. In *Water Distribution Systems Analysis 2008,* 1-16.

Savić, D., Bicik, J., Morley, M.S., Duncan, A., Kapelan, Z., Djordjević, S. & Keedwell, E.C. (2013). Intelligent Urban Water Infrastructure Management. *Journal of the Indian Institute of Science*, 93(2), 319-336.

Savić, D., Vamvakeridou-Lyroudia, L. & Kapelan, Z. (2014). Smart Meters, Smart Water, Smart Societies: The iWIDGET Project. *Procedia Engineering*, 89, 1105-1112.

Savić, D.A., Morley, M.S. & Khoury, M. (2016). Serious Gaming for Water Systems Planning and Management. *Water*, 8(10), 456.

Savić, D., Vamvakeridou-Lyroudia, L. & Kapelan, Z. (2017). Smart Meters, Smart Water, Smart Societies: The iWIDGET Project. *Procedia Engineering*, 89, 1105-1112.

Schwartz, H.-G. (2012). The Smart Cities Member States Initiative Helping Cities to Become the Drivers of Energy Innovation. GEODE Autumn Seminar, November 2012.

Sensus (2017). Smart Water Network. https://sensus.com/smart-water-network/ (last accessed on 28/04/2017).

Smart Cities Council (2017). Smart Cities Readiness Guide. http://readinessguide.smartcitiescouncil.com/article/introduction-smart-cities?page=0%2C1 (last accessed on 12/04/2017).

Sofoulis, Z. (2005). Big Water, Everyday Water: A Sociotechnical Perspective. *Continuum: Journal of Media & Cultural Studies*, 19(4), 445-463.

Sønderlund, A.L., Smith, J.R., Hutton, C.J., Kapelan, Z. & Savic, D. (2016). Effectiveness of Smart Meter-Based Consumption Feedback in Curbing Household Water Use: Knowns and Unknowns. *Journal of Water Resources Planning and Management*, 142(12).

Spence, M., Annez, P.C. & Buckley, R.M. (2008). *Urbanization and Growth*. World Bank Publications.

Sugiyama, M. (2015). *Introduction to Statistical Machine Learning*. Morgan Kaufmann.

Thames Water (2014). *Final Water Resources Management Plan 2015-2040,* https://corporate.thameswater.co.uk/-/media/site-content/thames-water/corporate/aboutus/our-strategies-and-plans/water-resources/our-current-plan-wrmp14/wrmp14_section_0.ashx?la=en (last accessed on 19/04/2017).

United Kingdom Water Industry Research (UKWIR). (2012). The Use of Artificial Neural Networks (ANNs) in Modelling Sewerage Systems for Management in Real Time: Volume 1 - Main Report (12/SW/01/2) (Project Final Report No. 12/SW/01/2). UKWIR, London, UK.

United Nation (2017). Goal 11: Make Cities Inclusive, Safe, Resilient and Sustainable. http://www.un.org/sustainabledevelopment/cities/ (last accessed on 12/04/2017).

Walker, D.J. & Savić, D.A. (2017). Predicting Infiltration with Temperature Data, Internal Report, Centre for Water Systems, University of Exeter.

RESILIENCE, FROM METAPHOR TO OPERATIONAL INDICATORS

FARHAD YAZDANDOOST(1)

(1) K. N. Toosi University of Technology, Tehran, Iran,
yazdandoost@kntu.ac.ir

ABSTRACT

Resistance is defined as the ability of a system to withstand a disturbance without any reaction, and resilience as the ability of a system to recover easily from a reaction to a disturbance. As a metaphor, resilience may be related to sustainability while in engineering practices it often implies quantifying practical/operational indicators by which levels and modes of resiliency may be assessed and achieved. To assess a system's resilience, one must specify which system configuration and which disturbances are of interest. The system may be defined as the socio-economic and/or physical characteristics of a basin where disturbances may affect the normal socio-economic and natural functioning of the society and the ecosystem. Conventional engineering approaches may be ideally addressed from a resilient perspective. Here, resilience based approaches for various engineering applications such as flood risk management, urban drainage systems, water distribution networks and water resources management are reported. Operational indicators have been identified in each case whereby practical variables may be quantified based on resilient approaches. Adopting operational resilience approaches has indicated enhanced management outcomes in comparison to conventional engineering approaches.

Keywords: Resilience; operational criteria.

1 INTRODUCTION

Resilience is the magnitude of disturbance that can be tolerated before a system moves to a different region of state space controlled by a different set of processes. Resilience has multiple levels of meaning: As a metaphor related to sustainability, as a property of dynamic models, and as a measurable quantity that can be assessed in field studies. The operational indicators of resilience have, however, received little attention in the literature (Carpenter et al., 2001).

In general, the word "resilience' has been used to describe the capability of a pressure-bearing system to be restored or to recover by returning to the initial state. Holling (1973) first introduced resilience into ecology as a measure to evaluate the ability of a system to adapt to the state variation while maintaining the ability to return to equilibrium. Handmer and Dovers (1996) believed that a system of greater stability would suffer less from a major disturbance and would quickly return to normal, and that a system of high resilience would be very unstable. Pimm (1984) assumed that resilience was the speed of the system to return to equilibrium after suffering from disturbance. Both perspectives were concerned with the preservation of the structure and functions of the system, but Holling emphasized the amount of disturbance a system could withstand, i.e., the stability, while Pimm's perspective was based on the equilibrium state and focused on the comprehensive capacity, including restoration, resistance, sustainability, and changes of a system after suffering a disturbance. The pioneering studies on ecological resilience by Holling and Pimm produced several different perspectives and a variety of concepts related to ecological resilience. However, no unified view has been developed as to the common accepted operational definition of resilience after 30 years of debate (Fu et al., 2011).

Although there has not been substantial progress in the ecological field of resilience research, the concept has been gradually applied in the research fields of social sciences and environmental changes to describe the behavioral responses in communities, institutions, and economic circles. Timmerman (1998) was the first to study the community's resilience to climate changes, and correlated resilience with vulnerability. Timmerman defined the term resilience as the measure or part of a system's capacity to recover from hazardous events. Studies of resilience over the past 30 years led to the establishment of the Resilience Alliance. The alliance is mainly made up of ecologists and ecological economists, aims to promote resilience studies, global sustainable development and defines resilience from three perspectives (Carpenter et al., 2001): "the amount of disturbance a system can absorb and still remain in the same state as a domain of attraction; the degree to which the system is capable of self-organization (versus lack of organization, or organization forced by external factors); and the degree to which the system can build and increase the capacity for learning and adaptation".

Inspired by such definitions, various theories were presented for resilient flood management approach in river basins and lowland rivers (De Bruijn, 2004; Yazdandoost and Bozorgy, 2008). Some studies, however, have attempted to develop indicators to quantitatively reflect the effectiveness of pertaining measures in considering the economic-technical aspects in urban drainage risk management systems (Tahmasebi Birgani and Yazdandoost, 2014; Tahmasebi Birgani et al., 2013). This research is carried out to investigate the impact of resilience on water scarce basins from an Integrated Water Resources Management (IWRM) perspective (Yazdandoost and Moradian, 2016). Attempts have been made to develop new indices for assessing resiliency and operations, in water distribution networks.

2 RESILIENCE: FROM DEFINITION TO OPERATION

2.1 Definitions

The stability of a system is highly dependent on both resilience and resistance. Resilience is a multidisciplinary concept which had been sought and developed into different fields of study (McDaniels et al., 2008). Two distinct views based on which the most definitions of resilience have formed are “engineering resilience” and “ecological resilience” (Holling and Meffe, 1996). The first view, termed “engineering resilience” focuses on system’s behaviour near stable equilibrium and was indicative of a system’s speed of return to an equilibrium following a disturbance. Based on this assumption, resilience can be measured by resistance to disturbances and rate of return to equilibrium. The second view, concentrates on a system’s behaviour near the boundary of a domain of attraction far from any equilibrium where instabilities can flip to another domain and is a buffer capacity or ability to absorb perturbation. This was measured as magnitude of a disturbance which can be absorbed before system changes its structure by changing variables and processes that control system’s behaviour.

In the context of flood management, De Bruijn (2004) used the two above definitions and defined resilience as "*the ease with which a system recovers from a disruption*" considering how a system reacts to disturbances. The recovery does not necessarily mean returning to the same situation as before flooding but it can be interpreted as returning to the normal or even better situation (De Bruijn, 2004),whilst, Liao (2012) argued that river cities resilience cannot be defined by engineering resilience. It can rather be defined as the capacity to put up with flooding and as a result of which the city reorganizes during physical damage and socioeconomic disruption occurrences. In fact, resilience is the ability of a social system to respond and recover from disturbances, and enables social system to reorganize, change and learn to respond to hazard (Cutter et al., 2008).

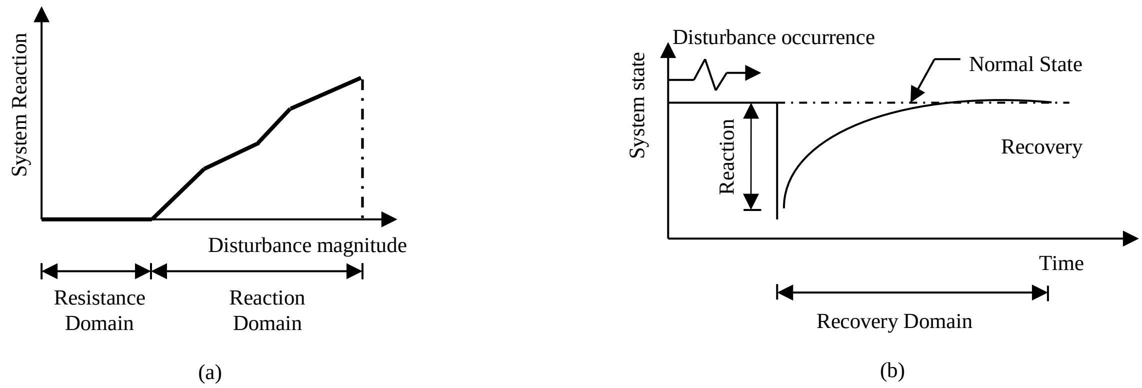

Figure 1. System’s behaviour in response to disturbance: (a) system’s reaction to a disturbance, (b) system recovery from a disturbance to a normal state (Tahmasebi Birgani and Yazdandoost, 2014).

Three aspects may be inferred from the definition of the stability of system on the basis of the system’s behaviour in response to disturbances. These aspects comprise: the system does not show specific behaviour, the system shows response and the system recovers from disturbances to the previous normal situation prior to the occurrence of disturbance. This may be suitably explained as a system’s behaviour under disturbances based on a response curve. When a system was affected by any disturbance, system’s response is different depending on the magnitude of disturbance (Fig. 1a). As shown in Fig. 1a, for small disturbances, the system may not react at all which implies the first perspective, whereas for larger ones, the system may react with its variation amplitude proportional to the increase in disturbance, and somehow implies the second perspective. The third aspect illustrated in Fig. 1b shows that the resilient system state, tends to return to the previous normal condition after reacting to disruption. It should be noted that the system recovery does not mean that the system should return to the exact same previous situation but the main characteristics of system should be restored.

Accordingly, three domains can be considered in these two schematic diagrams: resistance domain, reaction domain and recovery domain while quantifying these domains may enable evaluating the stability of a system to some extent. The resistance domain refers to the condition in which system has no reaction to disruption. In other words, system can easily bear the perturbation applied to it. In reaction domain, the system’s behaviour is different than it was in the resistance domain. This is a range in which the system cannot withstand the disturbance and will be inevitably affected by it. There are two considerable aspects in this behaviour: amplitude and trend of reaction. For a resilient system, it is more desirable for the reaction amplitude to be low and reaction trend to be more gradual. In addition, recovery domain can show how a system recovers from disturbances. The rate of this recovery process is significant to understand how fast a system can attain normal performance. Therefore, it seems in addition to system itself and its properties, disturbances, response to disturbances and the recovery should be described to define the stability of a system.

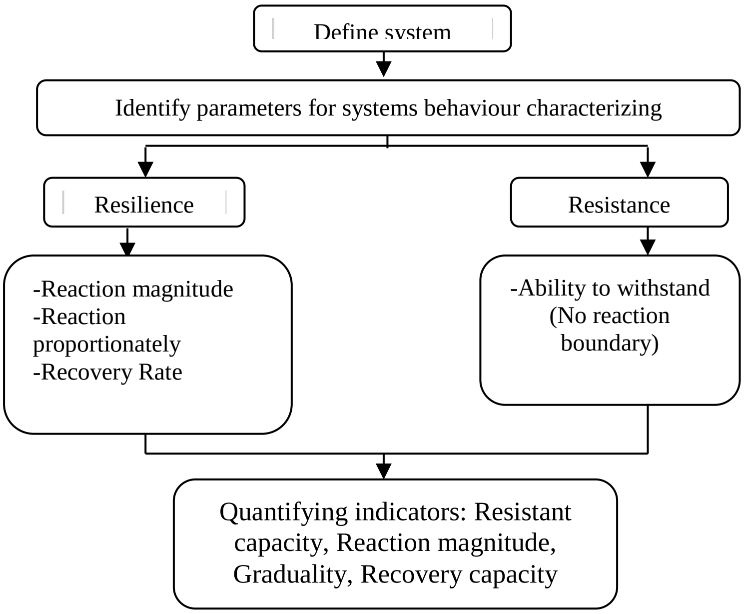

Figure 2. Steps to reach the stability of the system (Tahmasebi Birgani and Yazdandoost, 2014).

One of the most important characteristics of a stable system is that the system tends to return to previous normal state of operation but not the exact previous situation as it would have operated if no disturbance had occurred. Fig. 2 summarizes the framework suggested here to evaluate the stability of a system. It is thus important to identify parameters by which the system's behaviour in response to disturbances can be appropriately characterized. To operationalize definitions, one may develop a set of indicators based on domains defined above.

2.2 Operationalizing resilience

Owing to dependency of resilience on various variables such as demographic, economic and institutional variables, quantification of resilience is a complex task. However attempts have been made to address resilience within integrated approaches appropriate to various cases.

2.2.1 Flood risk management

De Brujin (2004) defined risk management as a set of actions that enables a region and enhances its sustainability. Resilience is defined in this context as the parameter that provides economic growth without damaging the environment. It had been further stipulated that stability is the ability of the system to resist disturbances without any reaction and in turn resilience is the ability of the system to recover easily from reaction to the disturbance. This leads to adoption of a system approach in which the system is defined as a viable socioeconomic plan susceptible to disturbance and disruption. Different indicators have been introduced for quantifying resilience, out of which the main three addressing response to disturbance are "recovery capacity", "Graduality" and "amplitude". The resilience of a system was directly proportional to gradual performance and recovery rate and inversely proportional to the amplitude.

Putting above definitions into practice requires measuring resilience. De Bruijn (2004) argued that the above definitions can be well comprehended by analyzing system’s reactions to disturbances. The resilience of a system is larger when the amplitude is smaller, the graduality is larger and the recovery rate is larger. The indicators for the amplitude were the Expected Annual Damage (EAD) and the Expected Annual Number of Casualties (EANC) (Equations 1 and 2). Graduality is indicated by comparing the relative increase of discharge in a river by the corresponding relative increase of damage (Equations 3 to 5). The recovery rate describes the rate of return from a state where flood impacts were visible to a normal state. De Bruijn (2005) introduced the three physical, economic and social factors which influenced recovery and used three tables for these factors to quantify the recovery rate on a scale from 1 to 10.

$$EAD = \int_{1/10000}^{p(D=0)} PD(P) d_P \qquad [1]$$

$$EANC = \int_{1/10000}^{p(D=0)} PC(P) d_P \qquad [2]$$

where:
EAD = Expected Annual Damage, EANC = Expected Annual Number of Casualties, P = Flood Probability, D(P) = Expected damage as function of probability, C(P) = Number of casualties as function of probability.

$$G = 1 - \sum_{n=1}^{n=N} \frac{\left|\Delta Q_n^{'} - \Delta D_n^{'}\right|}{200} \qquad [3]$$

where:

$$\Delta Q_n^{'} = Q_n^{'} - Q_{n-1}^{'} = \left[\frac{100*(Q_n - Q_{\min})}{Q_{\max} - Q_{\min}}\right] - \left[\frac{100*(Q_{n-1} - Q_{\min})}{Q_{\max} - Q_{\min}}\right] \qquad [4]$$

$$\Delta D_n^{'} = D_n^{'} - D_{n-1}^{'} = \left[\frac{100*(D_n - D_{\min})}{D_{\max} - D_{\min}}\right] - \left[\frac{100*(D_{n-1} - D_{\min})}{D_{\max} - D_{\min}}\right] \qquad [5]$$

where:
Q' = Relative discharge (%), Q = Discharge (m^3/sec), Q_{max} = Q (P=1/10000), Q_{min} = Highest Q for which D=0, D' = Relative damage (%), D = Damage as a function of Q, Dmax = D (Qmax), Dmin = 0, n = Ranking number of the discharge level. The above approach was adopted for the case of Gorgan River in the North-East of Iran (Fig. 3), where decision making procedure was required to determine the best flood risk management strategy for the basin based on resilient criteria.

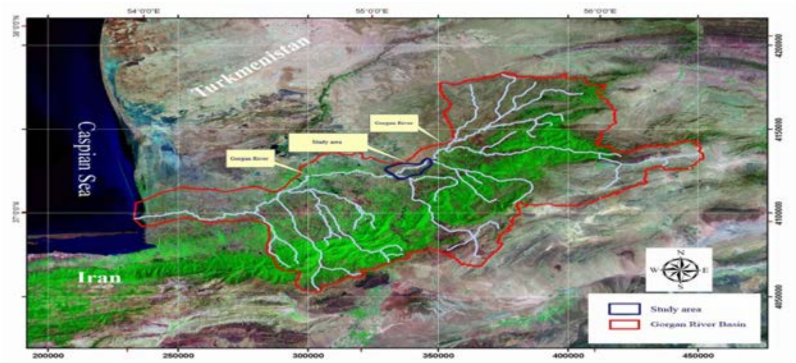

Figure 3. Gorgan River Basin, North-East of Iran.

Results indicated various estimations for resilience criteria for each strategy providing the grounds for an MCDM exercise to rank strategies (Table 1).

Table 1. Resilience indicators' values for different strategies.

Strategy		EANC	Graduality	Recovery Rate
1	Natural Condition	4.4	0.83	5.7
2	Flood Retention	1.9	0.80	6.0
3	Flood Control Levees	3.8	0.73	5.7
4	Flood Diversion Channel (Green River)	2.2	0.94	5.7
5	Flood Warning System	2.0	0.86	6.3
6	Flood Insurance	4.4	0.83	6.7
7	Flood Warning System + Flood Insurance	2.0	0.86	6.7

Performing an MCDM analysis would result in ranking of the strategies based on the resilience criteria. The results revealed that Strategy 7 (Flood warning & insurance) which was a non-structural and practically resilient strategy scores the best ranking and Strategy 5 (Flood warning) and Strategy 4 (Green River) scored as 2nd and 3rd ranks respectively. Strategy 2 (Flood detention reservoir) scores the 4th rank due to its high construction, operation and maintenance costs. The natural condition scores the lowest rank due to its high EANC and low recovery rate.

2.2.2 Urban drainage risk management systems

Urban Drainage Risk Management (UDRM) systems were considered to include the physical urban drainage systems as well as the encompassing geographical areas including streets and buildings, etc. which may potentially be adversely affected by pluvial urban flooding (Fig. 4). These effects can be investigated in the form of technical, environmental, social and economic aspects. In the current study, the technical and economic aspects of system had been considered. The technical aspects comprise of hydraulic parameters such as flood water depth and flood duration in urban drainage system nodes. The economic aspects of the system include the pluvial flood consequences on the urban areas which were interpreted as economic damages to buildings, urban infrastructure and the environment.

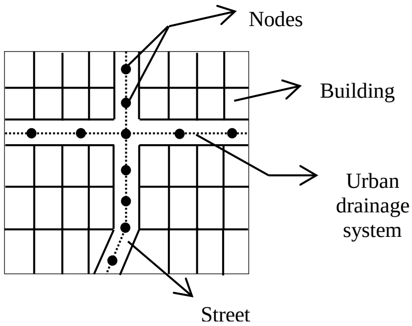

Figure 4. Schematic UDRM system.

To analyze resilience of the UDRM systems, the UDRM system itself, its response to rainfalls and its ability to recover from the pluvial flood should be determined. Response depends on several factors depending on the status of the community, such as the population density, vehicular traffic conditions, land use, proximity to hot spots, and etc. in the flooded area. Ability of recovery also depends on the physical, economic and institutional factors (Tierney and Bruneau, 2007) such as duration of flood water subsidence. Allocated budget to related organizations and appropriate distribution of relief centres in a city so as to provide timely services to flood affected people and places are also taken into consideration. The essential parameters used to quantify response and recovery in this research are summarized in Table 1. The rationales on choosing these parameters were the suggestion of various literature and experts' opinions.

A similar approach to that of the flood risk management has been adopted here regarding the ability of recovery of a system along a full range of rainfalls. In this sense, a UDRM system does not respond to the rainfalls which are within its tolerance (no reaction domain). Obviously, in this situation, the ability of a recovery was absolute (full recovery domain), although, this may not be verified prior to any system response. With the increase in rainfalls magnitude coinciding with Urban Drainage Systems (UDSs) failure, the response of the system proportionately raises (reaction domain), while the ability of recovery probably reduces (recovery reduction domain). However, appropriate activities may improve the ability of recovery against the same rainfalls in future. These processes are schematically depicted in Fig. 5 termed 'response-recovery (R-R) curves'. A consideration is given to the point of intersection of the two curves, termed "warning point", where after this point the percentage of recovery becomes numerically smaller than the percentage of response. In other words from this point onwards, it will be the rainfall to which urban authorities should pay further attention since the response would exceed the recovery resulting in further disorders. Representing R-R curve as such, can delineate analyzing the behaviour of UDRM systems faced with various rainfalls as a snapshot in time.

Here, indicators were modified to suit the urban drainage conditions while upholding the essence of resilience. As earlier stated, the EAD was often used as a risk indicator to reflect the adverse effects in terms of costs (Zhou et al., 2012). Accordingly, in this research, severity of the expected damage resulting in pluvial flood had been considered as the reaction to the rainfalls. For describing the magnitude of reaction to the different return period of rainfalls, the EAD has been used. EAD is determined by integration of flood risk over all return periods (Zhou et al., 2012) as stated by Chow et al. (1988):

$$EAD = \int_{h_d}^{\infty} f(h)\, D(h)\, dh \qquad [6]$$

in which, EAD is the expected annual damage ($MRial/year$), h_d is the design level which shows the total depth of rainfall with the specified return period above which pluvial flood damage occurs ($h > h_d$), $f(h)$ is the probability density function of total rainfall depth and $D(h)$ is the pluvial flood damage resulting from $h > h_d$. For quantifying the graduality, the resistance and the reaction domains were divided into N sections based on the number of rainfall events for which the UDRM systems have been assessed. Graduality was then measured as follows:

$$G = 1 - \frac{1}{2}\sum_{m=1}^{N}\left|\frac{\Delta h_m}{h_{max}-h_{min}} - \frac{\Delta D_m}{D_{max}-D_{min}}\right| \quad [7]$$

where:
G = graduality (-), N = number of sections gained by subtracting 1 from the number of rainfalls, Δh_m = change in rainfall depth for section m (mm), ΔD_m = change in damage for section m $(MRials)$, h_{max} = maximum total rainfall depth at the end of reaction domain (mm), D_{max} = maximum damage in all the UDRM that corresponds to h_{max} $(MRials)$, h_{min} = minimum total rainfall depth for the lowest return period of rainfalls (mm), D_{min} = minimum damage in all the UDRM that corresponds to h_{min} $(MRials)$.

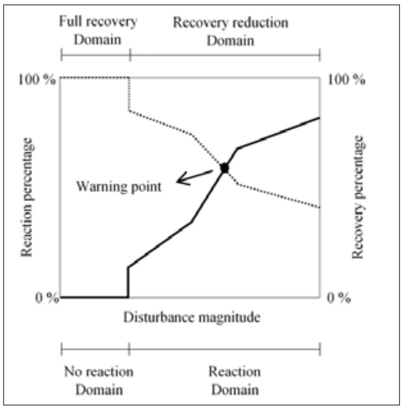

Figure 5. Schematic R-R curve (reaction: solid line, recovery: dotted line).

Recovery rate can be considered as the duration of system recovery from unsatisfactory condition to satisfactory one. In the case of UDRM systems, the current research defines recovery capacity as the time in which pluvial flood above urban drainage network nodes subsides. For quantifying recovery capacity, the weighting average of flooding time for all nodes was calculated and called recovery duration. Because of the importance of flood volume above each node, flood volumes have been assigned as weights. Following equations show the steps to quantify recovery capacity:

$$RD = \frac{\sum_{j=1}^{k} T_{fj}\, V_{fj}}{\sum_{j=1}^{k} V_{fj}} \quad [8]$$

where RD is recovery duration (hr) of urban drainage system for each flood event, T_{fj} is time of flooding for node j, V_{fj} is flood volume above node j and k is number of flooded nodes.

The 22nd municipal district of Tehran, located at the downstream of Kan River watershed and in the North-west of Greater Tehran, was chosen for the case study. The urban drainage system implemented over the study area includes the concrete channel network which conveys storm waters towards the outlet of Kan River. The layout of main channels of existing urban drainage system in the study area is depicted in Fig. 6.

A number of urban drainage Best Management Practices (BMPs) were investigated here as sustainably enhanced practical solutions, often conventionally adopted in engineering approaches. Corresponding resilience indicators were identified based on the described indicators (Table 2).

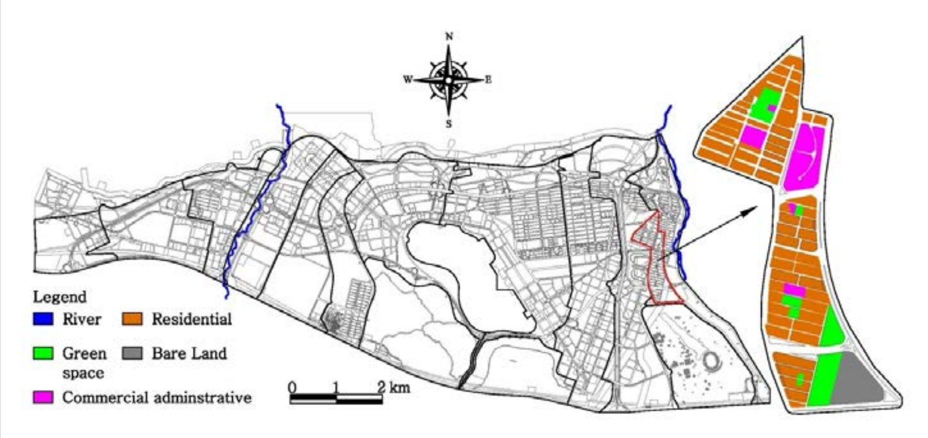

Figure 6. The study area land use.

Table 2. Indicators values for various BMP scenarios.

BMP Scenario	Resistance capacity (mm)	EAD$(MRials/year)$	Graduality	Recovery capacity
Current condition	18.56	1027.8	0.93	0.36
Green roof	26.51	313.9	0.72	0.48
Pervious pavement	30.99	91.6	0.46	0.68
Detention pond	26.51	205.9	0.62	0.49
Channel enlargement	26.51	153.7	0.55	0.72

It was clear that the persistence of a UDRM system cannot be well evaluated using one indicator such as designed rainfall or EAD. Adopting a system approach allows the study and comparison of various urban drainage measures based on the values of the associated indicators in the case study. It is generally expected that a persistent system has high values of resistance capacity, gradulity and recovery capacity and low values of reaction magnitude and the vice versa would be true for a non-persistent system. However, in practice different situations may occur calling for definition of weights for criteria based on common engineering practices.

Results showed that the proposed framework can help managers and urban planners to further appreciate the impacts of different urban drainage measure on the behavior of the UDRM system faced with extreme rainfall events. Additionally, indicators have the potential to be considered as urban drainage design criteria or to be utilized in decision making processes examining different criteria.

2.2.3 Resilient approach in IWRM

Water shortage had often been the source of competitions and conflicts amongst stakeholders. Integrated Water Resources Management (IWRM) is seen worldwide as appropriate means of conflict resolution. IWRM is the response to the growing pressure on water resources systems as a result of growing population and socio-economic developments. Water resources management had undergone a drastic change world-wide, moving from a mainly supply-oriented, engineering biased approach towards a demand-oriented, multi-sectoral approach, often labelled as Integrated Water Resources Management. Problems were somewhat exacerbated in water scarce basins where despite considerable developments in risk management techniques, management deficiencies persist due to numerous uncertainties.

Given the issues associated with water scarce regions, all sources of water supply, both in terms of quality and quantity, have to be carefully identified. Water systems' planning is often associated with too many uncertain parameters due to ambiguities in defining objectives, forecasts and assumptions. To achieve coherence, a broad perspective is therefore required to effectively establish the relationship between certain and uncertain parameters. Identification of parameters may then be followed by setting an allocation simulation model. Identifying the role of resilience based on IWRM may then be assisted by consideration of various scenarios encompassing of technical, economic, environmental and social aspects in an integrated framework. The base/reference framework for quantity and quality of water supply and demand may be deduced based on available data.

The above procedure had been utilized for the case of Lake Urmia basin. Lake Urmia, is one of the largest saltwater lakes on earth and a highly endangered ecosystem, is on the brink of desiccation. Considering no significant trend in the drought pattern, Lake Urmia's observed physiographic changes may be attributed to the adverse effects of unsustainable development plans and excessive irrigation projects in the basin. Once with a surface area of approximately half a million hectares, Lake Urmia's shoreline has been receding severely and in a relatively short period of time (Fig. 7) with no sign of recovery, leading to a significant shrinkage in the lake's surface area, which currently is decreased by around 88%.

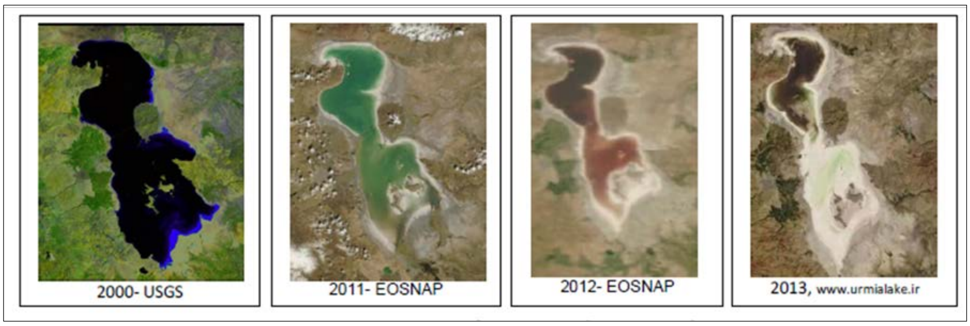

Figure 7. Lake Urmia's geophysical changes.

In terms of water utilization, a gradual reduction up to 40% in agricultural consumption, as the basin's highest consumer of water resources, had been introduced by the authorities to alleviate the immediate problems with desiccation of Lake Urmia.

The calibrated allocation model was used to simulate gains in storage volumes of Lake Urmia as a consequence of reduction in agriculture allocation. Order of priorities were set in the model to consider drinking water as first and agriculture and industry equally as second. Simulations were then projected to the year 2020. Table 3 shows the corresponding simulated results for lake volumes and basin unmet demands.

Table 3. Comparison of average lake volumes and basin unmet demands for 2015 to 2020.

Average unmet demand (BCM)	Average lake volume (BCM)	Scenario
2.84	1.529	No reduction in agriculture consumption
2.33	4.775	40% reduction in agriculture consumption

To observe the effect of resilience in this approach, different indicators were previously introduced, namely "recovery capacity", "Graduality" and "amplitude", which may be investigated and quantified. In order to obtain the recovery capacity it was necessary to determine the normalized weighted average of time of disturbance over the entire basin. This was performed using the same relationships previously used for interpretation of the recovery capacity in the case of urban drainage risk management (equation 8).

For representing the recovery capacity in a single number in a range between 0 and 1, the recovery duration values should be normalised and results were then averaged over the entire range of return periods. As a result, the duration of recovery should be determined for at least three different values of rainfall. The resulting value was termed as the normal duration of recovery. The normal duration of recovery may be found from:

$$NRD_i = \frac{RD_i - RD_{\min}}{RD_{\max} - RD_{\min}} \qquad [9]$$

in which, NRD is the normalised recovery duration and RD_{max} and RD_{min} are the maximum and minimum durations of recovery respectively. Eventually the recovery capacity, R, may be found from:

$$R = 1 - \frac{\sum_{i=1}^{n} NRD}{n} \qquad [10]$$

where, n is the number of rainfall events. This relationship shows that a higher recover capacity would imply a smaller low rainfall duration.

As for the graduality in this case, a modification was made to the previous case (equation 7) to adopt this relationship for water scarce basins by defining the low rainfall depth situation as:

$$h_{m\_famine} = h_{avg} - h_m \qquad [11]$$

in which h_{avg} is the minimum fifty year rainfall in mm and $h_{m\text{-}fanine}$ is the low rainfall depth. Substitution will result in:

$$G = 1 - \frac{1}{2}\sum_{m=2}^{N}\left|\frac{h_m - h_{m-1}}{h_{\max} - h_{\min}} + \frac{D_m - D_{m-1}}{D_{\max} - D_{\min}}\right| \quad [12]$$

$$D_m = 2\times10^6 \times (\frac{h_{avg} - h_m}{P_m})^{0.1681} \quad [13]$$

where, P is the probability of low rainfall. The damage is determined by a best fit to available damage data as a result of low rainfall and may not be adopted for other basins.

For the values of the amplitude, equation 1 was used with the following interpretation:

$$EAD = \sum_{i=1}^{n}(\Delta P_i \times D_i) \qquad \therefore \begin{cases} D_i = \dfrac{D_{i-1} + D_i}{2} \\ \Delta P_i = P_{x\geq x} - P_{x\geq x_{i-1}} \end{cases} \quad [14]$$

where, n = number of rainfall events, D = drought damage for section i (M IRRials), P = probability rainfall occurrence of section i and EAD = expected annual damage (M IRRials/year). Various ranges for the resilience indicators were determined from the above:

$0.83 < R < 1$

$0.77 < G < 1$

$EAD < 13.73 \quad (BIRRials / year)$

It was observed that the model would produce a relationship for the Lake Urmia's volumes versus varying different figures of reduction in the agriculture allocation up to a figure of 40%. As shown in Fig. 8, this relationship is by no means linear, clearly indicating that consideration of resilience indicators will imply a steady and constat rate of change after a braking point. This indicates that the systems would tend to resist, absorb and recover upon receiving a disturbance. It may be argued here that initially the volume of the lake would increase fairly linearaly as reduction in agricultur allocation increases up to a point where the basic characteristics of the system were recovered to its normal condition after reaction. From this point on variations were followed by a near horizontal line indicating further reductions in agriculture alocation would not have any reasonable meaningful effect on the gain in lake volume. In other words, if lake's volume is given first priority in the allocation model, reduction in agriculture allocation would have no effects on the results after a certain (braking) point.

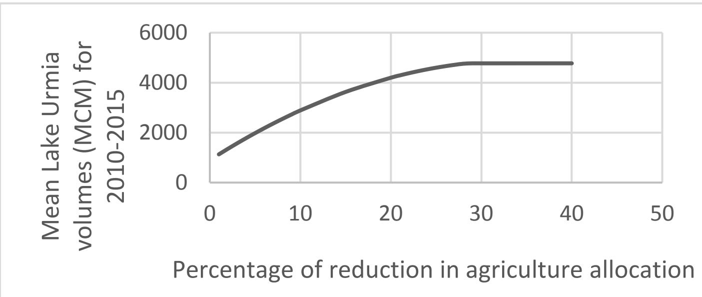

Figure 8. Percentage of reduction in agriculture allocation vs. Lake Urmia volume gains.

2.2.4 Resiliency in water distribution networks

Water Distribution Networks (WDNs) are among the vital infrastructures consisting many assets. Failure of each asset can cause multi aspects of risks and eventually lead to the operational disruption or serious consequences. Understanding the nature of risks and reducing the level of them have the most important role in risk management. Risks in water distribution systems can originate from natural incident like earthquakes, floods and etc., as well as artificial cases such as pipe break, power outage, service disruption and change in water quality. Supporting WDNs against these incidents may require exorbitant costs to implement reactive and proactive actions.

Resilience was evaluated here through introducing five new indexes measuring the role of each pipe asset failure in the operation of WDNs. These presented indexes were established based on some specific abilities previously defined and characterized for a resilience system. These selected features were the ability to reduce the magnitude and/or the duration of disruptive events, the ability to minimize the costs of a disaster and returning to the status quo in the shortest feasible time, the ability to propagate disruption in a gradual manner and the ability to recover from an unsatisfactory condition as soon as possible. In a very simplified form, Fig. 9 illustrates the functional state of a system before, during, and after a failure. The vertical axis of the diagram in Fig. 9 can represent any system performance measure (e.g., amount of water supplied to customers) as long as higher values indicate higher performances and the horizontal axis represents the time.

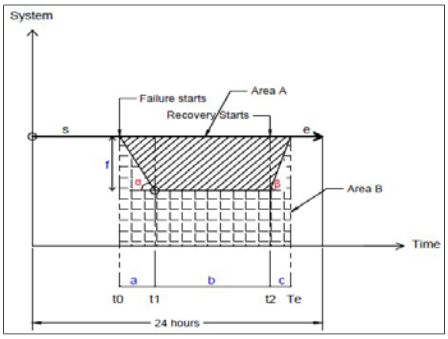

Figure 9. Functional state of a WDN system before, during and after a failure.

The five indexes of Graduality, Recovery Rate, Water Outage Time, Hydraulic Critical Index (HCI) and Regret Cost with their corresponding features in Fig. 9 are condensed in Table 4.

Table 4. Indexes introduced for the study.

index	section in figure 9	unit
Graduality	α	Lit/s²
Recovery Rate	β	Lit/s²
Water Outage Time	Te – t0	hour
HCI	-	percentage
Regret Cost	A/(A+B)*Water sales income	IR.Rial

Values of indicators were further represented in this case by the following relationships:
Graduality = Rate of Loss/Loss time, Recover Rate = Rate of Rise/Rise time, Water Outage Time = a+b+c,
HCI = Total supplied demands of network after the failure/Total supplied demands of network before the failure,
Regret Cost = [Unsatisfactory Area (A)/Total Area (A + B)] x 100

The above mentioned methodology was applied to a WDN in the south-west of Isfahan, Iran. The city's' area is around 36Km² and its population is estimated at 20000. The area is divided into three main districts namely; N, D, and W (Fig. 10).

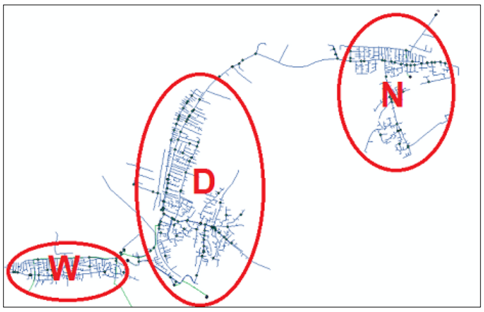

Figure 10. Case study's schematic water distribution network.

In order to quantify the proposed resilient indexes for the existing condition of the WDN, a toolkit was developed and used. This toolkit is able to simulate failure of each pipe and assess the indexes. Those pipes whose failures can create more unmet demand were the critical ones. Table 5 shows the measured indexes for some of the most critical pipes. It is worth noting that, while the higher amount of recovery rate was desired, the lower amount for the other indexes is favorable. Pipes 1 to Pipe 3 were those which are linked directly to the main reservoirs, and Pipe 4 to Pipe 6 is the connections between two main districts of the WDN. The pipes were arranged in order of their HCI level (criticality).

Table 5. Indexes and features of the critical pipes of the existing WDN.

FEATURE	UNIT	PIPE1	PIPE2	PIPE3	PIPE4	PIPE5	PIPE6
DIAMETERE	(Millimeter)	60	250	150	150	150	150
LENGTH	(Meter)	8.4	90.5	11.3	32.2	229.6	47.4
GRADUALITY	(Lit/s²)	17.66	0.28	6.06	1.41	0.15	0.46
RECOVERY RATE	(Lit/s²)	0.59	0.5	0.52	0.56	0.71	0.52
WATER OUTAGE TIME	(Hour)	6.07	6.18	6.06	6.07	6.22	6.1
HCI	(%)	16.67	12.77	12.68	11.42	10.96	9.86
REGRET COST	(MIR.Rial)	8.66	6.97	7.00	6.47	6.20	5.80

The results showed that the indexes introduced here, are efficient enough to cover the economic (Regret Cost), social (Graduality, Recovery Rate and Water Outage Time) and technical (HCI) perspectives of WDNs operation simultaneously. In this situation, by taking enhancing scenarios into account, the WDN can prosper into a more resilient one. This type of quantifying resilience of WDNs would help stakeholders making the best management decisions on repairing, replacing and etc.

3 CONCLUSIONS

Introduction of resilient strategies has made a marked difference to the traditional risk management approaches. It has been shown that for resilient strategies to be examined and exercised appropriately it is imperative to adapt a system of a holistic approach to various risk management issues. The role of resilient strategies may be further emphasized for their direct impacts on sustainable development. Evidently management strategies have shown higher ranks in decision making, indicating the need for a paradigm shift, particularly in developing communities, from purely engineering biased approaches to resilient management strategies. Operationalizing resilience leads to comprehension and appreciation of quantifiable measures when faced with risk management issues, thereby facilitating enhanced and sustainable decision making.

REFERENCES

Carpenter, S., Walker, B., Anderies, J.M. & Abel, N. (2001). From Metaphor to Measurement: Resilience of What to What? *Ecosystems*, 4(8), 765–781,

Cutter, S.L., Barnes, L., Berry, M., Burton, C., Evans, E., Tate, E. & Webb, J. (2008). A Place-Based Model for Understanding Community Resilience to Natural Disasters. *Global Environmental Change,* 18(4), 598-606.

De Bruijn, K.M. (2004). Resilience and Flood Risk Management. *Water Policy*, 6(1), 53-66.

De Bruijn, K.M. (2005). Resilience and Flood Risk Management: A System Approach Applied to Lowland Rivers. *PhD Thesis*, Delft University Press.

Handmer, J.W. & Dovers, S.R. (1996). A Typology of Resilience: Rethinking Institutions for Sustainable Development, Industrial and Environmental Crisis Quarterly. *Organization & Environment*, 9(4), 482–511.

Holling, C.S. (1973). Resilience and Stability of Ecological Systems. *Annual Review of Ecology and Systematics*, 4(1), 1-23.

Holling, C.S. & Meffe, G.K. (1996). Command and Control and the Pathology of Natural Resource Management. *Conservation Biology,* 10(2), 328-337.

Liao, K.-H. (2012). A Theory on Urban Resilience to Floods—A Basis for Alternative Planning Practices. *Ecology and Society,* 17(4).

McDaniels, T., Chang, S., Cole, D., Mikawoz, J. & Longstaff, H. (2008). Fostering Resilience to Extreme Events Within Infrastructure Systems: Characterizing Decision Contexts for Mitigation and Adaptation. *Global Environmental Change,* 18(2), 310-318.

Pimm, S.L., (1984). The Complexity and Stability of Ecosystems. *Nature*, 307(5949), 321-326

Tahmasebi Birgani, Y. & Yazdandoost, F. (2014). A Framework for Evaluating the Persistence in Urban Drainage Risk Management Systems. *Journal of Hydroenvironment Research*, 8(4), 330-342, doi:10.1016/j.jher.

Tahmasebi Birgani, Y., Yazdandoost, F. & Moghadam, M. (2013). Role of Resilience in Sustainable Urban Stromwater Management. *Journal of Hydraulic Structures*, 1(1), 44-53.

Tierney, K. & Bruneau, M. (2007). Conceptualizing and Measuring Resilience: A Key to Disaster Loss Reduction. *TR-News*, 250, 14-15, 17.

Yazdandoost, F. & Bozorgy, B. (2008). Flood Risk Management Strategies Using Multi-Criteria Analysis. In *Proceedings of the Institution of Civil Engineers-Water Management,* 161(5), 261-266).

Yazdandoost, F. & Moradian, S. (2016). A Resilient Approach to Integrated Water Resources Management in Water Scarce Basins. *Journal of Fundamental and Applied Sciences*, 8(3), 137-151.

Fu, Z.M., Xiang, Y., Liu, C.D., Li, Z.Y. & Wang, Z.J. (2011). Resilience of Hydraulic Structures under Significant Impact of Typhoons. *Water Science and Engineering*, 4(3), 284-293

Zhou, H., Wan, J. & Jia, H. (2010). Resilience to Natural Hazards: A Geographic Perspective. *Natural Hazards,* 53(1), 21-41.

WATER SECURITY ISSUE AND ADAPTIVE WATER MANAGEMENT OF CHINA FOR CHANGING ENVIRONMENT

XIA JUN[1]

[1] State Key Laboratory of Water Resources & Hydro Power Engineering Sciences, Wuhan University, Wuhan, China
[1] Institute of Geographical Sciences and Natural Resource Research, Chinese Academy of Sciences, Beijing, China
xiajun666@whu.edu.cn

ABSTRACT

This paper addresses the issue of water resources and its trends and development challenges in China. Also, the preliminary assessment of climate risks with current and future in the water sector are presented, particular in current Climate Risks for water resources management. Combined with author's research supported by the National Key Basic Research and Development Program (2010CB428400) in China, some of major discussions are given as future perspective on sustainable water utilization and adaptive water management for changing environment.

Keywords: Climate change; water cycle; water resources; vulnerability; adaptation.

1 INTRODUCTION

China, as a big developing country, is facing a huge challenge in managing water resources to support its economic boom. China has an immense territory of 9.6 million km^2 and relatively abundant water resources which ranks the sixth in the world after Brazil, the Russian Federation, Canada, the United States, and Indonesia in terms of absolute amount of annual runoff. However, given its large population of over 1.3 billion, China has a very low per capita amount which is about one quarter of the world average of water resources and, is therefore one of the countries with the severest shortage of water in the world. The Ministry of Water Resources completed a nationwide assessment of water resources in 2000 and reported the great challenge on water issue (Qian and Zhang, 2001; Xia, 2012). For instance, the spatial distribution of available water resources in China is remarkably uneven. The total amount of available water resources of China is about 814 BCM, accounted for 29% of the total water resources. The available water resources in South China is about 560 BCM in total and 1100m^3 per capita; while North China has overall 204.5 BCM amount of available water resources with only 359m^3 per capita. Annual mean precipitation, averaged from 1956 to 2002, decreases from the south to the north. The annual precipitations in South and North China are 1000-1500mm and 500-600mm, respectively, while the region between the Huaihe River and Yellow River has an annual precipitation of 600-1000mm. No significant long-term change in the country-averaged annual precipitation can be seen within the past 100 years. However, an obvious tendency towards drought in terms of annual or summer precipitation has been found in the Yellow River Basin and the North China Plain, especially the Shandong Province. Meanwhile, a significant wetting trend could be detected in the Yangtze River Basin and most parts of western China. The increased annual precipitation in the Yangtze River Basin is mainly resulted from the significant rising of summer rainfall, although winter precipitation also tends to increase (Ren, 2001). According to the past 50-year records, water resources of China varied significantly. As shown in Figure 1 (Zhang, 2009), the overall runoff in the country dramatically decreased in basins of Haihe River, Yellow River and Liao River, while moderately reduced in basins of Huai River, Songliao River, Pear River and Yangtze River.

Population of China is estimated to be 1.6 billion in 2030, and the total actual water use will be 710.1 BCM by then. Thus, considering social & economic growth and impact of environment change, available water resources will be more vulnerable. Available water resources per capita in North China will decrease from existing 359m^3 to 292m^3 in 2030, and water resources per capita in the whole country will be reduced from existing 628m^3 to 508m^3.

On the other hand, the impact of climate changes on water resources has become an important issue not only globally but also in China which prepares us to gain enough information in order to enable sustainable global water utilization (Xia et al., 2012). In line with global change, China's climate has witnessed significant change in the last 50 years. These changes included increased average temperatures, rising sea-levels, glacier retreat, reduced annual precipitation in North and Northeast China and significant increases in southern and northwestern China. Extreme weather and climatic events are projected to become more frequent in the future and water resource scarcity will continue across the country. Coastal and delta areas will face greater flood and storm risk from sea level rise and typhoon generation (Liu, 2001; Xia, 2008; 2012; Zhang and Wang, 2005). The possibility of global warming and subsequent changes to climate mean, extreme

  / ISSN 1562-6865 (Online) - ISSN 1063-7710 (Print)

events are altering the viability of existing water resources structures and influencing the safety of drinking water, ecosystem, flood protection, water development and exploitation in China. Potential negative impacts to the water sector goals include: Direct impacts, such as damages from extreme weather and climatic events to infrastructure, Indirect impacts, like health impacts that reduce labour productivity in agriculture, Underperformance, such as agricultural projects that fail when rainfall decreases, and 'Mal-adaptation', e.g. policies that inadvertently increases vulnerability, such as those encouraging migration into high risk areas.

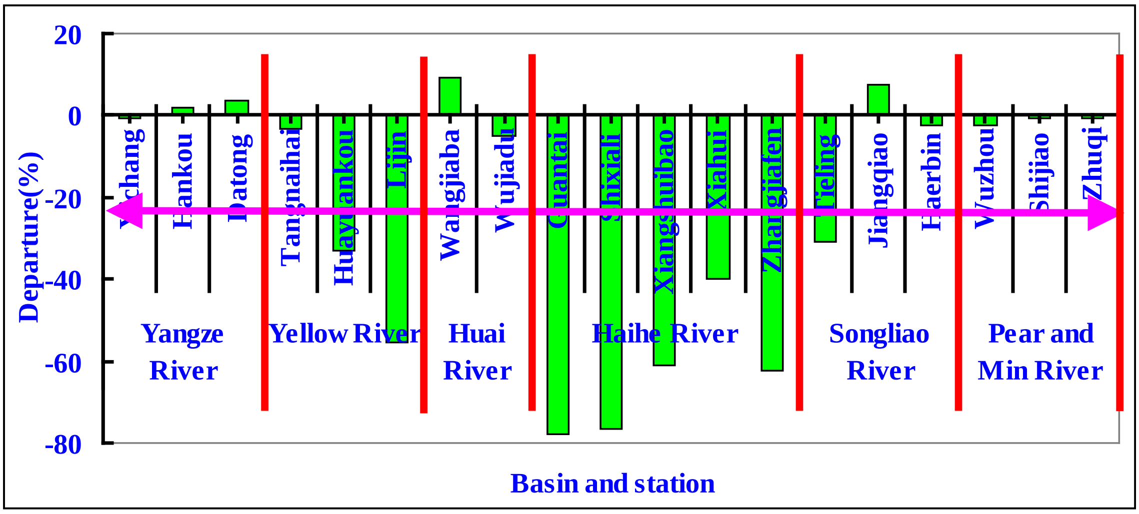

Figure 1. Trend of runoff change in main river basins in China by difference comparison of total runoff from 1950-1980 to 1981~2004 (Zhang, 2009).

Under the background of global warming, available water resources in northern China are decreasing, water consumption is increasing, and extreme hydrological events are occurring more frequently (Xia, 2012; Duan and Phillips, 2010). Such problems increase the vulnerability of water resources and will ultimately influence their allocation in China, thereby reducing the benefit of large water transfer and flooding control projects. It is thus necessary to explore four key scientific issues: How has the climate and water cycle changed historically? What will the changes be in the future? What is the mechanism of change and how should we adapt to these changes?

2 ONE OF MAJOR RESEARCHES ON UNDERSTANDING CLIMATE CHANGE AND WATER RESOURCES IN CHINA

The four questions are the research focus of the National Key Basic Research and Development Program with respect to, "The impact of climate change on terrestrial water cycle, regional water resources security and the adaptation strategy for Eastern Monsoon Region of China" (2010CB428400). These are the most prolific water science issues relating to the Earth's system. Under guidance from the project leader, the research team had been working for the past five years to obtain new ideas and knowledge to be applied by Ministry of Water Resources in P.R. China and other sections. These findings are briefly summarized in this paper.

In the past five years, the research team had obtained new knowledge and technological advances, and the things described can be addressed as follows:

(1) A gridded dataset has been developed in China which provides quality control for correlations based observations from high density meteorological stations (Liu and Xia, 2011);
(2) A new two-layered Land-Atmosphere Coupling Model and land data assimilation system has been developed. Research on the attribution aspect has shown that hydrological change in China was due to both natural climate variation and greenhouse gas emissions, in which the contribution of natural variability to precipitation accounts for about 70% and anthropogenic forcing accounts for 30% on average in the EMRC (Zhang et al., 2015). With future scenarios of increasing CO_2 emissions, the contribution rate from anthropogenic forcing will increase. Therefore, water resources management will face increasing risks associated with climate change;
(3) A workable and practical new approach has been developed using probability distribution where this quantitatively describes uncertainties from different GCMs and the model-self, and assesses climate change projections contained in IPCC AR5 for continental China (Liu and Xia, 2011);
(4) A new approach for non-stationary extreme flood frequency analysis related to climate change has been developed based on the climate change index method combined with hydrological frequency calculations (Wu et al., 2015);

(5) A new theory and method for quantifying water resource vulnerability has been developed based on the multivariate index system and functional approach, that can be linked with climate change, the socioeconomic impact of change, adaptive processes to change, and risk (Xia, 2010; Xia et al., 2014);

(6) Countermeasures and suggestions for adaptive water management in China have been proposed to deal with climate change. These include, the immediate promotion of adaptive management in relation to planning and construction of water resources at a national level, carrying out capacity-building of a water resources adaptation and decision-making system to deal with climate change as soon as possible, and actively implementing innovation-driven basic scientific research under the impact of climate change, and national water security development strategies for a changing environment.

The results showed significant benefits of the adaptive water management (see Figure 2). Even under the worst condition of climate change, the water resource vulnerability in EMRC can be reduced by 21.3% and the sustainable development degree can be increased by 18.4% if we carry out the adjustment and countermeasure of the adaptive water resources (Xia, 2012).

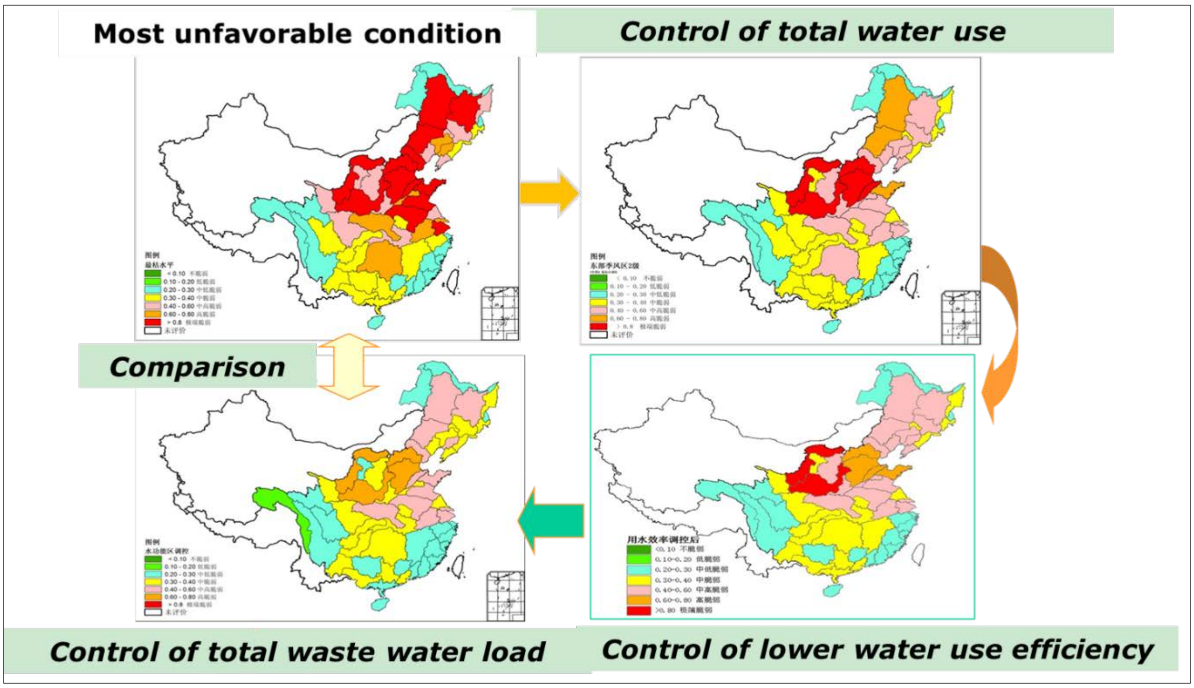

Figure 2. Vulnerability change after taking"Three Red-line Controls"policy (Xia, 2014).

3 CONCLUDING REMARKS

Impact of climate change to water sector in China will have higher reliability to increase water stress in China through changing of water cycle time-space distribution which extremely increases water disasters, such as floods and droughts. It is shown that the contribution of natural variability on changes in precipitation accounts for about 70% whereas anthropogenic forcing accounts for about 30% on regional average changes. With increasing of CO_2 emissions in future, there will probably be an increase in extreme flood and drought. In addition, together with rising temperature of 1°C in North China, the agricultural water consumption will increase to about 4% of total water consumption.

As climate change impacts become more apparent, adaptation is an increasingly important area of work around the world. Adaptation is a process to moderately cope with and take advantage of the consequences of climate change. Crucially, adaptation requires a process of ongoing monitoring and assessment in scientific understanding of climate change developments. To cope with climate change impact to water sector, China will face more challenges on its adaptive capacity and adaptive way to manage wisely water in both regions of the country. The existing water resource planning, design, and management of water division projects will be at high risk because of limited considerations of the impact of climate change. Even under the worst climate change scenario, water resource vulnerability in China can be reduced by 21.3% and the degree of sustainable development can be increased by 18.4% if adaptive management and countermeasures are implemented for dealing with climate change to ensure water security in China. Under the changing environment, it is thus crucial to modify existing water resource planning and management standards in major water conservancy projects.

Anyhow, China will play a leading role on solution of its water problem, and also face great challenges on how to process adaptive water management due to climate change and human activity. Opportunities and challenges will also arise to this great country at this great time.

ACKNOWLEDGEMENTS
This study is supported by the National Key Basic Research Development Program Project (2010CB428400) and the Natural Science Foundation of China (51279140).

REFERENCES
Chahine, M.T. (1992). The Hydrological Cycle and Its Influence on Climate. *Nature*, 359(6394), 373-380.
Duan, Q. & Phillips, T.J. (2010). Bayesian Estimation of Local Signal and Noise in Multimodel Simulations of Climate Change. *Journal of Geophysics Research*, 115(D18), 123.
Gulbenkian Think Tank on Water and the Future of Humanity (GTTWFH), (2013). *Water and the Future of Humanity: Revisiting Water Security*. Springer.
IPCC (2007a). *Climate Change 2007：The Physical Science Basis. Working Group I Contribution to the Fourth Assessment Report of the Intergovernmental Panel on Climate Change*. Cambridge University Press, Cambridge.
IPCC (2007b). *Climate Change 2007: Impacts, Adaptation and Vulnerability. Working Group II Contribution to the Fourth Assessment Report of the Intergovernmental Panel on Climate Change*. Cambridge University Press, Cambridge.
IPCC (2014a). *Climate Change 2014: Synthesis Report. Contribution of Working Groups I, II and III to the Fifth Assessment Report of the Intergovernmental Panel on Climate Change*. Cambridge University Press, Cambridge.
IPCC (2014b). *Climate Change 2014: Impacts, Adaptation, and Vulnerability. Part A: Global and Sectoral Aspects. Contribution of Working Group II to the Fifth Assessment Report of the Intergovernmental Panel on Climate Change*. Cambridge University Press, Cambridge.
Liu, C. & Xia, J. (2011). Detection and Attribution of Observed Changes in the Hydrological Cycle Under Global Warming. *Advances in Climate Change Research*, 2(1), 31-37.
Oki, T. & Kanae, S. (2006). Global Hydrological Cycles and World Water Resources. *Science,* 313(5790), 1068-1072, doi: 10.1126/science.1128845.
Pahl-Wostl, C., Downing, T., Kabat, P., et al., (2005). *Transition to Adaptive Water Management: The NeWater Project*. NeWater Working Paper 1, University of Osnabrück, Osnabrück, Germany, 1-17.
Qian, Z.Y. & Zhang G.D. (2001). Strategic Studies of Water Resources for Sustainable Development in China, Vol. 1 (in Chinese). *Chinese Water Resources and Hydropower Press*, Beijing, China, 1-10.
Wu, Z., Liu, Z., Xiao, H., et al., (2015). Assessing Impacts of Future Climate Change on the Risk of Using the Mengwa Flood Detention Area in Huaihe River Basin. *Progressus Inquisitiones de Mutatione Climatis*, 11(1), 1-7 (in Chinese).
Xia, J. & Zhang, Y. (2008). Water Security in North China and Countermeasure to Climate Change and Human Activity. *Physics and Chemistry of the Earth*, 33(5), 359–363
Xia, J. (2010). Screening for Climate Change Adaptation: Water Problem, Impact and Challenges in China. *International Journal on Hydropower & Dams,* 17(2), 78-81.
Xia, J., (2012). Special Issue: Climate Change Impact on Water Security & Adaptive Management in China. *Water International,* 37(5), 509-511.
Xia, J. & Chen, Y.D. (2001). Water Problems and Opportunities in Hydrological Sciences in China. *Hydrological Science Journal,* 46(6), 907-921.
Xia, J., Chen, J.X., Weng, J.W., et al. (2014). Vulnerability of Water Resources and Its Spatial Heterogeneity in Haihe River Basin, China. *Chinese Geographical Science,* 24(5), 525-539.
Yu, Y., Xie, Z.H. & Zeng, X.B. (2014). Impacts of Modified Richards Equation on RegCM4 Regional Climate Modeling Over East Asia. *Journal of Geophysical Research. Atmospheres*, 119(22), 12642-12659.
Zhang, J, Wang, G., Yang, Y., et al. (2009). Impact of Climate Change on Water Security in China. *Advances in Climate Change Research*, 5, 34-40.
Zhang, D.F., Gao, X.J., Luo, Y., et al. (2015). Downscaling a 20th Century Climate Change of a Global Model for China from RegCM4.0: Attributable Contributions of Greenhouse Gas Emissions and Natural Climate Variability. *Chin. Sci. Bull.,* 60(17), 1631–1642, doi:10.1360/N972015-00007(in Chinese).
Zhang, R. (2015). Natural and human-Induced Changes in summer Climate Over the East Asian Monsoon Region in the last Half Century: A Review. *Advances in Climate Change Research*, 6(2), 131–140.

REAL-TIME, ADAPTIVE, SELF-LEARNING MANAGEMENT OF LAKES

JÖRG IMBERGER[(1)], CLELIA L. MARTI[(2)], CHRIS DALLIMORE[(3)], DAVID P. HAMILTON[(4)], JUAN ESCRIBA[(5)] & GIULIA VALERIO[(6)]

[(1)] Department of Ocean Sciences, Rosenstiel School of Marine & Atmospheric Science, University of Miami, Miami, USA jimberger@rmsas.miami.edu

[(2)] Sustainable Engineering Group, Faculty of Science and Engineering, Curtin University, Perth, Australia clelia.marti@curtin.edu.au

[(3)] Hydronumerics Pty Ltd, Melbourne, Australia dallimor@hydronumerics.com.au

[(4)] Environmental Research Institute, University of Waikato, Hamilton, New Zealand davidh@waikato.ac.nz

[(5)] INYMA CONSULT SRL, Asunción, Paraguay jescribagm@gmail.com

[(6)] DICATAM, Universita degli Studi di Brescia, Brescia, Italy giulia.valerio@unibs.it

ABSTRACT

Lakes and reservoirs are increasingly threatened by anthropogenic activities, with serious environmental and financial consequences. In particular, nutrient loadings are increasing due to expanding human populations and food demand, and thermal stratification is increasing due to global warming. For deep lakes, this is leading to an increase of the seasonal water column stability, extending the duration of seasonal deoxygenation of hypolimnetic waters, as well as increasing the nutrient inventory within the bottom sediments. The large volume of deoxygenated hypolimnetic water and nutrient-enriched bottom sediments increase nutrient releases. This overturn brings the deoxygenated, nutrient rich hypolimnetic water into the euphotic zone, leading to increased primary productivity, organic enrichment, and providing a feedback mechanism for further degradation of the fauna and flora living in the epilimnion, potentially culminating in total death of aerobic organisms by asphyxiation. Reservoirs and shallow lakes are increasingly subjected to toxic algal blooms in response to changing patterns of stratification in combination with the increasing nutrient loadings. We use two examples to illustrate the problems presently encountered, the range of control strategies available to manage the consequences and then show how adaptive, real-time, self-learning technologies may be used to dynamically optimize the ecosystem health, as both the impacts and the system change with time. The first example is deep Lake Iseo in Italy. The period between overturns has increased from around every ten years to twenty years in Lake Iseo over the last 50 years. We show that the water column stratification may be controlled with solar-powered impellers, allowing the frequency of overturning to be regulated so as to prevent the buildup of large volumes of low-oxygen hypolimnetic waters. The second is shallow Lake Ypacarai in Paraguay. It has undergone rapid eutrophication, resulting in severe toxic algal blooms that are having a devastating impact on the economy of Paraguay. Using the numerical simulations of the lake ecosystem, we carried out a sensitivity analysis of the available controls for the mitigation of the algal blooms. The simulations demonstrate how a decrease in the nutrient loadings, decrease in the water levels, flushing of the lake with bore or river water and increase in water opacity provide multiple potential bloom control mechanisms. The results for both lakes indicate that a real-time adaptive management system using model forecasts could optimize environmental controls on attributes (e.g. cyanobacteria and dissolved oxygen) that would otherwise seriously deteriorate and impact the ecological processes throughout the lake ecosystems.

Keywords: Lakes; global warming; nutrient loadings; algal blooms; adaptive management.

  / ISSN 1562-6865 (Online) - ISSN 1063-7710 (Print)

1 INTRODUCTION

The traditional response to manage algal blooms in standing waters is to develop an environmental plan aimed at reducing external macronutrient loads (Paerl et al., 2016). Often, however, more often than not, the problem of increasing nutrient loads is ignored until, for example, a cyanobacterial bloom develops and/or fish kills occur (e.g. Kangur et al., 2016). At this point, the plans are taken off the shelf and a blame game is set into motion. Even when such plans are activated, they are often compromised by large inventories of macronutrients (legacy nutrients, Spears et al., 2014) stored in the bottom sediments, and reflecting historical excesses of catchment loads (Hamilton et al., 2016). This inventory is often mobilized unpredictably and rapidly in response to declining ecological condition in lakes (Zhu et al., 2014). Recent trends in environmental management have been to move away from management via fixed plans and abrupt, often politically driven responses, towards “adaptive, real-time, self-learning control and management”. There are three main reasons for this change. First, it is extremely difficult to impose a strict “plan” over a lake basin, as both natural and anthropogenic loadings evolve in response to multiple factors (e.g. climate, human populations, changes in weathering) so rigid control, involving prohibition or restriction of land use activities, is very expensive and rarely works. Second, the scale of human actions and the reach of actions have become global in the last 20 years or so. The outcome is that local actions aimed at improved practices can be diluted by political imperatives usually driven by global trends and economic incentives. The result is changing ecological functioning of both the lake basin and the lake itself, as well as the changes in weather, invalidating the assumption of statistical stationarity upon which conventional management plans are predicated. Third, sensor, communications and modeling technologies have all recently greatly improved, allowing decisions to be made in real-time, based on the dynamic feedback from the environmental domain coupled with real-time numerical simulations (e.g. Marti and Imberger, 2015, Reis et al., 2015). This allows non-stationary behavior to be better quantified, understood and managed.

Adaptive management recognizes the non-stationary nature of a system and consists of five, complementary, components (Marti and Imberger, 2015, Gunderson, 2015):

1. *Process field work and experimental studies aimed at identifying and quantifying the sensitivity of the controls on the system*. The basis of this scientific investigation is to understand the underlying ecological processes at catchment scale, quantify and predict their responses to anthropogenic impacts, and provide data suitable for testing the relative sensitivity of possible ecological controls.
2. *Numerical models to mimic the ecological function of the domain.* Fundamental process understanding is used here to set up relevant numerical models that are suitably resolved in time and space to simulate the responses from expected anthropogenic developments. Such models will first, contain deficiencies in their initial process descriptions and will therefore require additional process descriptions to be added as the system characteristics are described more completely, as anthropogenic impacts change, and with changes in community expectations over time.
3. *Real-time monitoring hardware.* Installation of critical real-time monitoring sensors provides opportunity for feedback of the system response and may be used to evaluate the simulation model results, *i.e.* for validation purposes (Hamilton et al., 2014).
4. *A Real-time Online Management System (RMSO).* This system allows the simulation models to run both in real-time and forecast mode and real-time data to be connected and fully integrated into the decision making, thus allowing:
    a. Custodians of the lake basin to be alerted, in real-time, of model and data stream departures from normal operating and/or ecological conditions.
    b. The deviation between model and data streams as feedback to assess the need for new process knowledge. This facilitates new algorithm development and cutting-edge science.
    c. Connection of the simulation models to “cloud” derived boundary conditions data streams, such as meteorological forcing from WRF [Weather Research and Forecasting Model (Skamarock et al., 2008)], open ocean forcing from HYCOM [HYbrid Coordinate Ocean Model (Chassignet et al., 2007)] and surface tide and wave characteristics from Wavewatch III (Tolman, 2002). Such boundary condition data streams, coming from the cloud, are now available for up to 20 years in forecast mode, allowing long time predictions to be made of the impacts of proposed developments. Given the advances in models, even a Monte Carlo approach can be used to arrive at optimum designs for new developments.
    d. Adapting a neutral objective function, such as the ISF [Index of Sustainable Functionality (Imberger et al., 2007)], that provides a quantitative measure of whether actions lead to mounting unwanted externalities.
    e. Disseminating the objective function value to the community and all stakeholders via the internet, providing a learning base for an educated stakeholder response that can stand up to special interest pressures.
5. *Solicit Stakeholder Feedback.* Set up close links with educational institutions in the lake basin, through social media, to provide a real life, local and sound educational tool. Use social media to

facilitate active communications with management system in place in other countries, to provide for comparative studies and facilitate rapid learning and uptake of universally acknowledged best practices.

In this contribution we focus on assessing the feasibility of using an adaptive management approach (Figure 1) in order to improve the health and resilience of lakes across the globe, to mitigate toxic algal blooms in shallow water bodies, and more generally to conserve flora and fauna of inland waters, as more biota are at risk of extinction in freshwater ecosystems than for any other ecosystem across the globe. We provide process evidence that the periodicity of overturning in large lakes may be controlled by using submerged impellers to artificially mix the water column and that toxic algal blooms are best mitigated with a multiple control strategy approach.

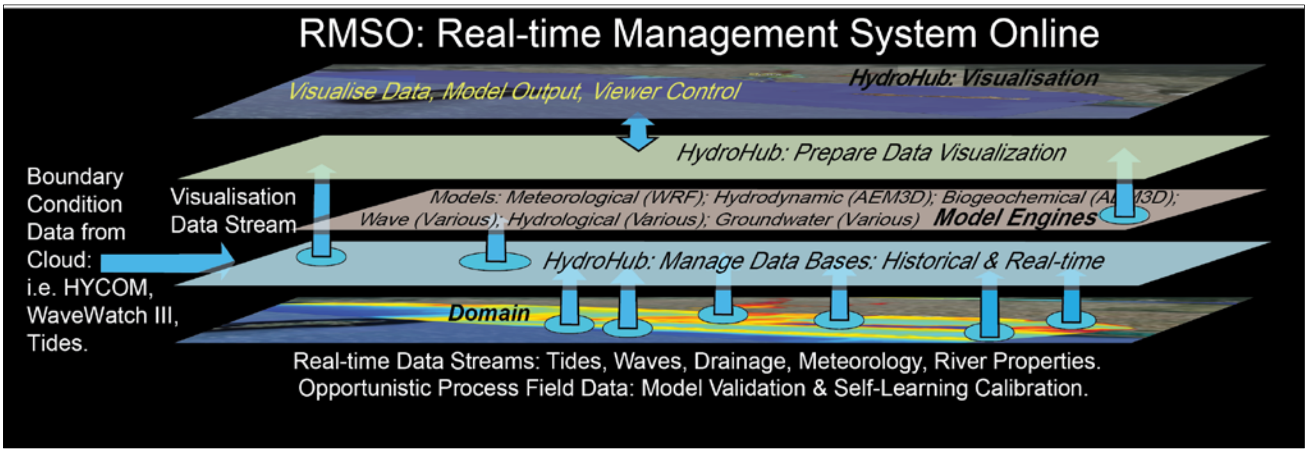

Figure 1. Schematic of a real-time adaptive management component structure and connectivity.

2 METHODS

2.1 Numerical Model

In this study, numerical simulations were conducted with the 3-dimensional coupled Hydrodynamic-Aquatic Ecosystem Model (AEM3D, Hodges and Dallimore, 2016) that was developed from the ELCOM-CAEDYM (Hodges et al., 2000, Romero et al., 2004) source code. The hydrodynamic solver uses the unsteady, viscous Navier-Stokes equations for incompressible flow with or without the hydrostatic assumption for pressure (Hodges et al., 2000). Calculated processes include baroclinic and barotropic responses, rotational effects, tidal forcing, wind stresses, surface thermal forcing, inflows, outflows, transport of salt, heat and passive scalars and mixing of all the state variable with either a mixed fraction algorithm or a Richardson Number dependent eddy diffusion coefficient. The hydrodynamic algorithms are based on the Euler-Lagrange method for advection of momentum with a conjugate-gradient solution for the free-surface height. Passive and active scalars (*i.e.* biogeochemical state variables, salinity and temperature) are advected using a conservative ULTIMATE QUICKEST discretization. The biogeochemical model includes a library of algorithms that represent the key biogeochemical processes (Romero et al., 2004) influencing water quality under the simulated physical conditions. Mixing and transport are solved separately to the rate of change due to the biogeochemical processes. The biogeochemical processes include primary production, secondary production, nutrient, carbon and metal cycling, oxygen dynamics and the transport and deposition of suspended solids. AEM3D can be run either in standalone hydrodynamic mode or as a fully coupled hydrodynamic biogeochemical model. The reader is referred to Marti et al. (2016) for similar application of the AEM3D model to Lake Iseo and for Lake Ypacarai, the default configuration was used for the hydrodynamics, but given that the focus was to understand the triggers for the toxic algal bloom observed in 2012, the configuration of the biogeochemical model component was adapted to include two phytoplankton state variables, but no higher levels of the food web.

2.2 Focus sites

2.2.1 Lake Iseo

The period between deep overturns is a decisive factor for the evolution of water quality and biocenosis in deep lakes, because the deep circulation oxygenates the hypolimnion (Boehrer and Schultze, 2008). Global warming is intensifying the thermal stratification of deep, mid-latitude lakes, leading to longer stratified periods, stronger thermal gradients across the thermocline and altered mixing conditions in the metalimnion (Peeters et al., 2002, Danis et al., 2004). Recent observations suggest that the time between complete water column overturn in deep lakes in general has increased by more than twofold in mid-latitude lakes, close to urban centres (Garibaldi et al., 2003). This is the result of three factors. First, increased phytoplankton growth in the surface layer increases the turbidity of the surface layer waters, causing the short wave radiation to be absorbed closer to the lake surface. Second, increasing greenhouse gases leads to an almost insignificant increase in incoming long wave radiation, but this amplified by the resulting increased humidity heat, resulting in a net increase of incoming long wave radiation, ΔQ_{LWI}, of approximately:

$$\Delta Q_{LWI} = 4\,\mathrm{Wm^{-2}}. \qquad [1]$$

Third, the increasing water column stability progressively shuts down the dissolved oxygen fluxes derived from surface aeration and production, while at the same time the increased phytoplankton biomass leads to an increase in oxygen demand, which in turn, fosters an enhanced dissolution of redox sensitive chemicals from the sediments into the lower part of the water column. In the extreme case, this initiates a transition for the lake to become meromictic. The water column potential energy is therefore a major factor influencing ecosystem health in a deep lake.

Lake Iseo is the fourth largest Italian lake in terms of volume, with a volume of 7.9 km^3, a surface area of 60.9 km^2 and a maximum depth of 256 m. The major inflows into Lake Iseo are the Oglio River and the Industrial Canal, entering the lake at the northern end, while the major outflow, the Oglio River, leaves the lake at the southwestern end (see Figure 2a). The lake is L-shaped with steep sides and with a 4.5 km^2 island in the central part of the basin. The wind field over the lake varies greatly spatially being strongly influenced by the island and the surrounding mountainous topography. This spatial variability is important as it determines which internal modes are excited by the wind forcing, which in turn, determines the mixing regimes in the lake (Valerio et al., 2012, Marti et al., 2016).

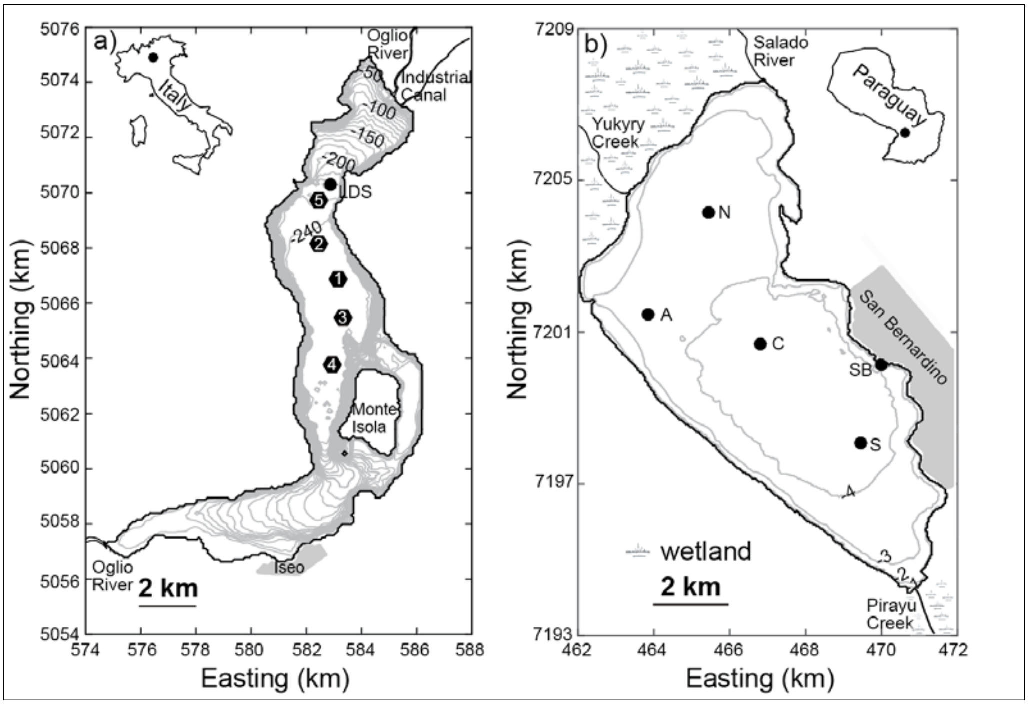

Figure 2. Location and bathymetry of (a) Lake Iseo and (b) Lake Ypacarai. Circles indicate the locations of the field data sampling stations. Hexagons in a) indicate the locations of the impellers. Contour values (in metres) are expressed relative to mean water level.

Lake Iseo shows a strong seasonally succession of phytoplankton consisting of cyanobacteria (mostly *Planktothrix rubescens*), green algae (mainly *Sphaerocystis schroeteri* and *Mougeotia spp.*) and diatoms (mainly *Fragilaria sp.* and *Diatoma elongatum*) (Garibaldi et al., 2003, Marti et al. 2016). Since the end of the 1980s, the deep layers of the lake have become more severely deoxygenated (see Figure 3) and the frequency of full overturn has changed from about once less than about 12 years before 1980 to 25 years in the period between 1980 and 2005. Also noticeable from Figure 3 is the increase in the rate of oxygen depletion of the hypolimnetic waters from an average of about 1 mg $L^{-1} y^{-1}$ in the 1990s to about 3 mg $L^{-1} y^{-1}$ in between 2006 and 2011.

These observed changes may be explained as follows. The reduction of the Secchi depth (Figure 3) from around 6 to 4 m over 20 years implies an increase of the extinction coefficient from about 0.28 to 0.42 m^{-1}. Assuming the increase in light absorption is predominantly due to higher concentrations of phytoplankton, then using the correlations established by Behrenfeld and Boss (2006), this implies a threefold increase of phytoplankton concentration in the surface layer. Assuming that the mass of organic matter falling into the hypolimnion, as dead algal cells, is associated with uptake of oxygen in this layer and that phytoplankton biomass in the surface layer is linearly related to the dissolved oxygen concentration, then the hypolimnetic oxygen uptake rate would have increased from 1 mg L-1 y^{-1} in the 1980s to 3 mg L-1 y^{-1} around 2010 (Figure 3). These biological changes combine with the small changes in the surface heat and momentum fluxes due to global warming. However, as shown by Tanentzap et al. (2008) and O'Reilly et al. (2015), each lake must be viewed on its own merits, as global warming is also known to force strong local weather changes. Thus, the small consistent increase in incoming long wave radiation due the greenhouse effect, may be overwhelmed by local variations in air temperature, wind speed and humidity that are changing on a global warming time scale, but at different rates and signs depending on the geographic regional location, all impacting on the heat budget of the surface layer. Thus, to gain a quantitative overview of how a particular lake responds to global warming and increased nutrient loadings, it is necessary to use local meteorological and stream flow data.

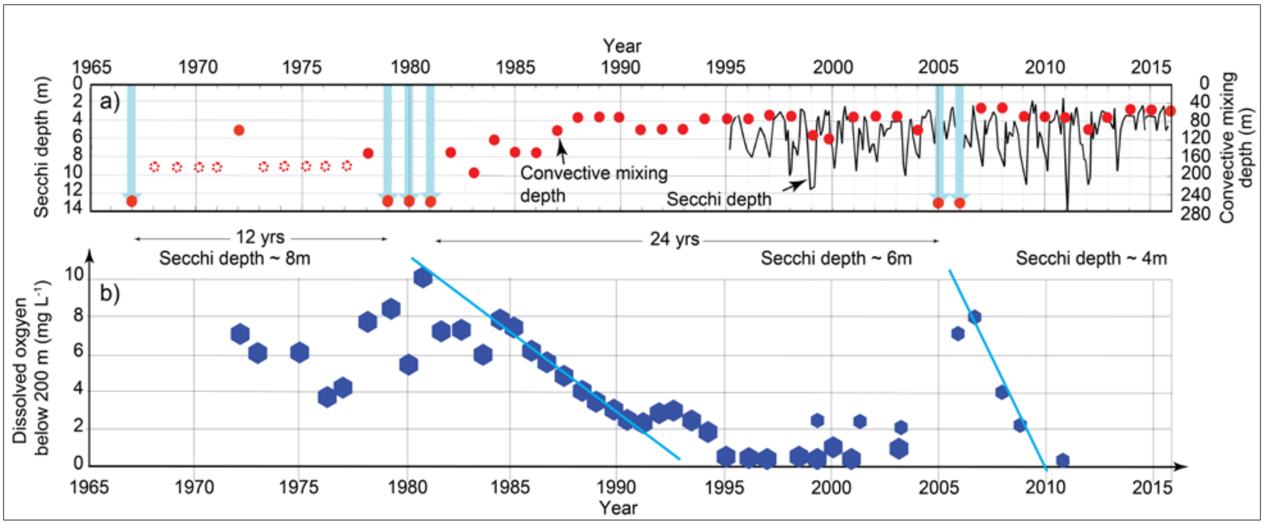

Figure 3. The time evolution, between 1965 and 2015 of the water column characteristics of Lake Iseo: (a) Secchi depth and convective mixing depth and (b) dissolved oxygen concentration at 200 m depth. Arrows in (a) indicate the full overturn of the lake. Lines in (b) represent the best fit during the period of oxygen depletion. (Data source: Bonomi and Gerletti, 1967; Cordella, 1976; Ambrosetti and Barbanti, 2005; Salmaso et al., 2007; Pilotti et al., 2013).

The objective of the present contribution is to show, by examining the response of a particular lake, Lake Iseo, with numerical simulations using AEM3D, that the increasing potential energy, due to heating from global warming heating, increasing extinction coefficient and increased solute in the hypolimnion, is small enough, at about 12 kW, to be countered with simply solar powered underwater impellers, described by Morillo et al. (2009) that individually were shown to have a mixing energy capacity of about 3 kW per impeller.

2.2.2 Lake Ypacarai

Lake Ypacarai, located in Paraguay, is approximately 30 km to the east of the capital Asunción (Figure 2b). The lake has a volume of 115 x 10^6 m^3, a surface area of 59.6 km^2, a maximum depth of 4 m and a mean depth of 2 m. The lake is located 62.7 m above sea level, and the associated river basin has an area of ~ 1100 km^2. The major inflows are the Yukyry Creek from the north and the Pirayú Creek from the south. The lake has only one outflowing river, the Salado River, which flows into the Rio de la Plata River via the Paraguay River to reach the Atlantic Ocean. It is important to note, as seen in Figure 2b, that there are extensive wetlands at the delta of Pirayú and Yukyry creeks. Under normal conditions, when the wetlands are not flooded, they intercept and abate the nutrient and sediment loads coming from the basin, before they reach the lake proper and add humic acids to the water (Imai et al., 1999) that will be shown below to influence active algal growth.

Lake Ypacarai and its basin ecosystems are the holiday destination and principal place of leisure for the population of Asuncion, so they have a major economic and tourism value. Lake Ypacarai is also the water source for the city of San Bernardino (Figure 2b), which has a population that can exceed 50,000 in the summer tourist season. In the last 50 years, the expansion of the urban areas of Asuncion towards the lake and the associated changes in land use, in most of the lake basin, have resulted in a marked deterioration of the water quality in the tributary streams increasing the nutrient, heavy metals and sediment loadings to the lake, adversely impacting the ecological health of both the lake and the wetlands (Stanley, 2009). Furthermore, most of the population does not have access to a sewage network and effluents are simply discharged directly into the ground by cesspools and septic tanks. The total annual loads of nutrients reaching the wetlands were estimated to be in the order of 5,450 t of total nitrogen (TN) and 1,180 t of total phosphorus (TP). Over 60% of the loads are generated in the Yukyry creek basin and about 55% are produced by the population through the disposal of sanitary wastewater, while the animal farming activities are responsible for 35% of the total. The remaining 10% is from other sources. The annual organic load was estimated to be in the order of 24,000 t of BOD5, 70% of which is produced by the disposal of sanitary wastewater and 20% by urban runoff. The rest is from other sources (Consorcio BETA Studio - Thetis, 2015). These loads do not all reach the lake, but undergo some reduction during their journey to the lake due to the natural remediation capacities of the wetlands. Such reduction depends on the time the pollutants stay in the wetlands. It is estimated that the wetlands of the Yukyry creek, when the inundation is optimum, capture somewhat more than 70% of the total loads coming from the basin, before the water reaches the lake (Consorcio BETA Studio - Thetis, 2015). In addition, the data collected since the intense cyanobacteria bloom in 2012, show that the concentration of dissolved organic carbon (DOC) is a function of the extent of inundation of the wetland, as quantified by the surface water level. The lake is characterized by low transparency (0.10 - 0.20 m), high suspended solids concentration (70 - 80 mg L^{-1}) and high concentrations of DOC coloring the water when it is most strongly influenced by wetland inputs. The lake is a eutrophic to hypertrophic water body (Consorcio BETA Studio - Thetis, 2015) characterized by high nutrient concentrations (TP ranges from 0.005 to 0.55 mg L^{-1} and TN from 0.5 to 3 mg L^{-1}) and in the last 15 years, high concentrations of cyanobacteria (e.g. *Microcystis, Anabaena*). During the period September 2012 to December 2012, high numbers of the cyanobacterium *Cylindrospermopsis raciborskii* were observed (~ 1,000,000 cells mL^{-1}) (OPS, 2012). This period corresponded to a time when a bridge construction in the Salado River outflow caused high water levels in the lake. In the following months of 2013, the abundance of this species remained high, with values of about 100,000 cells mL^{-1} (Benitez et. al., 2015).

Traditional management strategies for the alleviation of toxic algal blooms, are based on reduction of the various form of P and or N, but as mentioned above, with respect to Lake Iseo, reducing the macronutrient loadings is made difficult by perception in developed countries that pollution is a right, and also, when it is successfully implemented, it is very expensive (Hammerl and Gattenhoehner, 2003). Analogous to Lake Iseo, the question here in Lake Ypacarai is whether the real-time adaptive management methodologies can be used in form of water level control, maximizing the export of color from wetland and possibly flushing the lake with nutrient free groundwater. Here, we explore the sensitivity of the water quality in the lake to the above controls.

3 RESULTS

3.1 Lake Iseo

The objectives of the Lake Iseo simulations were first, to quantify the effect of a small increase in incoming long wave radiation the result of global warming and a small increase in the extinction coefficient, the result of increasing primary production, on the water column stability of the lake. Second, to show, by the example of Lake Iseo, that the above two increases of potential energy may be kept in check, or even reversed by mixing the water column with submerged impellers, of the type described by Morillo et al. (2009). To achieve this objective only the hydrodynamic code was applied to the Lake Iseo bathymetry (Figure 2a), using the dataset by Pilotti et al. (2013). The model was run on an 80 m x 80 m horizontal grid with a vertical resolution ranging from 0.5 m in the diurnal surface layer to 25 m at the bottom. Three cases were simulated. First, a 2012 base simulation was run using measured forcing data (Figure 2a) and a measured extinction coefficient of k = 0.40 m^{-1}. The year 2012 was chosen as good field validation data were available for that year. Second, a simulation mimicking the lake behaviour in the 1990s, referred to as the 1990 case, was run by using the same meteorological forcing data but reducing the incoming long wave radiation by 4 W m^{-2} and changing the extinction coefficient to k = 0.28 m^{-1}. Third, a mixing impeller simulation, based on the 2012 base case was run with five mixers located at the thermocline (see Figure 2a) pushing water down with a thrust of 4600 N each (Morillo et al., 2009). The metric used to quantify the difference between the three cases was the amount of energy required to fully mix the lake to its average temperature at any point in time; the energies were then normalised to the 1990 case as shown in Figure 4. As expected, the increased radiation and extinction coefficient of the 2012 case leads to a significant increase in the stability of the water column during the warming period. As seen from Figure 4b, the five impellers are able to negate the increase in the water column stability and return the water column potential energy back to the 1990 case in a period of four months. Work is currently in progress to derive a dynamic control algorithm for the location of the impellers that would minimize the impeller energy input.

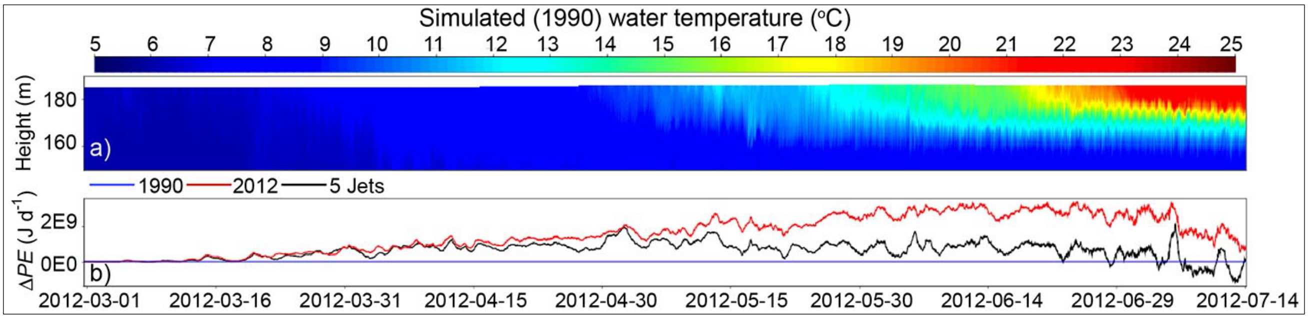

Figure 4. (a) Thermal structure of the top 40 m for the one year simulation with k = 0.27 m^{-1} and no extra heating: 1990 case. (b) The energy required to fully mix the water column relative to the 1990 case for the 2012 case and the 2012 case with 5 impellers pointing down located dynamically at the middle of the thermocline. .2 Lake Ypacarai

The domain of Lake Ypacarai was discretized with a uniform horizontal grid spacing of 80 m, with a vertical resolution of 0.10 m in the upper 0.50 m, and expanding gradually to 0.25 m at depth. Grid resolution studies at finer scale showed no significant difference in model results. The appropriate algorithms in the hydrodynamic model were activated to include atmospheric exchange, inflow and outflow dynamics, turbulent mixing dynamics and Coriolis forcing. The flow was assumed hydrostatic. The biogeochemical model was configured to simulate two groups of phytoplankton (cyanobacteria and diatoms) and the dynamics of phosphorus, nitrogen, dissolved oxygen (DO), silicon, organic matter and one group of suspended solids. Algal biomass was modeled as carbon (C) converted to chlorophyll a (Chl a), with a constant C: Chl a ratio. Phytoplankton dynamics was based on simple growth limitation functions (Hodges and Dallimore, 2016) being constrained to temperature, nutrients, and light, as well as silica in the case of diatoms, mortality, excretion, respiration, settling, and resuspension. Cyanobacteria (*Microcystis aeruginosa*) and diatoms (*Aulacoseira* sp.) were assigned to have constant buoyant and sinking velocities, respectively. The calibration/validation simulations were conducted for a one-week period, starting on 16 September 2015 for which period in-lake field data were available (Figure 2b, INYMA CONSULT SRL, 2015). The model time step was set to 120 seconds. During the period of simulation, the inflows from the Yukyry and Pirayú creeks were negligible and the outflow was assumed to balance the inflows so the lake was assumed closed, with only meteorological forcing acting on the surface. The simulation was driven with 15-minute air temperature, relative humidity, shortwave radiation and 3-hour cloud cover data from a meteorological station located in Asuncion, ~ 30 km northwest of the lake, and 10-minute wind speed and direction data from a meteorological station located in San Bernardino, at the eastern side of the lake. The simulation was initialized with horizontally and vertically homogenous temperature, DO, nutrients (NH_4, NO_3, PO_4 and SiO_2), suspended solids and Chl a (nominally *Microcystis aeruginos*a and *Aulacoseira* sp.) constructed from measured data on 17 September 2015 by averaging data from the five stations shown in Figure 2b. For the validation period the water depth was 2.98 m. The ecological parameters values were derived from the literature (Romero et al., 2004, Reynolds, 2006). The hydrodynamic model did not require calibration, as the physical aspects of water movements in reservoirs are fairly well understood. The water quality model was calibrated by adjusting the Secchi depth through the suspended solids attenuation coefficient. The simulation results achieved are shown in Figure 5, together with field data from the Central station (C in Figure 2b). Horizontal variability was small during the simulation period.

A series of simulations of the hydrodynamics and phytoplankton biomass were conducted in order to explore strategies to mitigate the severity of high biomass algal blooms (cyanobacteria *C. raciborskii)* as observed in 2012 in Lake Ypacarai. These simulations were aimed at testing mitigation strategies to minimize the impact of the phytoplankton bloom and were conducted for a period of 30 days starting on 9 September 2012. The simulations were driven with air temperature, relative humidity, shortwave radiation, wind speed and direction data recorded at 15-minute intervals and cloud cover data recorded at 3-hour intervals from the same meteorological station located in Asuncion, ~ 30 km northwest of the lake. Constant inflow and outflow rates were assumed for the Pirayú and Yukyry creeks and Salado River (2m^3 s^{-1}, 7m^3 s^{-1} and 6m^3 s^{-1}, respectively). For the 2012 period, the water depth was 3.98 m. Due to the lack of inflow temperature data, the two inflows temperatures were estimated as three-day running averages of the air temperature data. Constant values of DO, nutrients (NH_4, NO_3, PO_4 and SiO_2), suspended solids and Chl a (as *C. raciborskii,* the dominant species in the lake, no diatoms were counted) obtained from unpublished data were used for the inflows. The simulations were initialized with horizontally and vertically homogenous values of water temperature, DO, nutrients, suspended solids and Chl a compiled from different sources (Benitez et al., 2015, Consorcio Beta Studio-Thetis, 2015).

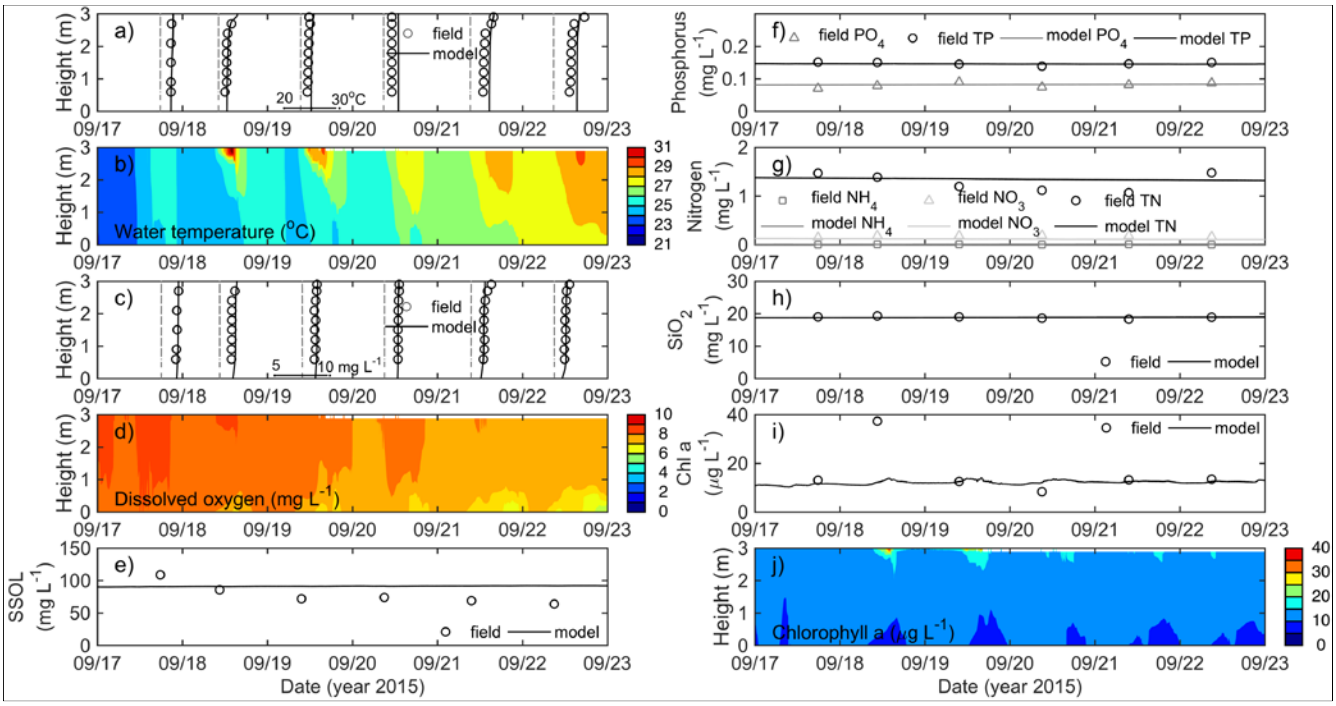

Figure 5. Measured in-lake field data and simulated results at the Central station for the validation period in 2015: (a) measured and simulated water temperature profiles, (b) simulated water temperature contours, (c) measured and simulated dissolved oxygen profiles, (d) simulated dissolved oxygen contours, (e) measured and simulated depth-averaged suspended solids (SSOL) concentrations, (f) measured and simulated depth-averaged PO_4 and TP, (g) measured and simulated depth-averaged NH_4, NO_3 and TN, (h) measured and simulated depth-averaged SiO_2, (i) measured and simulated depth-averaged Chl a, and (j) simulated Chl a contours.

The validated model configuration for 2015 was applied to the one-month period in September and October 2012, the time of the major cyanobacteria bloom. The simulation results for the base case, which we shall refer to as the “mockup”, shown in Figure 6a-h, uses the best estimate for the forcing and initial conditions. The objective was to determine the conditions responsible for the 2012 bloom. Given the paucity of good initial conditions and inflow data, and the absence of any in-lake data during the bloom, such comparisons could not be made, but it will be instructive to see whether the validated model configuration, with realistic forcing and initial conditions, would produce a bloom or bloom tendencies in October. As shown in Figure 6h, the assumed initial cyanobacteria concentration of 30 µg L^{-1} grew to a little under 40 µg L^{-1} in the period from 09/09 to 09/23, then reached a maximum concentration of around 65 µg L^{-1} by 10/09 or about 500,000 cells mL^{-1} with the most rapid growth occurring in the last week of the simulation period. The rate of growth was completely determined by the combination of light limitation and temperature expressed quantitatively by the product of the maximum rate of growth, μ_{max}, times the availability of light, f(I), times the temperature function, f(T), *i.e.* μ_{max} x f(I) x f(T) = 0.7 x 0.2 x 1.4 = 0.2 d^{-1}, implying a doubling time of the concentration field of between three and four days, which conforms to what is seen in Figure 6h; neither P nor N limited growth at any time of the simulation. The results, from this mockup simulation, show that during a bloom, the phytoplankton grow in the diurnal surface layer, whenever there is sufficient light, the water temperature is near that required for optimum growth and the wind is weak enough so as not to mix the blooming phytoplankton more than approximately one meter below the photic depth (Figure 6c,h from 09/20 to 10/09); the one meter is because the assumed rise rate is 1 m d^{-1}. In summary, the mockup simulation suggests that the conditions conducive for the occurrence of a bloom in Lake Ypacarai are that the diurnal mixed layer is comparable, in depth, to the photic depth plus the rise distance per day. Nutrients are more than plentiful, but the growth seems to almost completely be controlled by the availability of light. To test the above light limitation hypothesis a number of scenarios were run. First, the water level was reduced by 1.20 m with same water quality as the mockup case. As seen in Figure 6i, the reduced depth prevented the cyanobacteria from being mixed out of the light zone plus 1 m (> 2) and this caused, as expected, an enhanced phytoplankton growth, the concentration reaching nearly 90 µg L^{-1} by the end of the simulation period. The second way to influence the light climate in the water column was to activate the action of the wetlands and increase the background extinction coefficient and DOC in both the inflows and the initial conditions of the simulations. A scan of the available data of Secchi, the depths revealed an extreme condition where the Secchi depth was only about 15 cm. Figure 6j shows that the cyanobacteria could not grow under these conditions. A second simulation with this extinction coefficient adjustment and reducing the water level again by 1.20 m is shown in Figure 6k. Both scenarios conformed to the assumed hypothesis. The deeper water case (Figure 6j) showed a dramatic growth reduction that was mitigated by reducing the water depth (Figure 6k), as discussed above.

Underneath Lake Ypacarai lies a deep unchartered confined groundwater aquifer, 160 km to the east of the Lake is a further very large confined aquifer and the Paraguay River is also reasonably close by all suggesting a scenario where, when the RMSO unit predicts a pending bloom, additional water is used to partially flush the lake. Figure 6l shows the result for the case of an additional flow of 22 m^3 s^{-1} that would be sufficient to flush the complete lake in 60 days. The impact is noticeable, but not dramatic at the Central station. With a focused design perimeter beaches could, however, be protected in this way.

The past scenario was verifying the obvious, if nutrients are reduced sufficiently, the algal blooms will be prevented (Figure 6m). To avoid the cyanobacteria concentrations from rising above 40 µg L^{-1}, the initial nutrient concentrations and loading had to be reduced to around 1% of the mockup case. In practice, this change would, however, not take effect, until all nutrients in the sediments were also used up.

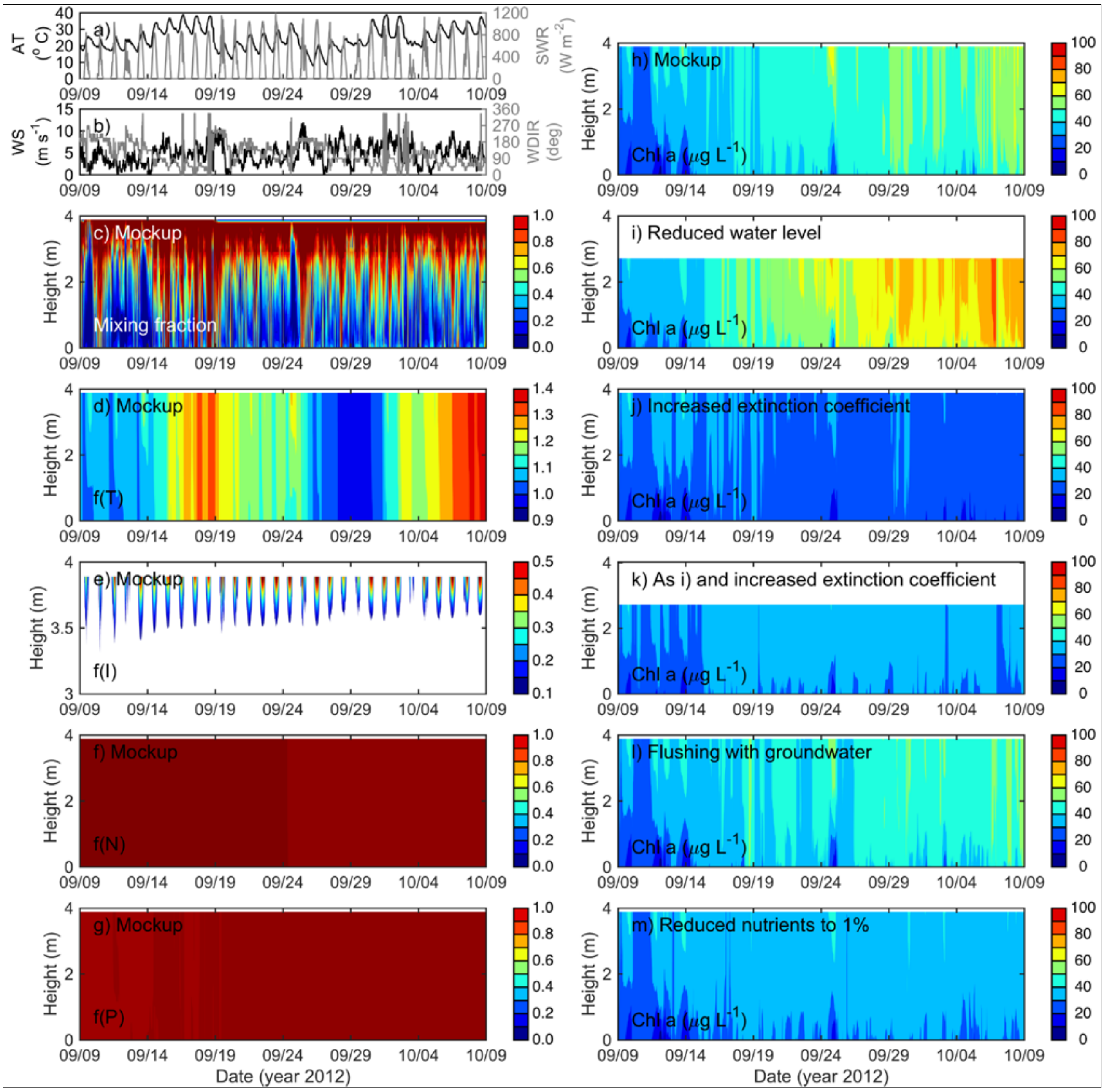

Figure 6. Times series of meteorological data and simulated results at the Central station for 2012: (a) Air temperature and short wave incoming radiation, (b) wind speed and direction, (c) mockup: simulated mixing fraction, (d) mockup: simulated rate of growth temperature dependence f(T), (e) mockup: simulated light limitation function f(I), (f) mockup: simulated nitrogen limitation function f(N), (g) mockup: simulated phosphorous limitation function f(P), (h) mockup: simulated Chl a concentration, (i) water level reduced with no other controls: simulated Chl a concentration, (j) increased extinction coefficient only to mimic possible

wetland restructuring with vegetation rich in tannins: simulated Chl a concentration, (k) water level reduced by 1.20 m, and extinction coefficient increased to mimic the action of the wetlands, in increasing yellow substances, at lower water level: simulated Chl a concentration, (l) adding 22 $m^3 s^{-1}$ of clean water to Pirayú inflow, designed to mimic flushing of the lake: simulated Chl a concentration, and (m) TP and TN inflow and initial concentrations reduced to 1% of those estimated for mockup: simulated Chl a concentration.

4 DISCUSSION

4.1 Lake Iseo

The Lake Iseo simulations clearly demonstrated that submerged impellers may be installed to control the water column stratification even in large deep lakes. A simple magnitude estimate analysis demonstrates the nature of the impeller action. The increase in incoming long wave radiation, is absorbed in the first few millimeters of the lake water column and is then distributed over the diurnal surface layer by the wind and night cooling, as shown schematically in Figure 7. Over a 24 hour cycle, from say 06:00 to 06:00 of the next day, we may assume that estimates of the temperature, θ', and the resulting relative potential energy increase due to global warming (GW), $\Delta PE|_{GW}$, of the diurnal surface layer are given by:

$$\theta' = \frac{\Delta Q_{LW}\Delta t}{\rho_0 C_P h_m} \sim 0.004^{\circ}\mathrm{C\,yr^{-1}} \quad [2]; \text{ and } \quad \Delta PE|_{GW} = A_0 g \alpha \theta' \rho_0 h_m \left(\frac{H}{2} - \frac{h_m}{2}\right) \sim 6.42\times10^{8}\,\mathrm{J d^{-1}} \quad [3]$$

where $h_m = (h_1 + h_2)/2 = 20$ m, ρ_0 is a reference density, $H = 124$ m is the mean water depth, and C_P is the specific heat, $A_0 = 60.9 \times 10^6$ m^2 is the lake surface area, g is the acceleration due to gravity and α□is the coefficient of expansion due to heat.

The low oxygen condition in the hypolimnion is known to be causing a small increase of hypolimnetic salinity of around 0.002 psu per year. In terms of the water density, this corresponds to a temperature change of around 0.001 ºC yr^{-1} implying that potential energy increase associated with the salinity increase is smaller than that due to the change of potential energy due to global warming and can easily be overcome with impellers placed in the hypolimnion.

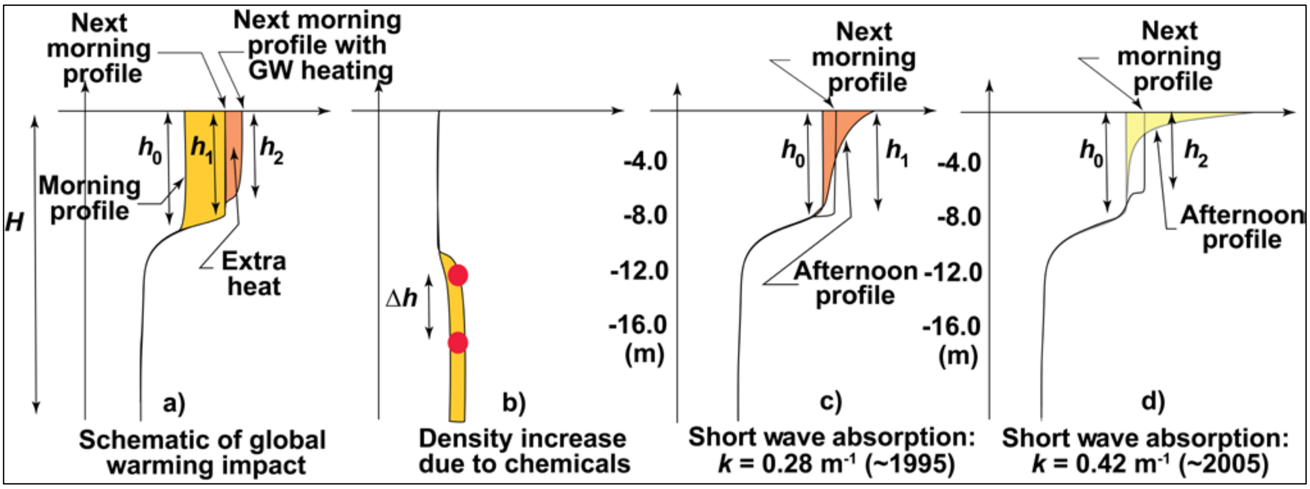

Figure 7. Schematic of the effect of global warming and increased primary production: (a) effect of increase in incoming long wave radiation, (b) density increase of the hypolimnetic waters due to dissolved chemicals, Δh = distance needed to raise extra mass for mixing, (c) short wave radiative heating with deep penetration, (d) short wave radiative heating with shallow penetration.

The effect of an increasing extinction coefficient (Figures 7c-d) is twofold. First, the larger the extinction coefficient, the closer to the water surface the incoming short wave radiation is absorbed and the larger the associated *PE* introduced to the water column and second, as shown in Figure 4d, a larger extinction coefficient, for the same incoming short wave radiation leads to slightly raised water surface temperature and thus a slightly increased long wave outgoing radiation, offsetting the increased long wave incoming radiation (Eq. [1]).

As shown in Figure 4, Lake Iseo experienced a threefold increase in the surface layer phytoplankton concentration over 20 years, which led to a 50% increase in the extinction coefficient. Suppose the short wave heat is distributed through the water column as described by Beer's law:

$$Q_{SW} = Q_{SWO}e^{kx_3} \quad -H < x_3 < 0 \qquad [4]$$

Where Q_{SW} is the short wave radiation at depth x_3, Q_{SWO}, is the short wave radiation entering at the water surface and k is the extinction coefficient. By way of illustration, consider the case where morning convective mixing has homogenized the diurnal surface layer to a depth a little greater than the Secchi depth establishing a uniform temperature, θ_0 over the depth of the surface layer. Carrying out a heat budget over the surface layer, using the absorption relationship (Eq. [4]) leads to a temperature profile $\theta'(x_3,t)$ given by:

$$\theta'(x_3,t) = \left(\frac{k\overline{Q_{swo}}}{C_P\rho_0}\right)e^{kx_3} + \theta_0 \quad [5], \text{ implying } \Delta PE_{sw} = \frac{\alpha\overline{Q_{swo}}gA_0t}{2C_P}\left(H - \frac{1}{k}\right) \qquad [6]$$

Where $\overline{Q_{swo}}$ is the time average incoming short wave radiation and $\rho'(x_3) = \alpha\rho_0\theta'$. Substituting values in Eq. [5] for a time average incoming radiation value of $\overline{Q_{swo}} = 500\,\mathrm{Wm^{-2}}$, suggests a surface temperature differential of 1.5 ºC for k_1 = 0.283 m^{-1} and 2.2 ºC for k_2 = 0.42 m^{-1}, respectively. The associated *PE* change, given by Eq. [6] using the above values leads to a value $\Delta PE'_{SW} = 4.578\mathrm{x}10^8\ \mathrm{Jd^{-1}}$.

The change in the outgoing long wave radiation emitted from the water's surface is given by the emission relationship:

$$\Delta Q_{LWO} = \varepsilon_w\sigma\left[(273+2.2)^4 - (273+1.5)^4\right] \qquad [7]$$

where $\varepsilon_w = 0.96$ is the emissivity coefficient of the water and $\sigma = 5.7\mathrm{x}10^{-8}$ is the Stefan-Boltzmann coefficient. Substituting the values in Eq. [7] implies that the outgoing long wave radiation would increase by about 3.2 W m^{-2}, which approximately equals the extra short wave coming towards the earth, due to greenhouse gases back radiation (Eq. [1]). Thus to first approximation, in Lake Iseo, in terms of heating, the anthropogenic impact of global warming (Eq. [1]) approximately balances extra back radiation, (Eq. [7]) induced by increased phytoplankton biomass, the result of increased nutrient loadings in contributing streams. By contrast, the changes to the potential energy are additive so that implying that bulk estimates of $\Delta PE' = (\Delta PE'_{SW} + \Delta PE'_{GW}) \sim 10^9\ \mathrm{Jd^{-1}}$, comparable to the simulation result as seen in Figure 4b.

The above estimates are clearly dependent on the daily cycle of heating cooling, which is accounted in the numerical simulations (Figure 4). Further insight may be gained by examining two extreme diurnal cycles. First, consider a day when the lake is exposed to a steady wind, strong enough to maintain a well-mixed surface layer preventing the buildup of the surface temperature (Eq. [5]). For such a day, the changes to outgoing long wave back radiation would be minimal, but the potential energy contributions (Eq. [3] and [6]) would be additive. By contrast, for a day with little wind during the sunshine hours, a clear sky and strong solar radiation, the near surface waters would stratify, so that the two radiation inputs would cancel, but again the *PE*'s would add. The above scale estimates suggest that the anthropogenic effects of global warming and increased nutrient loadings add approximately 10^9 J d^{-1} of potential energy to the lakes water column, explaining the simulation results shown in Figure 4. This additional potential energy must be overcome by the meteorological forcing if the historical pattern of complete overturn is to be maintained. For lakes, such as Lake Iseo, where the water column stability is in a delicate balance with meteorological forcing, this increasing potential energy, coupled with increased nutrient loadings, is leading to the period between overturns to progressively increase and if nothing is done three consequences are likely. First, the endemic fauna and flora will most likely be eliminated at the next complete overturn that will sweep low oxygen water into the surface layer. Second, in lakes that contribute to carbon sequestration, such as Lake Iseo, the increase in macronutrient loadings supports increased carbon sequestration in combination with increasing the water column stability. The sledgehammer approach of reducing the nutrient loadings targets both the stability and the sequestration rate, by comparison, mixing with impellers selectively targets only the increasing water column stability (Schindler, 2012). Third, in the long term, these lakes will become meromictic with a continually increasing concentration of dissolved chemicals.

4.2 Lake Ypacarai

We may inspect the phytoplankton growth simulation in Lake Ypacarai and write the phytoplankton growth equation in non-dimensional form:

$$\frac{\partial C'(x_i,t)}{\partial t'} + N_A v'_i \frac{\partial C'(x_i,t)}{\partial x'_i} - N_M \frac{\partial C'(x_i,t)}{\partial x'_3} = \varepsilon'_j(x_i,t)\frac{\partial^2 C'(x_i,t)}{\partial x'^2_j} + N_G \mu'(x_i,t)C'(x_i,t)$$

$$C' = \frac{C}{C_0},\ x'_i = \frac{x_i}{h},\ v'_i = \frac{v_i}{U},\ \varepsilon'_j = \frac{\varepsilon_j}{\varepsilon_j^{(0)}}, \mu' = \frac{1}{\mu^{(0)}}\left\{\mu_{max}\left[Min(f(N),f(P),f(I),)f(T)\right] - Rf(S) - M\right\}$$

$$\text{and}\quad N_A = \left(\frac{Uh}{\varepsilon^{(0)}}\right);\ N_M = \left(\frac{Vh}{\varepsilon^{(0)}}\right)\ N_G = \left(\frac{\mu^{(0)}h}{\varepsilon^{(0)}}\right) \qquad [8]$$

Where C is the algae concentration and μ_{max} is the maximum rate of growth. This maximum growth is constrained by the availability of nitrogen, f(N), availability of phosphorous, f(P), and light, f(I). Furthermore, these constraints are modulated by a temperature function f(T); the growth is small if the water temperature is too cold, occurs at a maximum rate at an optimum temperature and death occurs when the water temperature becomes warmer than a critical temperature. R is the respiration and excretion loss term, f(S) is a salinity modifier for this term and is set to 1 for freshwater. M is the removal of phytoplankton due to grazing by zooplankton and bivalves. Given that here, we are illustrating the control of phytoplankton biomass through changing the physical regime of the water column we may assume that M = 0. The function, R:

$$R(T) = k_r \vartheta^{(T-20)} \qquad [9]$$

Where k_r is the respiration rate coefficient, T is the water temperature and ϑ is the temperature multiplier.

An understanding may be gained of the relative importance of each term in Eq. [8]. The vertical diffusion coefficient ε_3 is related to the mixing fraction, $\eta_{(i)}$ in AEM3D as follows:

$$\varepsilon_3 = \frac{\eta_{(i)}\Delta_3^{(i)}}{\Delta t} \qquad [10]$$

Where $\eta_{(i)}$ designates the ith interface and $\Delta_3^{(i)}$ is the vertical grid spacing at the ith interface. The non-dimensional ratios in Eq. [11] indicate the relative importance of advection relative to mixing, N_A, phytoplankton vertical migration relative to mixing, N_M, and phytoplankton growth relative to mixing, N_G, respectively. The main offending phytoplankton species, cyanobacteria, have a rise velocity, V = 1 m d^{-1}, the scale for the rate of growth $\mu^{(0)}$ = 10^{-5} s^{-1}, the mean depth h = 3 m, and the vertical diffusion coefficient may be estimated from Eq. [10]. When the non-dimensional ratios are equal to 1, then the particular processes change the phytoplankton concentration at the same rate as the concentration is changed by mixing. If we assume h = 1 m, U = 0.1 m s^{-1}, V = 1 m d^{-1} = 1.16 x 10^{-5} m s^{-1} and $\mu^{(0)}$ = 1 d^{-1} = 1.16 x 10^{-5} s^{-1}, then a balance occurs as follows:

$$N_A = 1 \Rightarrow \varepsilon^{(0)} = Uh \sim 10^{-1}\mathrm{m^2s^{-1}} \Rightarrow \eta_{(i)} \sim 0.08 \qquad [11]$$

$$N_M = 1 \Rightarrow \varepsilon^{(0)} = Vh \sim 1.2\mathrm{x}10^{-5}\mathrm{m^2\,s^{-1}} \Rightarrow \eta_{(i)} \sim 0.14 \qquad [12]$$

$$N_G = 1 \Rightarrow \varepsilon^{(0)} = \mu^{(0)}h \sim 8.1\mathrm{x}10^{-6}\mathrm{m^2\,s^{-1}} \Rightarrow \eta_{(i)} \sim 0.1 \qquad [13]$$

This analysis may be used to put the various scenarios simulated (Figure 6) into context. The diffusion coefficient (mixing fraction) will, in practice, be a function of the water depth and the meteorological surface fluxes. In extreme bloom situations, it is most likely that the concentration of phytoplankton will also affect the vertical mixing coefficient, especially when the mixing fraction is small, but little seems to be known about the possibility that the water may become non-Newtonian. In Lake Ypacarai, the water depth is controlled by an adjustable gate and so offers a possibility of using the water level as a control. However, for the effect of the water level to be properly quantified, a surface wave model must be included, this is beyond the scope of the present contribution. Also, the lake is too large for the meteorological fluxes to be influenced by the height of fringing vegetation. However, the water depth in the lake also appears to have a strong influence on the background extinction coefficient and through the light limitation function the effective rate of growth, $\mu^{(0)}$.

Thus, apart from flushing the whole lake with groundwater, controlling the light climate, through manipulating the wetland participation by adjusting the lake level to maximize the leaching of tannins from the wetland vegetation offers the most effective, practical and cost efficient management strategy.

4.3 Global relevance

By considering in detail, the globally relevant issues facing deep and shallow lakes, in Lake Iseo and in Lake Ypacarai, it has been possible to identify strategies for avoiding the anthropogenic disasters awaiting many inland standing water bodies. Combining the identified control strategies with an adaptive real-time, self-learning methodology, will provide solutions on a global scale that will yield positive results with a much higher probability than catchment cleanup programs and at a fraction of the cost. European governments are currently spending billions of Euros to remove P and N from contributing rivers. By way of example the Bodensee cleanup program (Hammerl and Gattenhoehner, 2003) reduced the PO_4 concentration from 90 µg L^{-1} in the 1980s to 6 µg L^{-1} in 2016 at a cost of over 20 EU Billion. However, even if this astronomical cost is ignored the side effect or in legal jargon, the “externality” of the cleanup action were, first, the fisheries in the lake crashed and secondly the desired reduction of phytoplankton biomass would have resulted in a reduction of greenhouse gas sequestration. Given that the world’s lakes and reservoirs sequester approximately three times more carbon than all the world’s oceans, returning the world’s lakes to their original trophic level will necessitate that a similar reduction in global anthropogenic emissions of greenhouse gases (Tranvik et al., 2009).

The priority for the management of shallow lakes, such as Lake Ypacarai, is clearly to gain a quantitative understanding of possible controls on the light climate together with a quantitative cost benefit of reducing the nutrient loading to a particular lake.

5 CONCLUSIONS

The potential energy in the water column stratification of deep lakes is relatively small and is therefore amenable to modification with a very small number of submerged impellers. By coupling the depth of the impellers and the impeller speed to a real-time adaptive management system with an appropriate ISF, it will be possible to control the lake aquatic ecology in order to optimize the lake’s function, conservation, water supply, hydropower, flood control and or carbon sequestration. On the other hand, for shallow lakes it was shown that the main, realistic, control of the aquatic ecosystem health lies in the control of the light climate. Again, using a real-time adaptive management system coupled with real-time data streams, running in forecast mode, would allow real-time Monte Carlo searches for the least risk action to prevent algal blooms.

6 REFERENCES

Ambrosetti, W. & Barbanti, L. (2005). Evolution towards Meromixis of Lake Iseo (Northern Italy) as Revealed by its Stability Trend. *Journal of Limnology*, 64(1), 1-11.

Behrenfeld, M.J. & Boss, E. (2006). Beam Attenuation and Chlorophyll Concentration as Alternative Optical Indices of Phytoplankton Biomass. *Journal of Marine Research*, 64(3), 431-451.

Benitez, G.A., Avalos, C., Araujo, C., Acosta, R., Escobar, A., Franco, G., Astigarraga, O., Peralta, I. & Cardozo, C. (2015). Influencia de los actores ambientales en la biodiversidad de cianobacterias en el lago Ypacarai. *Congreso Paraguayo de Recursos Hídricos*, Universidad Nacional de Asunción, Paraguay, Asunción, 11.

Boehrer, B. & Schultze, M. (2008). Stratification of Lakes. *Review of Geophysics,* 46(2), 1-27.

Bonomi, G. & Gerletti, M. (1967). Il Lago d'Iseo: primo quadro limnologico generale (termica, chimica, plancton e benton profondo). *Mem. Ist. Ital. Idrobiol.*, 22, 149-175.

Chassignet, E.P., Hurlburt, H.E., Smedstad, O.M., Halliwell, G.R., Hogan, P.J., Wallcraft, A.J., Baraille, R. & Bleck, R. (2007). The HYCOM (HYbrid Coordinate Ocean Model) Data Assimilative System. *Journal of Marine Systems*, 65(1), 60-83.

Consorcio Beta Studio - Thetis (2015). *Diagnóstico de la situación actual del Lago Ypacaraí y de su Cuenca*, Informe de avance, Paraguay, Asunción.

Cordella, P. (1976). Ricerche idro-biologiche sul lago d'Iseo. I. Lineamenti della ricerca, condizioni chimico-fisiche, nutrienti algali. *Rivista di Idrobiologia*, 15, 205-236.

Danis, P.A., von Grafenstein, U., Masson-Delmotte, V., Planton, S., Gerdeaux, D. & Moisselin, J.M. (2004). Vulnerability of Two European Lakes in Response to Future Climatic Changes. *Geophysical Research Letters,* 31(21)*,* 1-4.

Garibaldi, L., Anzani, A., Marieni, A., Leoni, B. & Mosello, R. (2003). Studies on the Phytoplankton of the Deep Subalpine Lake Iseo. *Journal of Limnology*, 62(2), 177-189.

Gunderson, L. (2015). *Lessons from Adaptive Management: Obstacles and Outcomes. In Adaptive Management of Social-Ecological Systems*. 27-38. Springer Netherlands.

Hamilton, D.P., Carey, C.C., Arvola, L., Arzberger, P., Brewer, C., Cole, J.J., Gaiser, E., Hanson, P.C., Ibelings, B.W., Jennings, E., Kratz, T.K., Lin, F.P., McBride, C.G., de Motta Marques, D., Muraoka, K., Nishri, A., Qin, B., Read, J.S., Rose, K.C., Ryder, E., Weathers, K.C., Zhu, G., Trolle, D. & Brookes, J.D.

(2014). A Global Lake Ecological Observatory Network (GLEON) for Synthesising High–Frequency Sensor Data for Validation of Deterministic Ecological Models. *Inland Waters*, 5(1), 49-56.

Hamilton, D.P., Salmaso, N. & Paerl, H.W. (2016). Mitigating Harmful Cyanobacterial Blooms: Strategies for Control of Nitrogen and Phosphorus Loads. *Aquatic Ecology*, 50(3), 351-366.

Hammerl, M. & Gattenhoehner, U. (2003). *Lake Basin Management Initiative - Experience and Lessons Learned Brief*. Lake Constance/Bodensee. Lake Basin Management Initiative Regional Workshop for Europe, Central Asia and the Americas, USA, Vermont.

Hodges, B.R., Imberger, J., Saggio, A. & Winters, K.B. (2000). Modeling Basin-Scale Internal Waves in a Stratified Lake. *Limnology and Oceanography,* 45(7), 1603-1620.

Hodges, B.R. & Dallimore, C. (2016). *Aquatic Ecosystem Model: AEM3D, v1.0*, User Manual. Hydronumerics. Australia, Melbourne.

Imai, A., Fukushima, T. & Matsushige, K. (1999). Effect of Iron Limitation and Aquatic Humic Substances on the Growth of Microcystis Aeruginosa. *Canadian Journal of Fisheries and Aquatic Sciences*, 56(10), 1929-1937.

Imberger, J., Mamouni, E.A.D., Anderson, J., Ng, M.L., Nicol, S. & Veale, A. (2007). The Index of Sustainable Functionality: A New Adaptive, Multicriteria Measurement of Sustainability - Application to Western Australia. *International Journal of Environment and Sustainable Development*, 6(3), 323-355.

INYMA CONSULT SRL (2015*). Evaluación de la calidad fisicoquímica y biológica del Lago Ypacarai, afluentes y del Rio Salado. Reporte técnico*, Paraguay, Asunción.

Kangur, K., Ginter, K., Kangur, P., Kangur, A., Nõges, P. & Laas, A. (2016). Changes in Water Temperature and Chemistry Preceding a Massive Kill of Bottom-Dwelling Fish: An Analysis of High–Frequency Buoy Data of Shallow Lake Võrtsjärv (Estonia). *Inland Waters*, 6(4), 535-542.

Marti, C.L. & Imberger, J. (2015). A Real-Time Management System for the Swan-Canning River Basin and its Receiving Waters, Western Australia, Australia. *E-proceedings of the 36th IAHR World Congress*, the Netherlands, The Hague, 1-10.

Marti, C.L., Imberger, J., Garibaldi, L. & Leoni, B. (2016). Using Time Scales to Characterize Phytoplankton Assemblages in a Deep Subalpine Lake during the Thermal Stratification Period: Lake Iseo, Italy. *Water Resources Research*, 52, 1762-1780.

Morillo, S., Imberger, J., Antenucci, J. & Copetti, D. (2009). Using Impellers to Distribute Local Nutrient Loadings in a Stratified Lake: Lake Como, Italy. *Journal of Hydraulic Engineering,* 135(7), 564-574.

OPS, Panamerican Health Organization (2012). *Aparición de la cyanobacteria Cylindrospermopsis raciborskii en Lago Ypacarai,* Boletín Informativo.

O'Reilly, C.M., Sharma, S. & Gray, D.K. (2015). Rapid and Highly Variable Warming of Lake Surface Waters Around the Globe. *Geophysical Research Letters,* 42(24), 773-781.

Paerl, W.H., Gardner, W.S., Havens, K.E., Joyner, A.R., McCarthy, M.J., Newell, S.E., Qin, B. & Scott, J.T. (2016). Mitigating Cyanobacterial Harmful Algal Blooms in Aquatic Ecosystems Impacted by Climate Change and Anthropogenic Nutrients. *Harmful Algae*, 54, 213-222.

Peeters, F., Livingstone, D.M., Goudsmit, G.H., Kipfer, R. & Forster, R. (2002). Modeling 50 Years of Historical Temperature Profiles in a Large Central European Lake. *Limnology and Oceanography*, 47(1), 186-197.

Pilotti, M., Valerio, G. & Leoni, B. (2013). Data Set for Hydrodynamic Lake Model Calibration: A Deep Pre-Alpine Case. *Water Resources Research*, 49(10), 7159-7163.

Reis, S., Seto, E., Northcross, A., Quinn, N.W.T., Convertino, M., Jones, R.L., Maier, H.R., Schlink, U., Steinle, S., Vieno, M. & Wimberly, M. (2015). Integrating Modelling and Smart Sensors for Environmental and Human Health. *Environmental Modelling and Software*, 75, 238-246.

Reynolds, C.S. (2006). *Ecology of Phytoplankton*. Cambridge University Press, 1-267.

Romero, J., Antenucci, J. & Imberger, J. (2004). One- and Three- Dimensional Biogeochemical Simulations of Two Differing Reservoirs. *Ecological Modelling*, 174(1), 143-160.

Salmaso, N., Morabito, G., Garibaldi, L. & Mosello, R. (2007). Trophic Development 0f the Deep Lakes South of the Alps: A Comparative Analysis. *Fundamental and Applied Limnology*, 170(3), 177-196.

Schindler, D.W. (2012). The Dilemma of Controlling Cultural Eutrophication of Lakes. *Proceedings of the Royal Society B*, 1-12.

Skamarock, W., Klemp, J.B., Dudhia, J., Gill, D.O., Barker, D., Duda, M.G., Huang, X.Y. & Wang, W. (2008). *A Description of the Advanced Research WRF Version 3*. NCAR Technical Note, Boulder, Colarado, USA.

Spears, B.M., Maberly, S.C., Pan, G., Mackay, E., Bruere, A., Corker, N., Douglas, G., Egemose, S., Hamilton, D., Hatton-Ellis, T., Huser, B., Li, W., Meis, S., Moss, B., Lürling, M., Phillips, G., Yasseri, S. & Reitzel, K. (2014). Geo-Engineering in Lakes: A Crisis of Confidence? *Environmental Science & Technology*, 48(17), 9977-9979.

Stanley, K.P. (2009). *Ypacarai Watershed Management Planning in the Asuncion Metropolitan Region. In Water and Urban Development Paradigms*. Taylor & Francis Group, London.

Tanentzap, A.J., Yan, N.D., Keller, B., Girard, R., Heneberry, J., Gunn, J.M., Hamilton, D.P. & Taylor, P.A. (2008). Cooling Lakes While the World Warms: Effects of Forest Regrowth and Increased Dissolved

Organic Matter on the Thermal Regime of a Temperate, Urban Lake. *Limnology and Oceanography*, 53(1), 404-410.

Tolman, H. (2002). *User manual and system documentation of WAVEWATCH-III*, version 2.22. US Department of Commerce, NOAA, US, Washington.

Tranvik, l.J., Downing, J.N., Cotner, J.B., Loiselle ,S.A., Striegl, R.G., Ballatore, T.J., Dillon, P., Finlay, K., Fortino, K., Knoll. L.B., Kortelainen, P.L., Kutser, T., Larsen, S., Laurion, I., Leech, D.M., McCallister, S.L., McKnight, D.M., Melack, J.M., Overholt, E., Porter, J.A., Prairie, Y., Renwick, W.H., Roland, F., Sherman, B.S., Schindler, D.W., Sobek, S., Tremblay, A., Vanni, M.J., Verschoor, A.M., von Wachenfeldt, E. & Weyhenmeyer, G.A. (2009). Lakes and Reservoirs as Regulators of Carbon Cycling and Climate. *Limnology and Oceanography*, 54(6), 2298-2314.

Valerio, G., Pilotti, M., Marti, C.L. & Imberger, J. (2012). The Structure of Basin Scale Internal Waves in a Stratified Lake in Response to Lake Bathymetry and Wind Spatial and Temporal Distribution: Lake Iseo, Italy. *Limnology and Oceanography*, 57(3), 772-786.

Zhu, M., Paerl, H.W., Zhu, G., Wu, T., Li, W., Shi, K., Zhao, L., Zhang, Y., Qin, B. & Caruso, A.M. (2014). The Role of Tropical Cyclones in Stimulating Cyanobacterial (*Microcystis* Spp.) Blooms in Hypertrophic Lake Taihu, China. *Harmful Algae*, 39, 310-321.

SMART PLATFORM WITH HYDRO-INFORMATICS FOR SMART WATER MANAGEMENT

JAE-YOUNG AHN[1]

[1] Hyper-Connectivity Source Technology Research Department, Electronics and Telecommunications Research Institute, Yusung, Deajeon city, Korea,
ahnjy@etri.re.kr

ABSTRACT

This paper deals with the technical directions to the realization of promising smart water management (SWM) solutions, focusing on smart water platform that accommodates emerging information technologies to enable the efficient integration of entire water management process and system in an efficient way. Issues on the standard structure of water management system with interoperability, adoption of IoT platform to smart water grid (SWG), horizontal integration of SWG system, necessity of smart water application platform (SWAP), big data and hydro-informatics, and decision support system (DSS) for water grid, have been examined. The vision, "SWM platform with advanced hydro-informatics empowered by big data and CPS (cyber-physical system)", brought in this paper will give rise to further researches on great-sphere economy scale of water management issues and faying surface effects in between socio-economic and environmental hydro-ecosystems.

Keywords: Smart Water Management (SWM); hydro-ecosystem; hydro-informatics; IoT platform.

1 SMART WATER MANAGEMENT (SWM)

The need of smart water management (SWM) has been increasingly justified, and the technical solutions to realize it have been diversely suggested; however, the definitive scope and technical direction in a standardized way of promising design framework have not been clearly pictured enough yet. SWM starts from the idea to integrate ICT into the water management domain to enhance efficiency of its operation, by winning over the spatial and temporal limitations residing in the domain. Since there have been numerous suggestions on various field of solutions to address the issues in SWM, the terminology has come to generally representing all the technical efforts to drive any improvement in water management domain by adopting ICT. Most of those efforts can be categorized into three directions of technical challenges; the first is to correspond water shortage and water hazard due to climate change, the second is to act for environment and sustainability endangered by the increase of mega city and population, and the third is to address the need of better quality and efficiency in water usage in compliance with economic development. Such challenges have been recognized as the driving force of SWM for recent years (Martyusheva, 2014; ITU, online; 2010; WWF, 2015).

2 SMART WATER GRID (SWG)

SWG has been propounded in many places either as a synonym of SWM or as a new concept of taking “grid” feature as for the vehicle of innovation in SWM. It is used to focus more on the areas where the direct outcomes from the application of ICT are expected, such as water conservation, efficient management of scarce water resource, leakage detection in ageing infrastructure, and asset management (Martyusheva, 2014). Technical effort currently put in SWG are concentrated to help measuring, monitoring, and the distribution of water as a result of environmental issues has not been fully identified and compiled (ITU, online). Obviously, ICT can play a special role to help towards better distribution, management, and allocation of water; those must be the focal areas for ICT in water management (ITU, 2010) and the areas are actually corresponding to the business of water operators. Related definitions focusing on “drinking water business” can be cited as the following: *Smart Water is the application of IT in water management so as to optimize the performance of drinking water and sanitation services and monitor water quality* (Gourbesville, 2015; 2016). *Smart Water Grid is an intelligent water management system that efficiently produces, transports, stores, distributes, and manages a variety of water resources. It is the system that resolves the spatial-temporal imbalances of water resources and enhances the efficiency and effectiveness of water resources management by applicable scales* (Telecommunication Standardization Sector, 2013). It is understandable that the allocated meanings of SWG are focusing first on the business areas out of environmental water issues. ICT for SWG requires a new investment, and the entities in drinking water business are the most likely afford it when they find economy from the technology and the use of it (Libelium World, online; WWF, 2015). The term SWG used in this paper will be considered for its business aspect firstly, and for its “grid” feature of realization secondly.

3 WATER AND INFORMATION NETWORK

Korea has carried projects on SWG that implement the informatized drinking water circulation system based on AMI (advanced metering infrastructure), multi-source water intake blending, waste water reclamation, and water information system for consumers (Lee, 2015). Hitachi suggested the concept of intelligent water system to implement systems based on a platform of "water cycle traceability" that utilizes ICT to monitor the status of water quality, water quantity, and other environmental factors and treats water resource management as a flow of both water and information (Onishi and Kageyama, 2011). There were many other trials to develop similar systems that actively utilize the information networking together with water system. A new terminology Smart Water Network (SWN) has been used in recent years at a definition and justification as the following: that is an integrated set of products, solutions and systems that enable utilities to remotely and continuously monitor and diagnose problems, prioritize and manage maintenance issues and use data to optimize all aspects of the water distribution network (Sensus, online). Its aimed goal and pursuing value are similar with SWG; however, SWN concerns more on the synergies in the integrated operation of data network and water distribution network.

4 CONVERGED REFERENCE MODEL

Such an effort to deal with the information flow and physical flow of drinking water processing system in the integrated way is the typical aspect of ICT convergence system, which should be captured in a standard reference model to lead the support from market and following researches. There were efforts to develop standard models of promising SWG systems (Ahn, 2015; Ye et al., 2016), and previous works on smart (power) grid architecture model (SGAM) that is reasonable to be applied to SWG for further materialization with standard reference models (CEN-CENELEC-ETSI, 2014; 2014). Figure 1 proposes a basic reference model of convergence system that applies the interworking scheme of SGAM (CEN-CENELEC-ETSI, 2014) to the standard information system model of water management system (Ahn, 2015). It shows how the physical process of water management system are structured in relation with information management system, and figures the vertical flow of information value from the horizontal flow of water process layer to upper layers of business. The model helps the standards development of interworking functions in each layer of information system, as well as the layer-wise systematic installation of smart control functions on the top of lower layer facilities.

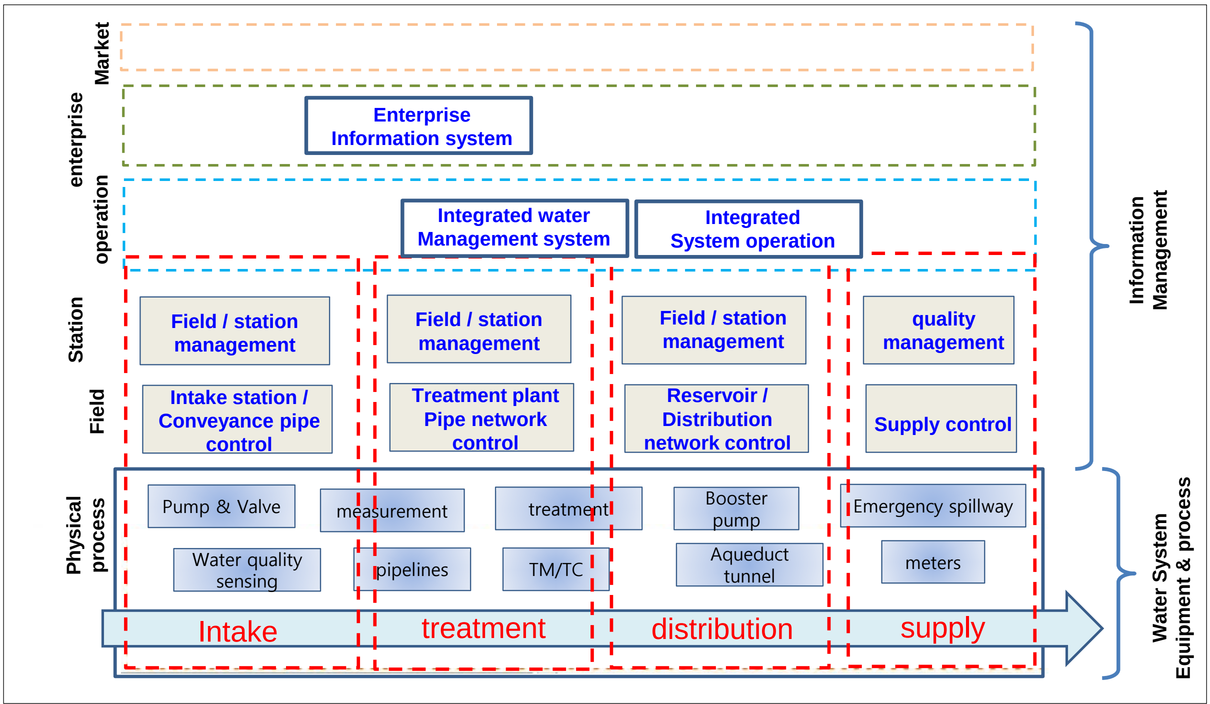

Figure 1. Convergence model of water management system.

5 IOT PLATFORM FOR SWG

SWG deploys a wide scale of sensor networks for AMI and AMR (Automatic Meter Reading), as well as for monitoring field systems and networks. It also builds actuators and additional control facilities such as SCADA (supervisory control and data acquisition) to control industrial process (Martyusheva, 2014; Monnier, 2013). Since SWG is seeking the synergies in the system level integration of the resources in the water business entities, accommodating such sensors and control facilities in an integrated way is naturally desired. A reliable platform should be brought into SWG system, which is to attach field devices through standard procedures, to provide common service functions to control the resources conveniently, and to help users to select advanced services with their preferred level of intelligence.

IoT (Internet of things) technology has been advanced remarkably for the past decade, and a number of standards to connect machines and devices are developed by dominant standards organizations; oneM2M, one of popular standard group on IoT, has released the standards on IoT platform equipped with the common functionalities for IoT services and system control (oneM2M, online). Figure 2 illustrates how IoT platform can be placed in the structure of a domain of water management system. It is not only the extended accommodation of new field devices in a standardized way, but also the functional augmentation of the supervisory system in the field domain, a standard capability to accumulate data collected from the devices, and the service delivery channel to connect it to the upper level of information processing. IoT platform is the primary part of smart platform of SWG, which bridges the operation of sensor devices towards the smart service potential based on the accumulated data processing.

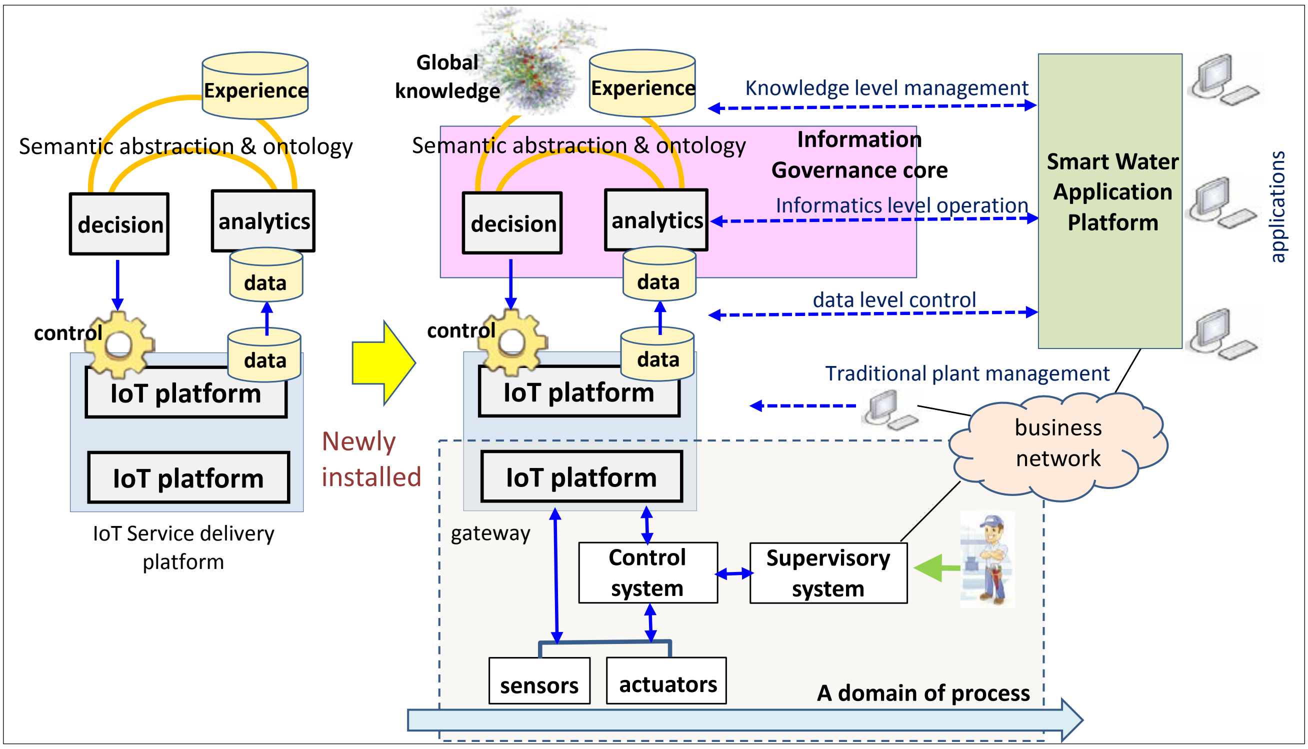

Figure 2. Smart platforms for water management system.

6 INTEROPERABILITY AND HORIZONTAL INTEGRATION OF FIELD DOMAINS

Platforms generally support interoperability and help horizontal integration of systems, as those are based on the standardized common interface and functionalities. The field devices appeared in Figure 2 are connected to the platform with standard interface that provides the flexibility in the extended installation of facilities. Datasets collected from the devices and control systems are delivered through the IoT platform with standard functions that enable the shared use of the data among various service functions. Those features of standard interface and interoperability are applied commonly in each field domain of water process, so that the consistent service interworking between the platform functions in every domain and consequently the entire system interoperability is established in the level of service delivery platforms. It means the enhancement of accessibility to the data of every field domain from enterprise level perspectives, which contributes to the improvement of cost effectiveness and flexibility of information system installation.

7 SMART WATER APPLICATION PLATFORM (SWAP)

SWG system implements a bunch of information system such as for water process control, resource and asset management, enterprise business and management information, customer support, and many others. Previous research identified 16 categories of business process in water management enterprise (Gourbesville, 2016; Lian, 2016), which can help the provisioning of data for the recognized areas to implement. There were other efforts to design water management systems to be more efficient by applying the integration scheme for the realization of water service applications (Choi et al., 2016; NewFields, online). The integrated system should be equipped indeed with flexibility to correspond to technology advancement and the change of user requirements, in order to preserve the value of integrated system. A platform to realize such a flexibility in a smart water company is required as for the name of smart water application platform (SWAP). It should provide common functions of various information systems in the water industry and to support installation, amendment, management and deletion of the applications along with the changing requirements.

SWAP plays the role as a data hub supporting the business requirements of water industry, and the accesses to datasets are categorized in different abstraction levels; it could be data and control level that works on the direct connection in between IoT platform and SWAP, or information level operation based on the result of big data and analytics, or knowledge level management that utilizes the accumulated experience and global knowledge as for decision criteria. Separating the data abstraction part from the application (water information systems) development part is one of the key benefits of SWAP, as it helps to separate evolution of data governance from the business ecosystem.

8 BIG DATA AND HYDRO-INFORMATICS

Data used in SWAP could be mediated by IoT platform, as the platform provides field data acquisition and accumulation function as its basic. Data will be collected from traditional supervisory systems, as well as from the newly deployed SWG sensors and facilities; data from smart meters, smart sensors and smart services, remote sensing, etc. will be collected and applied to the enterprise data governance, in order to be used in any application of water business. There are other data sources in global context, concerned with water business directly, such as weather forecasting information provided by public authorities and any large scale of linked open datasets like semantic webs. All those sources can be simply categorized as in business dimension, in distinction to other two categories of the sources in natural dimension and social dimension; natural dimension is about the water as one important component of the natural environment, and social dimension is about the interaction of water environment and the human society (Chen and Han, 2016).

Amount of such data is immense due to the advancement of information technology (Gourbesville, 2009), so that it prompts the data governance in the water enterprise into the inevitable big data era (Chen and Han, 2016). Big data is in a form of database equipped with high speed data I/O and parallel data processing, which is capable to deal with various types of datasets. It can provide the data as streaming, or as a kind of warehouse that integrates structured and unstructured datasets. Application of it into hydro-informatics is natural, as "big data" often refers simply to the use of predictive analytics, user behavior analytics, or certain other advanced data analytics methods that extract value from data (Wikipedia, online). Data governance core in which a decision support system (DSS) for data mining is equipped, in a water enterprise, is to prepare the necessary datasets for the analytics and business domain applications, by metadata mining and integration of data collected from the various sources (Guerrero et al., 2017).

Application of big data to hydro-informatics drastically enhances its capability, as it provides not only the means to handle large datasets for a precise calculation, but also the new analytical tools on knowledge discovery and its utilization for better understanding and engineering of water. Big data extends the work of hydro-informatics towards the cooperation with data to boost creative ideas and new value findings. For instance, computational-intensive analysis such as the numerical simulation and modelling to find an optimal design of water distribution network can be shifted to an information-based research, by associating environmental and experimental knowledge to the analysis; information on when and where the water is being consumed, and how the water demand and weather condition be changed, can be applied as major factors to seek for structural innovation point as well as to compensate the analytics calculation (Chen and Han, 2016; Gourbesville, 2009).

9 GRID WITH DSS

Grid has been taken into water management, as the terminology SWG references the smart (power) grid system for electricity management. The primary motivation of SWG is to cut the cost for the management of scarce water resource and for the leakage from ageing water infrastructure, by enhancing the capability to monitor and manage pressure, quality, flow rate, and temperature of water distribution system (Martyusheva, 2014). The operation of a grid system, generally for resource rebalancing, is feasible when the production, consumption, and storage of the resource are within a single domain of ecosystem, and when their horizontal coherency is developed to exchange the resources in bidirectional and reciprocal way (Gourbesville, 2014; Yoldaş et al., 2017; Ma et al., 2017).

However, water is weighted material that costs energy for transportation, so that its flow against the direction of gravity and hierarchy of distribution system associates with more expenses and limits. That property with the expense of quality management for sewage retreatment hurdles the efficient realization of reverse transmission mechanism in a small scale of SWG (Lee, 2015; Onishi and Kageyama, 2011). Though there were some experiments of *micro grid* for enhancing the performance of water distribution network (Castro-Gama et al., 2016; Sophocleous et al., 2016), rather the wide area water relocation systems, built in USA and Australia, focusing on pipelines installation are still referenced more as the promising cases of SWG (WWF, 2015).

Such an understanding situates us to consider the structural feature of SWG as an optimal supply chain management with economic load balancing between multiple value chains, rather than to think about a loop for the resource recycling as focal issue. Potential of cost optimization from SWG is in the larger scale of value chains model that is out of a single operator’s span of control and business (Gemma, 2014; Shahanas and

  / ISSN 1562-6865 (Online) - ISSN 1063-7710 (Print)

Sivakumar, 2016). Value chain of drinking water is the largest among others as it is built on the basic of our socioeconomic ecosystem, and others on irrigation and industrial system, waste water treatment, desalination are alongside it. A correlated cost model graph, based on the supply chain analysis for the production, delivery, demand and purchase, is required to determine the holistic optimization of the ecosystem to which SWG designate its span of control.

Hydro-informatics is equipped within the SWG in a form of decision support system (DSS) to help with the simulation of the planned system, to find minimum cost or maximum benefit of the operation, development of alternative structure to help system performance, etc. (Di Nardo et al., 2016; Guerrero et al., 2017; Li et al., 2017; Gourbesville et al., 2016). As the type of SWG system suggested in this paper focuses on the collaboration in between multiple operators, multiple hydro-ecosystems equipped with multiple DSSs can be working independently within a SWG. Figure 1 shows a tier of *market* at the top of the structure, which will issue the interworking of DSSs in different hydro-systems.

Operators install ICT facilities more, mostly for controlling and monitoring of physical world in the context of SWG, to extend the capability to collect environmental context from the sensors deployed in wide area. Adding natural dimension data to the big data system mentioned above, it establishes a SWG equipped with rich data of environmental context and grid system of interrelated supply chains of operators working in a physical area. That is the larger framework comprising of the concept of IWRM (Agarwal et al., 2000; Al Radif, 1999; Frevert et al., 2000) which is focusing on geographical incorporation of water management systems; SWG is developed based on the socioeconomic ecosystem model which helps the optimized control among multiple operators, and on the environmental model with big data that is capable to do the best of our economic system at the faying surface of both ecosystems (Kashefipour et al., 2002; Sabenije, 1996). The cost model at the faying surface between socioeconomic and environmental ecosystems is indeed desired, as the SWG in here is focusing on the “values” as the main criteria of systems design. Economic impact on the environment by the resource intake and pollution should be calculated, within a context of climate change, and those factors should be included in the evaluation of DSS in SWG. It is to shift the design of SWG from water business level to global sphere economy level, by developing the linkage model of value chains in between socioeconomic and environmental ecosystem.

10 CPS WITH VR

Big data does not only provide the capability for the predictive analytics, user behavior analytics, or any extract value from data (Wikipedia, online), but also accumulates experiences and knowledge to drive *AI powered DSS* to enable autonomous control of IoT systems (Ingebrigtsen, 2007). However, water system is basically a critical infrastructure that is conservative to have unmanned autonomous control, so that a cooperative working under human supervision is inevitable even in a very intelligent system. One of the mechanism to help human intervention to complex physical system in remote site for monitoring and control operation is Cyber-Physical Systems (CPS) (Wikipedia, online). It is implemented as a highly interconnected and integrated system that include engineered interacting networks of physical and computational components (Kaur and JayPrakash, 2014; Cyber Physical Systems Public Working Group, 2016). It actually gives a functionality to project physical system to virtual world, to connect virtual control to physical action, and to guarantee reliable operation between virtual and physical world (Yu and Xue, 2016). It can be implemented in the data governance core in Figure 2 as a platform between IoT platform and SWAP, for the efficient handling of the facilities in SWG and its projected presentation in virtual space. CPS support for the simulation and monitoring does not only cause the inundation of data at the integrated water management center, but also gives rise to the need of accelerating implication of data coming into the data center. Virtual reality (VR) can be the best combination for CPS, to make advance in the data visualization of the system. It captures the huge datasets from remote sites into the data format for communication, sharing, seeing, rendering, hearing, and writing, to present the field situation and information with icons, logos, graphic images, character sets, etc. It is the extreme achievement of the knowledge based operation of SWG in cooperation with human operator.

11 CONCLUSIONS

This keynote paper addresses the issues on the platforms required in the development of SWM system. Though many SWM technologies are emerging, the practical structure of SWM in a holistic and standardized viewpoint is few. This paper is to pave the way to the future vison of the SWM system, while focusing on the holistic structure of the SWG system and appropriate application of ICT into the system in a context of incremental advancement of smartness support. Key challenges suggested in this paper are on the development of cost model for the interaction at the faying surface between economic and environmental ecosystem, and development of hydro-informatics based on IoT big data. SWAP, DSS, CPS and VR are all challenging areas where ICT can play a crucial role to drive innovation in the field of water management.

REFERENCES

Martyusheva, O. (2014). Smart Water Grid – Plan B Technical Report, *Master Thesis*. Dept. of Civil and Environmental Engineering, Colorado State University.

International Telecommunication Union (ITU). (undefined). FG-SWM, available online, http://www.itu.int/en/ITU-T/focusgroups/swm/Pages/default.aspx.

Mauree, V. (2010). *ICT as an Enabler for Smart Water Management*, ITU-T Technology Watch Report, ITU Telecommunication Standardization Bureau, 23.

Gourbesville, P. (2015). @qua: ICT for Water, In *7th World Water Forum*, Daegu & Gyeongbuk, Korea.

Telecommunication Standardization Sector (2013). Summary of the First Meeting of the Focus Group on Smart Water Management (FG SMW), SMW-O-0001, International Telecommunication Union.

Libelium World (undefined). Smart Water: Pipe Control to Reduce Water Leakages in Smart Cities. Libelium Comunicatciones Distribuidas S.L. http://www.libelium.com/smart_water_wsn_pipe_leakages/.

The 7th World Water Forum (2015). Science and Technical Process White Paper, 7th World Water Forum, Korea, http://eng.worldwaterforum7.org/outcome/fo/view.asp?notice_seq=35&key=&keyWord=&sh_forum_gb=&page=1.

Lee, S. (2015). Smart Water Management with ICT for Water Efficiency, Security and Welfare, In 7th World Water Forum, Korea.

Onishi, M. & Kageyama, K. (2011). Smart Water Management and Usage Systems for Society and Environment. *Hitachi Review*, 60(3), 164-171, http://www.hitachi.com/rev/pdf/2011/r2011_02a_110.pdf.

Sensus (undefined). Intelligent Water Management for Your Utility. https://sensus.com/smart-water-network.

Ahn, J. (2015). *Standardization Gap Analysis for Smart Water Management*, ITU-T Focus Group on Smart Water Management Deliverable TR2.1, 3. https://www.itu.int/ifa/t/fg/swm/docs/Finalized_Deliverables/.

Ye, Y., Liang, L., Zhao, H. & Jiang, Y. (2016). The System Architecture of Smart Water Grid for Water Security. *Procedia Engineering*, 154, 361-368.

CEN-CENELEC-ETSI (2014). *SGAM User Manual - Applying, Testing & Refining the Smart Grid Architecture Model (SGAM), Version 3.0*, Smart Grid Coordination Group.

CEN-CENELEC-ETSI (2014). *SG-CG/M490/G_Smart Grid Set of Standards, Version 3.1*, Smart Grid Coordination Group.

Monnier, O. (2013). A Smarter Grid with the Internet of Things. *Texas Instruments*, http://www.ti.com/lit/ml/slyb214/slyb214.pdf.

oneM2M (undefined). *Function Architecture*, No. TS-0001-V2.10.0, oneM2M, http://www.onem2m.org/technical/published-documents.

Gourbesville, P. (2016). Key Challenges for Smart Water. *Procedia Engineering*, 154, 11-18.

Lian, G.L. (2016). Analysis of Current ICT Solutions in Water Business Processes. *Procedia Engineering*, 154, 3-10.

Choi, G.W., Chong, K.Y., Kim, S.J. & Ryu, T.S. (2016). SWMI: New Paradigm of Water Resources Management for SDGs. *Smart Water*, 1(1), 1-12.

NewFields (undefined). Vertical System Integration Horizontal System Integration- Smart Water Grid City Blueprint, http://www.newfields.com/sites/default/files/pictures/SWG_City_Blueprint.pdf.

Chen, Y. & Han, D. (2016). On Big Data and Hydroinformatics. *Procedia Engineering,* 154, 184-191.

Gourbesville, P. (2009). Data and Hydroinformatics: New Possibilities and Challenges. *Journal of Hydroinformatics*, 11(3-4), 330-343.

Guerrero, J.I., García, A., Personal, E., Luque, J. & León, C. (2017). Heterogeneous Data Source Integration for Smart Grid Ecosystems based on Metadata Mining. *Expert Systems with Applications*, *79*, 254-268.

Gourbesville, P. (2014). Challenges on Smart Water Management and Ways to Overcome Them, *Smart Water Grid International Conference 2014*.

Yoldaş, Y., Önen, A., Muyeen, S.M., Vasilakos, A.V. & Alan, İ. (2017). Enhancing Smart Grid with Microgrids: Challenges and Opportunities. *Renewable and Sustainable Energy Reviews*, 72, 205-214.

Ma, T., Wu, J. & Hao, L. (2017). Energy Flow Modeling and Optimal Operation Analysis of the Micro Energy Grid based on Energy Hub. *Energy Conversion and Management*, 133, 292-306.

Castro-Gama, M.E., Pan, Q., Jonoski, A. & Solomatine, D. (2016). A Graph Theoretical Sectorization Approach for Energy Reduction in Water Distribution Networks. *Procedia Engineering*, 154, 19-26.

Sophocleous, S., Savic, D., Kapelan, Z., Shen, Y. & Sage, P. (2016). A Graph-Based Analytical Technique for the Improvement of Water Network Model Calibration. *Procedia Engineering*, 154, 27-35.

Gemma, P. (2014). *Smart Water Management in Cities*, Contribution from Huawei to ITU-T Focus Group on Smart Water Management, SWM-I-0026r1, https://www.itu.int/ifa/t/fg/swm/docs/1403-Geneva/in/.

Shahanas, K.M. & Sivakumar, P.B. (2016). Framework for a Smart Water Management System in the Context of Smart City Initiatives in India. *Procedia Computer Science*, 92, 142-147.

Di Nardo, A., Cavallo, A., Di Natale, M., Greco, R. & Santonastaso, G.F. (2016). Dynamic Control of Water Distribution System based on Network Partitioning. *Procedia Engineering*, 154, 1275-1282.

Guerrero, J.I., García, A., Personal, E., Luque, J. & León, C. (2017). Heterogeneous Data Source Integration for Smart Grid Ecosystems based on Metadata Mining. *Expert Systems with Applications*, 79, 254-268.

Li, Y., Rezgui, Y. & Zhu, H. (2017). District Heating and Cooling Optimization and Enhancement–Towards Integration of Renewables, Storage and Smart Grid. *Renewable and Sustainable Energy Reviews*, 72, 281-

294.
Gourbesville, P., Du, M., Zavattero, E. & Ma, Q. (2016). DSS Architecture for Water Uses Management. *Procedia Engineering*, 154, 928-935.
Agarwal, A., delos Angeles, M.S., Bhatia, R., Chéret, I., Davila-Poblete, S., Falkenmark, M, Gonzalez-Villarreal, F., Jønch-Clausen, T., Aït Kadi, M., Kindler, J., Rees, J.A., Roberts, P., Rogers, P., Solanes, M. & Wright, A. (2000). *Integrated Water Resources Management*. TAC Background Paper No.4., Global Water Partnership, Stockholm, Sweden.
Al Radif, A. (1999). Integrated Water Resources Management (IWRM): An Approach to Face the Challenges of the Next Century and to Avert Future Crises. *Desalination*, 124(1-3), 145-153.
Frevert, D., Lins, H., Fulp, T., Leavesley, G. & Zagona, E. (2000). The Watershed and River Systems Management Program: An Overview of Capabilities. In *Proceedings of Watershed Management and Operations Management 2000*, 1-4.
Kashefipour, S.M., Lin, B., Harris, E. & Falconer, R.A. (2002). Hydro-Environmental Modelling for Bathing Water Compliance of an Estuarine Basin. *Water Research*, 36(7), 1854-1868.
Sabenije, H.G. (1996). Water and Environmental Resources Management – How to Cope with Our Ever Increasing Demands? *Annual Conference of the Korea Water Resources Association*, 3.
Wikipedia (undefined). Big Data, https://en.wikipedia.org/wiki/Big_data.
Ingebrigtsen, N. (2007). The Difference between Data, Information and Knowledge. Infogineering, http://www.infogineering.net/data-information-knowledge.htm.
Wikipedia (undefined). Cyber-Physical System, https://en.wikipedia.org/wiki/Cyber-physical_system.
Kaur, K. & JayPrakash, L.T. (2014). Modeling and Simulation of Cyber Physical Systems: A Case of an Adaptive Water Management System, In *Confluence the Next Generation Information Technology Summit (Confluence), 2014 5th International Conference,* 267-273.
Cyber Physical Systems Public Working Group (2016). *Framework for Cyber-Physical Systems-Release 1.0*, National Institute of Standards and Technology, https://s3.amazonaws.com/nist-sgcps/cpspwg/files/pwgglobal/CPS_PWG_Framework_for_Cyber_Physical_Systems_Release_1_0Final.pdf.
Yu, X. & Xue, Y. (2016). Smart Grids: A Cyber–Physical Systems Perspective, *Proceedings of the IEEE*, 104(5), 1058-1070.